Project No: 603502

DACCIWA

"Dynamics-aerosol-chemistry-cloud interactions in West Africa"

Deliverable

D4.4 Aerosol influences on cloud properties

<u>**Due date of deliverable:**</u>	31/05/2018
<u>**Completion date of deliverable:**</u>	05/06/2018

Start date of DACCIWA project:	1st December 2013	**Project duration:**	60 months

Version:	[v1.0]
File name:	[D4.4_Aerosol_influences_on_cloud_properties_v1.0.docx]

Work Package Number:	**4**
Task Number:	**4**

<u>**Responsible partner for deliverable:**</u>	**UNIVMAN**
Contributing partners: **UNIVLEEDS, MO, KIT**	**UNIVMAN, UCA (previously UBP), UPMC, DLR,**

Project coordinator name:	Prof. Dr. Peter Knippertz

Project coordinator organisation name:	Karlsruher Institut für Technologie

Dissemination level		
PU	Public	**X**
PP	Restricted to other programme participants (including the Commission Services)	
RE	Restricted to a group specified by the consortium (including the Commission Services)	
CO	Confidential, only for members of the consortium (including the Commission Services)	

Nature of Deliverable		
R	Report	**X**
P	Prototype	
D	Demonstrator	
O	Other	

Copyright

DOCUMENT INFO

Authors

Author	Beneficiary Short Name	E-Mail
Hugh Coe, Jonathan Taylor, Hazel Jones, Chris Dearden, Sophie Haslett	UNIVMAN	hugh.coe@manchester.ac.uk jonathan.taylor@manchester.ac.uk hazel.jones@manchester.ac.uk
Alfons Schwarzenboeck, Joel Ferreira de Brito, Regis Dupuy	UCA	A.Schwarzenboeck@opgc.univ-bpclermont.fr j.brito@opgc.univ-bpclermont.fr R.Dupuy@opgc.univ-bpclermont.fr
Adrien Deroubaix, Laurent Menut, Cyrille Flamant	UPMC	adrien.deroubaix@lmd.polytechnique.fr menut@lmd.polytechnique.fr cyrille.flamant@latmos.ipsl.fr
Christiane Voigt, Valerian Hahn	DLR	Christiane.Voigt@dlr.de
John Marsham, Phil Rosenberg, Paul Field	UNIVLEEDS	J.Marsham@leeds.ac.uk P.D.Rosenberg@leeds.ac.uk P.Field@leeds.ac.uk
Paul Field	MO	P.Field@leeds.ac.uk
Konrad Deetz, Bernhard Vogel	KIT	konrad.deetz@kit.edu bernhard.vogel@kit.edu

Changes with respect to the DoW

Issue	Comments
-	-

Dissemination and uptake

Target group addressed	Project internal / external
Scientific	Internal and external

Document Control

Document version #	Date	Changes Made/Comments
0.1	02/05/18	Template with general structure
0.2	15/05/18	Draft with contributions from all institutions
0.3	18/05/18	Full draft including introduction and summary for approval by the general assembly
1.0	05/06/18	Final document approved by the general assembly

Table of Contents

1   Introduction

DACCIWA focusses on the densely populated coastal area of southern West Africa (SWA). The UNO (2015a) indicates that more than half of the global population growth between now and 2050 will be related to Africa. Nigeria had a population of 182 million in 2015 (rank 7) that is predicted to rise to 399 million (rank 3). Accompanied with these projections, Liousse et al. (2014) has shown that the African anthropogenic emissions will significantly increase from 2005 to 2030 if no emission regulations were implemented. In the "business as usual" scenario an increase in emissions of CO, NO_x and SO_2 by factors of 3.2, 5.6 and 6.5, respectively, is projected from 2005 to 2030. Furthermore, UNO (2015b) expects that urbanization will increase significantly. For Nigeria the population fraction living in urban areas is estimated or projected to be: 47% (2014), 54.1 % (2030) and 62.7% (2050). These huge social and economic developments will take place at the same time as large scale land use changes and future global climate change. These will combine to significantly impact the West African Monsoon (WAM) in a variety of different ways. To both predict the changes on the monsoon and to quantify the impacts requires a detailed knowledge of meteorological characteristics, cloud physics, and dynamics, as well as air pollution, yet at the present time our understanding is extremely poor. DACCIWA comprises expertise in modeling and observation including weather and climate science, air pollution, cloud microphysics, and radiation and deploys this expertise to shed light on the area of interest.

This deliverable describes the progress made in understanding the key processes driving both stratocumulus clouds across the DACCIWA region and how aerosols across the region influence the properties of clouds, through which they may subsequently modify precipitation, radiation, and dynamical and land surface interactions. The work carried out as part of WP4 to deliver these outcomes includes direct analysis of the observational data set obtained during the DACCIWA intensive experimental period (June – July 2016) and model assessments of key processes. The modelling framework covers a range of scales of physical and chemical complexity and geographical extent. Large Eddy Modelling (LEM) has been carried out to examine detailed cloud processes in a dynamical framework that resolves dynamics. Regional numerical weather prediction models have been used both with prescribed aerosol fields but including detailed two-way interactions to perform sensitivity studies of aerosol-cloud-radiation interactions and also in models that fully describe the emissions of aerosols and their precursors and link these to cloud properties and feedbacks. The DACCIWA observational dataset (previously reported on in D4.3) has been used extensively to constrain and challenge model results. Important processes have been investigated in the coupling of aerosols, clouds, radiation, energy budget, dynamics, and precipitation using this hierarchy of models.

Each of the models used in these assessments are described in Section 2 including an overview of their setup and the runs that were carried out. The main findings are then described. The observational findings are presented first since these framed the model simulations and were used to challenge model results. The main model findings are described broadly in scale order beginning with small scale microphysical processes and ending with large regional scale interactions. At the end of the report the main findings are discussed in the summary.

2 Description of models, setup and runs

The following section contains descriptions of relevant features of each of the models used in this report. While model descriptions were covered in detail in D4.2, this section focuses more on how the models were set up to be relevant to an investigation of cloud-aerosol interactions in the DACCIWA region.

2.1 MONC (UNIVMAN)

MONC is a re-write of the original Met Office Large Eddy Model (LEM). It can be coupled to the Cloud-AeroSol-Interactions-Microphysics (CASIM) module (Shipway and Hill, 2012; Hill et al., 2015) – a multi-moment scheme allowing the investigation of changes in mass mixing ratio and number concentrations of cloud droplets, rain and aerosols. MONC experiments have been performed using both CASIM and the simple cloud scheme, where for the latter case, there is only a single prognostic (cloud mass mixing ratio) with sedimentation of cloud droplets, autoconversion of cloud to rain and aerosol information not specified.

2.1.1 Model initialisation and configuration

All simulations are based on conditions at Savé and use a domain size of 7.5 x 7.5 km in the horizontal (30 m grid spacing), and a vertical extent of 2 km (10 m spacing up to 1.5km, increasing to 20 m spacing between 1.5 and 2 km), where the top 500 m is a sampling layer to prevent unwanted gravity waves. The first two hours of each simulation are discarded to allow for model spin-up. Periodic boundary conditions are used in all cases.

MONC is initialised using profiles of potential temperature, total water mass mixing ratio and horizontal wind components, shown in Figure 2.1, from the 0330 UTC radiosonde launched from the Savé ground site, interpolated onto the model grid with a vertical resolution of 10 m. The cloud liquid water mass mixing ratio profile is calculated assuming an adiabatic cloud parcel ascent from cloud base to cloud top (i.e. between 350 m and 500 m when RH is at water saturation in Figure 2.1b). The total water mass mixing ratio profile is then calculated as the sum of the cloud liquid water and the water vapour mixing ratio at each model level. This supersaturated profile results in the immediate production of a clouds layer via condensation in the first model time-step.

Over a period of 7.5 hours within the model, the wind fields from 0330 UTC are relaxed to those from the 1100 UTC radiosonde (see Figures 2.1c, d) to allow the model to maintain the low level jet throughout the simulation. A constant large-scale subsidence of 5×10^{-6} s^{-1} is imposed throughout the domain.
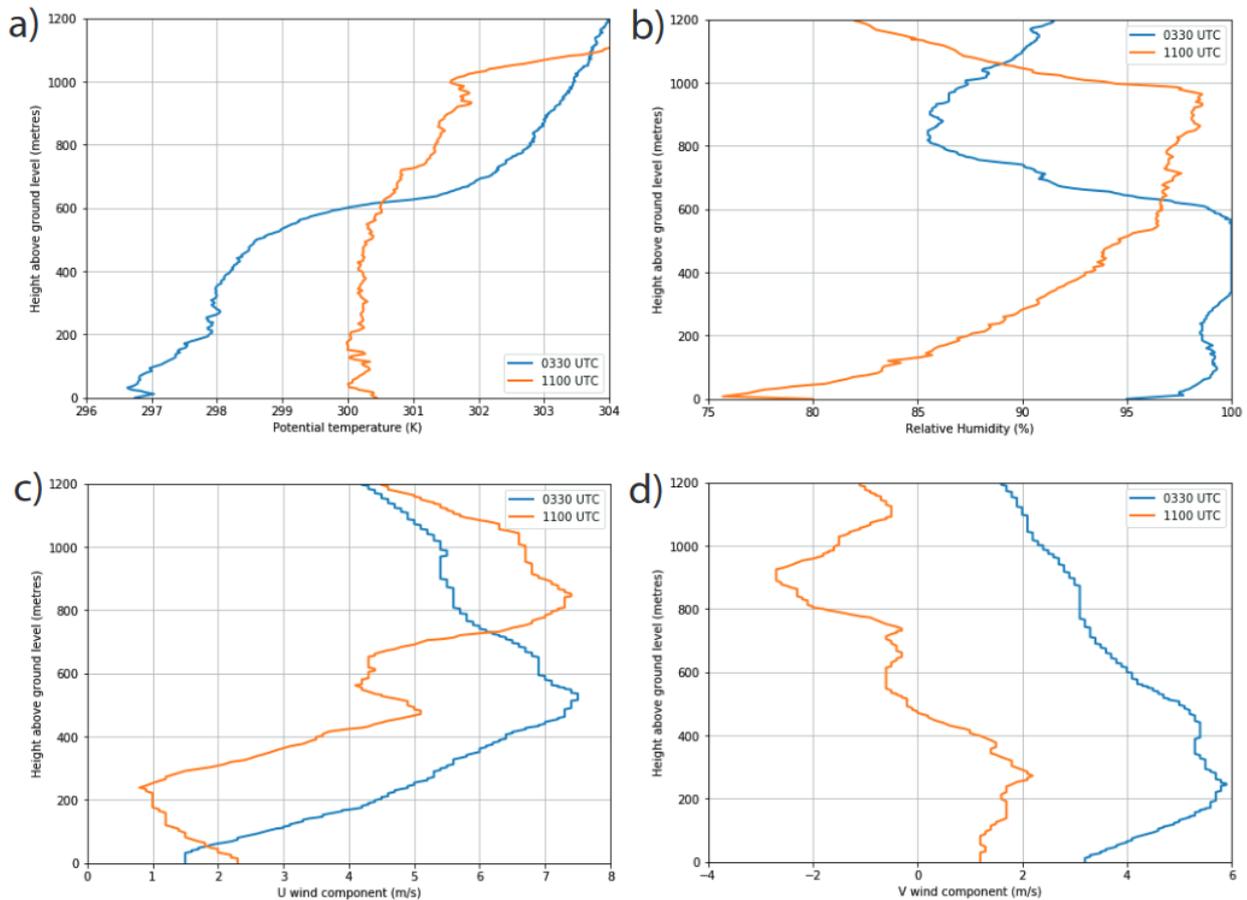
Figure 2.1 - Profiles of a) potential temperature, b) relative humidity, c) u wind component and d) v wind component from radiosondes launched at Savé on 5 July 2016 at 0330 UTC (blue) and 1100 UTC (orange).

Radiation is accounted for via coupling MONC with the Suite of Community Radiative Transfer codes based on Edwards and Slingo (SOCRATES) called on a three minute time-step. This allows the effects of long wave cloud top cooling and short wave absorptions within the cloud layer to be represented in the model. Surface fluxes are prescribed by ground site measurements at Savé, so there is no feedback between changes in cloud cover, LWP and the land surface radiation budget.

2.1.2   Model experiments

CASIM_NO_PROC denotes the experiment where CASIM is used to predict the evolution of the mass and number concentration for both cloud droplets and rain. Droplet activation is based on the Abdul-Razzak scheme, with aerosol specified as a single accumulation mode log-normal distribution following the analysis of regional aerosol properties by Sophie Haslett at UNIVMAN (section 3.1.1). Aerosol mass and number fields are completely passive in this experiment, and used only to determine the number of droplets activated.

SIMPLE_CLOUD denotes the use of the simple cloud scheme.

2.2   Unified Model (UNIVLEEDS/MO)

The Unified Model (UM) is a suite of numerical weather prediction and climate simulation software that is capable of producing both global and local area simulations of the atmosphere at resolutions from ~100 m to ~100 km and on both climate and numerical weather prediction time scales. It uses a Semi-Lagrangian dynamics scheme (Wood et al. 2014). Subgrid fluxes are parameterized using a 1st order closure boundary layer scheme with a non-local term (Lock et al 2000, Lock 2001, Lock & Edwards 2011). It is relevant to note that the boundary layer scheme considers well mixed layers

generated by both surface heating and cloud top radiative cooling of stratocumulus. These layers may be either coupled or decoupled as appropriate for the stability profile. The UM can be run with a variety of physical parameterisations and can be coupled to different surface models.

A recently developed cloud microphysics parameterisation for the UM is the Cloud AeroSol Interactions Microphysics (CASIM), the same scheme as used in MONC. CASIM permits simulations to be initialised with a user defined multi-mode profile of aerosol where each mode can act as cloud condensation nuclei or ice nuclei. These nuclei are activated by one of a selection of activation scheme to generate cloud droplets. The aerosol is advected and can be optionally modified by cloud processes. The cloud droplets and precipitation may be represented by one, two or three moments. CASIM includes a sub-grid cloud scheme based on Smith (1990) to represent cloud cover on smaller scales than the grid resolution. It has been used to successfully represent stratocumulus (Grosvenor et al., 2017) and convective clouds (Miltenberger et al. 2018).

In order to test the sensitivity of the meteorology in West Africa to aerosol concentration we have run a set of limited domain simulations each using the CASIM microphysics with different aerosol concentrations. Our limited area domain covers approximately 1650 km E-W by 880 km N-S with a resolution of approximately 4.4 KM and a 30 s time step centred upon lat 6° and lon 2.5°. This model is one-way nested into a global simulation. Both models have 70 levels, concentrated towards the surface (10 m resolution at the surface). The selection of physical parameterisations is based on the well tested operational runs used for UK weather forecasting by the Met Office. In particular, the convective parameterisation is switched off allowing moist convection only by the resolved scale dynamics. The only significant difference from the UK forecasting runs is that we use the CASIM microphysics. Within the CASIM microphysics we use two moment cloud droplets and two moment precipitation. This allows us to investigate the impact of droplet size upon the cloud microphysics. We provide the model with a single mode of aerosol to act as condensation nuclei and a single mode of aerosol to act as ice nuclei and do not utilise cloud processing of the size distribution. The condensation nuclei aerosol is composed of a single accumulation mode and we use the Shipway (2015) activation scheme which generates the number of activated droplets as a function of aerosol particle size and updraft velocity. The four simulations have condensation nuclei concentrations at the surface of 100, 300, 1000 and 3000 cm^3. In all cases the mass mixing ratio of aerosol is kept approximately constant up to 5 km and then exponentially decays to the top model level.

2.3   The model system COSMO-ART (KIT)

The regional-scale model framework COSMO-ART combines the operational weather forecast model COSMO (Baldauf et al., 2011) of the German Weather Service (DWD) with the ART modules (Aerosols and Reactive Trace gases, Vogel et al., 2009). Gas phase chemistry and aerosol dynamics are online coupled with the meteorology. Aerosol particles are treated via a modal approach, considering mineral dust, sea salt and anthropogenic aerosols as well as secondary aerosols. Latter can be formed by nucleation of sulfuric acid. The processes condensation, coagulation, and dry and wet deposition are taken into account. The formation of secondary organic aerosol is realized via a VBS (volatility basic set) approach (Athanasopoulou et al., 2013). COSMO-ART is able to consider the direct and indirect aerosol effect. Schematically, the link between the atmospheric state and treatment of air pollution (trace gases and aerosols) is shown in Figure 2.2.
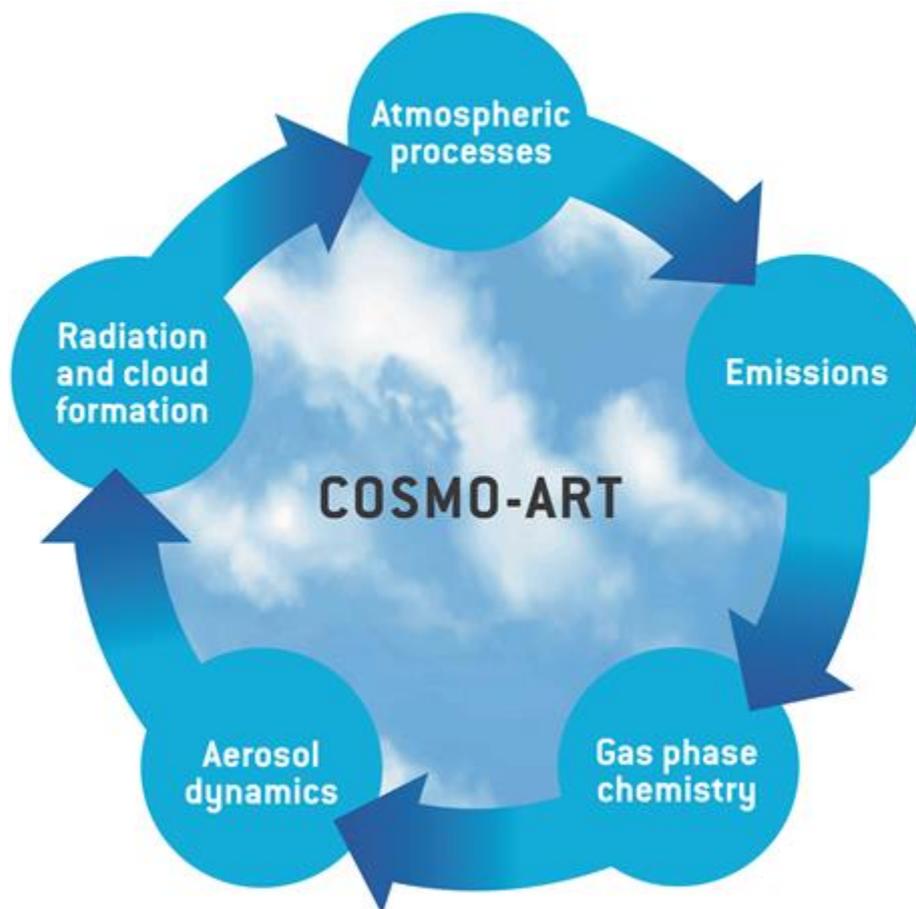
Figure 2.2 – Scheme of the COSMO-ART model structure.

In this study (Deetz et al., 2018), the regional-scale model framework COSMO-ART is applied to Southern West Africa (SWA) for a summer monsoon process study on 2 – 3 July 2016 to assess the aerosol direct and indirect effect on clouds and the atmospheric dynamics. The modelling study is supported by observational data obtained during the extensive field campaign of the project DACCIWA (Dynamics-Aerosol-Chemistry-Cloud Interactions in West Africa) in June–July 2016.

To assess the sensitivity of the aerosol direct effect (ADE) and the aerosol indirect effect (AIE) on the meteorological conditions, two factors F_{ADE} and F_{AIE} were introduced in COSMO-ART, which allow to scale the total aerosol mass and number densities, respectively, by simultaneously preserving the underlying aerosol distribution. All aerosol modes are changed uniformly by the factors but the scaling is limited to the derivation of the aerosol optical properties in case of ADE and the aerosol activation in case of AIE. Table 2.1 summarizes the realizations used in this study.

Table 2.1 - Overview of the COSMO-ART realizations capturing the variation in the aerosol amount with respect to the Aerosol Direct Effect (ADE) and Aerosol Indirect Effect (AIE).

Abbreviation	Description of Simulation
$AIE_{0.1}ADE_{0.1}$	$F_{AIE} = 0.1$ and $F_{ADE} = 0.1$
$AIE_{0.25}ADE_{0.25}$	$F_{AIE} = 0.25$ and $F_{ADE} = 0.25$ (clean case)
$AIE_{0.5}ADE_{0.5}$	$F_{AIE} = 0.5$ and $F_{ADE} = 0.5$
$AIE_{1.0}ADE_{1.0}$	$F_{AIE} = 1.0$ and $F_{ADE} = 1.0$ (reference case)
$AIE_{2.0}ADE_{2.0}$	$F_{AIE} = 2.0$ and $F_{ADE} = 2.0$
$AIE_{4.0}ADE_{4.0}$	$F_{AIE} = 4.0$ and $F_{ADE} = 4.0$ (polluted case)

2.4   WRF-CHIMERE (UPMC)

WRF-CHIMERE is an online access model, which is composed of the meteorological model (WRF) and the chemistry-transport model (CHIMERE). The Weather Research and Forecasting (WRF) model is a mesoscale non-hydrostatic meteorological model that includes several options for physical parameterizations of the different atmospheric processes. CHIMERE is a chemistry-transport model suitable for a widely range of air quality applications extending from urban to hemispheric scale (Mailler et al, 2017).

The coupling online of the two models is described in Briant et al. (2017) and is done by using the version 3.7.1 of WRF and CHIMERE 2017. The models are coupled through the external coupler OASIS3-MCT (Valcke et al., 2015).

In its current version, WRF-CHIMERE allows both one and two way coupling. In the one-way coupling, WRF feeds CHIMERE with sub-hourly frequency exchanging 28 meteorological variables through the OASIS interface implemented in the models. The two-way interaction includes the aerosol direct and indirect effects through the exchange (with sub-hourly frequency) of aerosol parameters.

For the direct effect, aerosol optical properties are diagnosed with Mie theory at different wavelengths starting from the aerosol size distribution predicted by CHIMERE and are used in WRF to force the radiative transfer calculation of both short and longwave radiation through the RRTMG radiation scheme (Iacono et al., 2000). CHIMERE sends aerosol information to WRF including Aerosol Optical Depth (AOD), Single Scattering Albedo (SSA), and Asymmetry.

The indirect effect is diagnosed in the model via the cloud microphysics scheme of Thompson and Eidhammer (2014), which is an aerosol aware microphysics parameterization including a scheme for cloud droplet nucleation. In this scheme, aerosol activation into droplets is done at cloud base as well as anywhere in cloud where the number of activated aerosols is larger than the existing droplet concentration. Following Ghan et al. (1997), the number of aerosol particles activated as cloud droplets in each section of the CHIMERE size distribution is calculated using a maximum supersaturation determined from a Gaussian spectrum of updraft velocity and internally mixed aerosol properties. CHIMERE sends aerosol information to WRF including Aerosol size distribution, bulk hygroscopicity, ice nuclei, and deliquesced aerosols.

For this study, we used the Hemispheric Transport of Air Pollutants (HTAP) anthropogenic emissions dataset with a native horizontal resolution of 0.1x0.1 degrees since the anthropogenic emissions developed within the DACCIWA project were not ready during the period of model development and when the simulations were carried out (end of 2017). It is probable that these HTAP emissions are less correct and accurate than those produced for the project. For the main emitted species, NOx, VOCs, OC, BC, SOx, PPM, emissions fluxes are disaggregated and reaggregated following the chemical mechanism, horizontally interpolated on the WRF-CHIMERE grid and vertically distributed as a function of the activity sectors.

The model domains are presented in Figure 2.3. Two domains are defined: the larger domain represents the whole surface presented in the Figure 2.3: from 9W to 5E in longitude and from 1N to 11N in latitude. The second domain is zoomed on Accra, Lomé, Cotonou and Savé and enables to have a fine horizontal resolution for the area covered by the flights measurements. These horizontal domains are used both by WRF and CHIMERE, to avoid spatial interpolation between the two models and during the coupling. On the other hand, the vertical resolution is different when WRF has more vertical levels in order to resolve convective cells as well as possible.
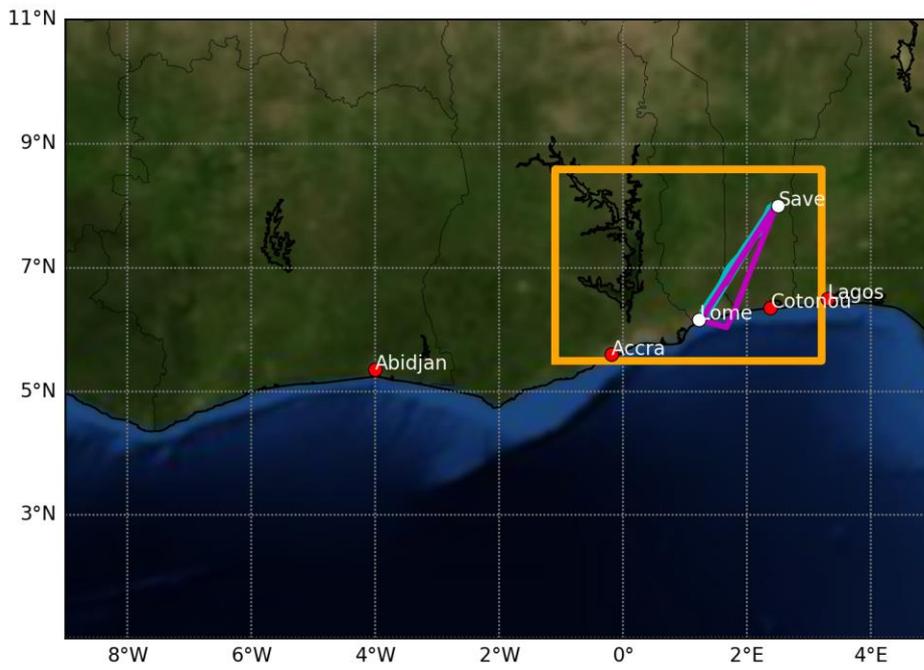
Figure 2.3 - Map of the modelling domain with location of the major cities (red and white dots). Superimposed are the flight tracks of the two research aircrafts on 5 July the German Falcon (blue line) and the French ATR-42 (violet line). The orange square presents the focused area

3 Influence of local pollution and Central African biomass burning low-level clouds in SWA (UNIVMAN, UPMC, DLR, UBP)

This analysis is being led by Jonathan Taylor and Hugh Coe (UNIVMAN). The objectives are

1. Compare the broad-scale cloud properties during the DACCIWA project to previous overviews of the region, to assess how representative the study region and period were
2. Provide a statistical overview of aerosol properties across the DACCIWA region
3. Provide a statistical overview of in situ properties of low-level clouds across the DACCIWA region
4. Assess the relative impacts of local urban emissions and transported background pollution on cloud properties in the region

The relative effects of local emissions and regional background pollution on the in situ cloud properties were investigated by mapping aerosol and cloud measurements across the region. These results were then used in process and regional modelling studies, to improve assessments of the impacts of increasing urban emissions on regional cloud, and consequently precipitation and climate, under different pollution scenarios.

3.1 Measurement data

3.1.1 In situ observations

Each aircraft was equipped with a suite of instrumentation to measure basic meteorological variables such as temperature, humidity, pressure, and winds. Accumulation mode aerosol composition was measured by aerosol mass spectrometer (AMS), on the Twin Otter and ATR. Aerosol size distributions were measured using a scanning mobility particle sizer (SMPS) on the ATR. The cloud condensation nuclei concentration (CCN) was measured with a CCN counter on the ATR. NO_x concentrations were measured using online chemiluminescence / photolytic conversion detectors. The cloud and aerosol measurements are described in more detail D4.3, while the gas-phase measurements are described in D3.3.

Cloud drops 3 – 50 µm in diameter were measured using a CDP on the Twin Otter, CDP and/or FCDP on the ATR, and a CAS on the DLR Falcon. Details of the data processing for the different platforms are given in D4.3. Data were considered in-cloud when the measured liquid water content (LWC) was greater than 0.1 gm^{-3}. Measurements of CDNC are reported in number per standard cubic centimetre (scm^{-3}), corrected to standard pressure of 1013.25 hPa and temperature of 273.15 K.

A difficult challenge with the DACCIWA dataset is ensuring the cloud drop number concentration (CDNC) measurements on the different platforms are comparable. Each instrument had its sample area measured using a droplet gun prior to the campaign, and sizing was calibrated in the field using glass beads of known size and refractive index. No direct inter-aircraft comparisons were conducted during the flying campaign, partly due to air traffic restrictions. This means a statistical comparison of the cloud probes is the best comparison possible. Figure 3.1 shows normalised histograms of CDNC from the three aircraft, over the geographical region with the most data points (both in terms of total time in cloud and number of days of cloud sampling). The similarity of the shape of the distributions shows that the CDNC measurements are comparable.
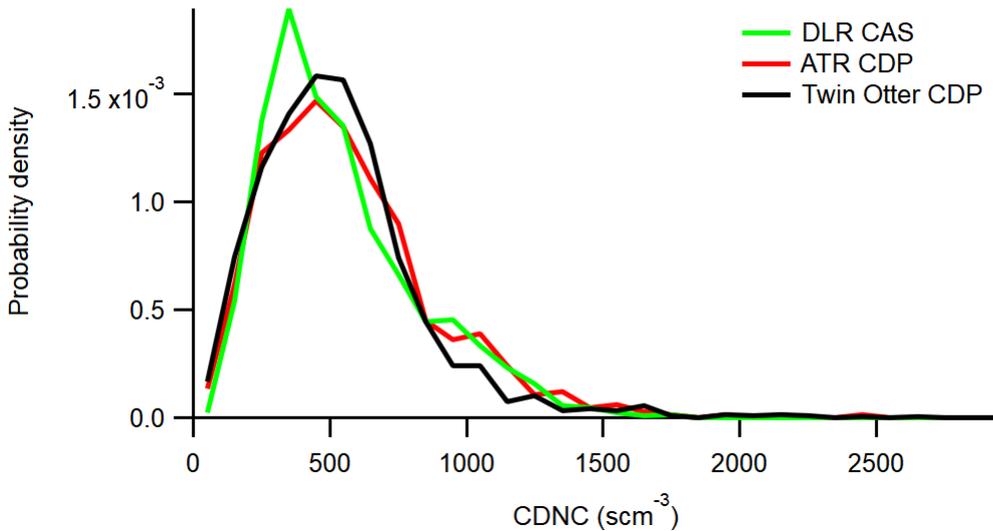
Figure 3.1 - Normalised histograms of CDNC from the three aircraft platforms. Data are taken from all flights with cloud penetrations over Togo/Benin below 1km AMSL.

3.1.2 Cloud satellite measurements

We used the optimal cloud analysis (OCA) product (Watts et al., 2011) taken from the Meteosat SEVIRI spectrometer. This product provides cloud top pressure (CTP) and cloud optical thickness (COT) for the top two cloud layers (looking from above), for scans every 15 minutes. We use this product to derive the low-level cloud fraction (for pressures above 680 hPa, or altitudes below around 3.5km AMSL). Comparison with the low- level cloud fraction (LLC) using ceilometers based near Save and Kumasi showed that this satellite-derived product agreed with ground measurements (Fig. 3.2) within 10% cloud fraction, capturing both the absolute values and also the diurnal cycle.
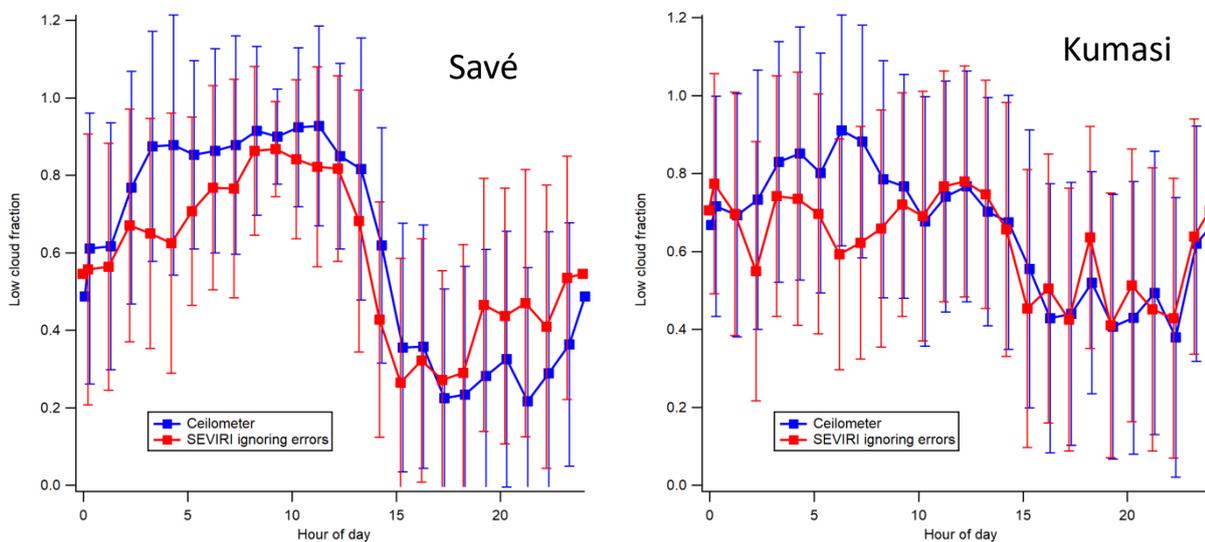
Figure 3.2 - Comparison of the diurnal cycle of LLC fraction from satellite and ground-based measurements.

3.2   Results

3.2.1   Diurnal cycle of low-level cloud cover

Figure 3.3 shows the average diurnal cycle of LLC fraction over Togo and Benin, plotted versus latitude. LLC peaks around 1000 UTC, and falls to a minimum around 1800. Cloud cover is generally higher inland than offshore, except for the period in the late afternoon / early evening. A

region of more extensive cloud cover is seen developing overnight, around 50 – 150 km inland. The greatest cloud cover is seen around 250 km inland that begins to develop overnight but becomes particularly pronounced during daylight hours. A further region of greater cloud cover is seen just inland of the coast- this may be sea breeze clouds developing from mid-morning to the early afternoon, and moving up to 50 km inland before dissipating. Less cloud cover is seen over all inland areas between 1600 – 2300. By taking the mean over several weeks we lose the extremes of these values- on some evenings cloud cover was zero and on some mornings it reached 100%. This averaging allows us to assess which features are statistically robust, and minimises transient features in the cloud field.

Figure 3.4 shows the orography of West Africa, and a map of LLC fraction at the 1000 peak. The LLC fraction decreases dramatically north of 10 – 11N. South of this decrease, the largest LLC fractions are seen on the upwind side of slopes, and the lowest on the leeward sides. This is in agreement with van der Linden et al. (2015). The features in our mean LLC fraction over the region are broadly similar to those derived by van der Linden et al (2015), meaning the measurement period is likely to be representative of a typical monsoon season. The absolute values we present are more in line with the synoptic observations than the satellite measurements in the previous work, as the LLC fraction product here takes into account times when LLC would not be visible due to higher cloud obscuring the view. Figure 3.4 also shows the major population centres in the region. Despite the presence of urban emissions, there is no clear effect on peak cloud cover downwind of the major cities.
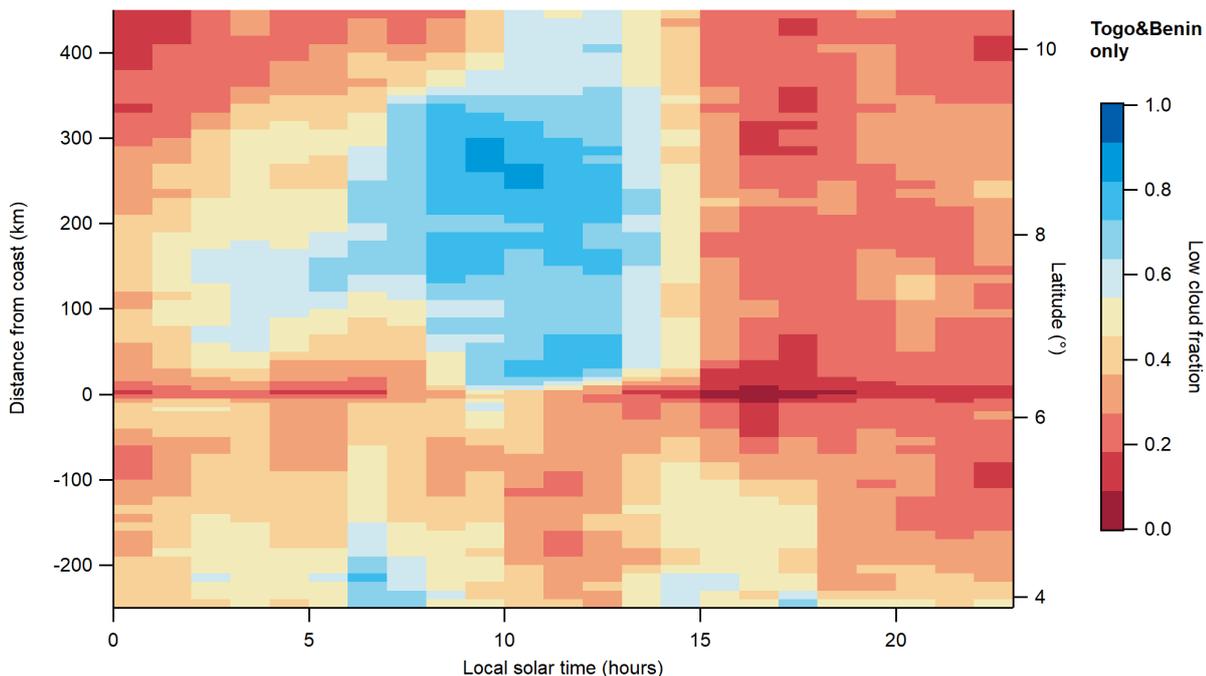

Figure 3.3 - Mean diurnal cycle of LLC fraction over Togo/Benin throughout the DACCIWA aircraft campaign.
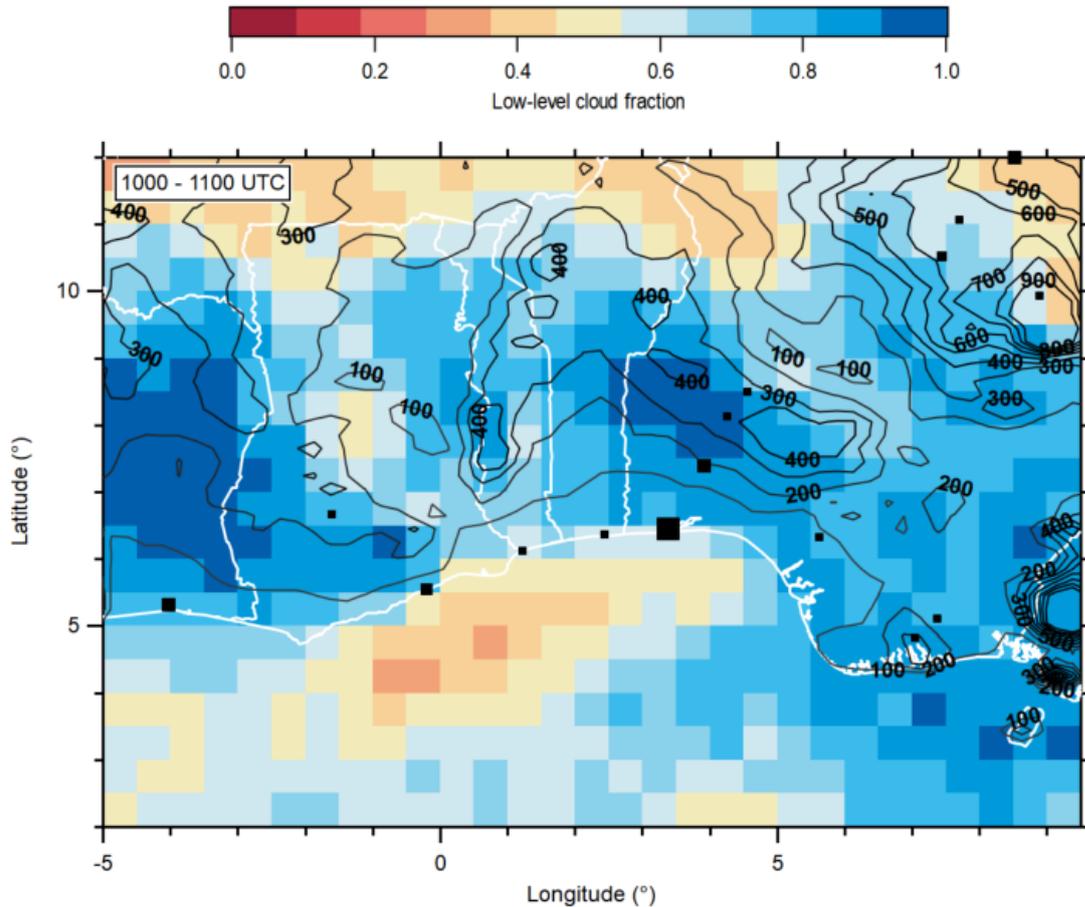
Figure 3.4 - Map of mean low-level cloud fraction between 1000-1100 UTC over West Africa. The black lines show the orography, labelled in m AMSL, and the black squares show major population centres.

3.2.2   Regional variation in aerosol properties

Aerosol data were separated into upwind marine and inland data. The thickest plumes of urban outflow were extracted by choosing only data from the top 5% of NO_x concentrations, within 60 km of Abidjan (Côte D'Ivoire), Accra (Ghana), Lomé (Togo) and Cotonou (Benin). The rest of the inland data was considered to be continental background.

Figure 3.5a shows a comparison of boundary layer aerosol size distribution measured in these different category areas. Significant variation can be seen both between and within regimes in the number of smaller, Aitken mode particles. These small particles are emitted from urban centres but grow quickly in the atmosphere; large Aitken mode populations are therefore indicative of a local aerosol source. In contrast, the number concentration of accumulation mode particles, with an average diameter near 200 nm, is remarkably consistent across the three regimes: 80% of the data lie within ±30% of the median in all cases. An average accumulation mode concentration of 600 cm^{-3} was measured in the upwind marine air and around 850 cm^{-3} in the continental background, which shows that the air mass already contains the majority of these particles before being influenced by urban emissions.

Figure 3.5b shows aerosol mass and number concentrations, with mass classified by chemical species. Upwind marine air contains a submicron mass of around 7 µg m^{-3}. Comparing this with the continental background mass loading indicates that more than 80% is already present upstream of any near-field sources. Even in the concentrated city plumes represented by the urban

outflow regime, an enhancement due to urban emissions was only factor of two greater. The relative chemical composition of the aerosol mass in all three regimes was remarkably similar.

The lack of variability in the accumulation mode concentration and chemical composition is evidence that much of the aerosol originates from a common source. Furthermore, the similarity between the accumulation mode concentration in upwind marine and background continental aerosol identifies the dominant source of this aerosol to be from outside the region, upwind of both locations. This is further corroborated by the similarity in the aerosol chemical composition across the three regimes. Our evidence shows that the majority of the aerosol mass in the West African boundary layer originates from the boundary layer of the eastern tropical Atlantic Ocean and is present before the air mass is influenced by coastal cities.
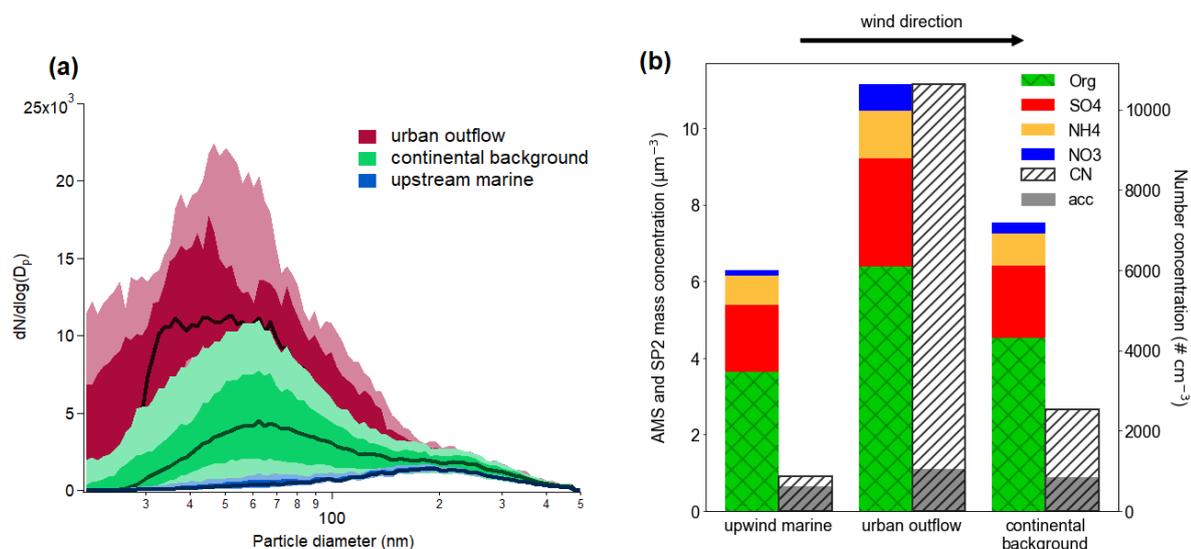

Figure 3.5 - Boundary layer aerosol composition. Panel (a) shows size distributions of aerosol in urban outflow, continental background and upstream marine regimes. Panel (b) shows the chemical composition and condensation nucleus (CN) concentration in each of these three regimes. Shaded regions in the CN bar show the number of aerosols in the accumulation mode.

To provide further evidence of the source of these emissions, modelling simulations running GEOS-Chem were used to compare the regional aerosol field with emissions of biomass burning switched on and off. These simulations showed a significant contribution to regional aerosol in SWA from biomass burning in central Africa. These results are reported in further detail in D3.4.

Further simulations were carried out using COSMO-ART, with fire emissions turned on and off, as shown in Figure 3.6. Again, the model captured the transport of biomass burning emissions from the southern hemisphere to the boundary layer in the DACCIWA region. The influence of the transported aerosol was to shift clouds into a regime with higher CDNC and lower effective radius.
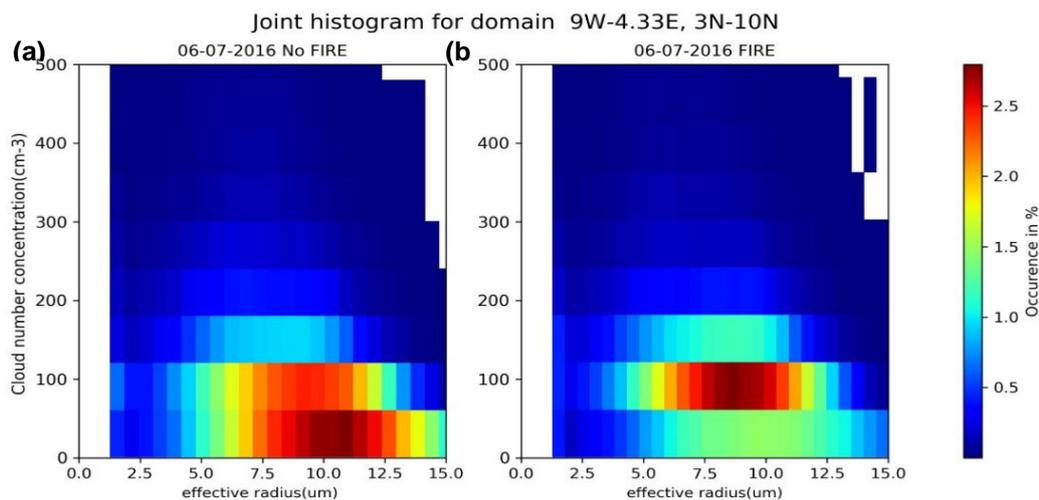
Figure 3.6 - Two-dimensional histogram showing cloud properties in the NO FIRE (left) and FIRE (right) simulations.

3.2.3   Regional variation in cloud microphysics

To investigate the effect of local emissions on cloud microphysical properties, we collated cloud measurements below 1 km in altitude from all three aircraft and compared them with distance to the coast on a north/south axis, as shown in Figure 3.7. The heterogeneous nature of the dataset means that some areas and some days have large numbers of data points recorded, while others have relatively few. This can potentially lead to bias in the data when averaging, as a day with a large number of cloud measurements could be given more weight than one with fewer clouds measured. To prevent this bias, the average data shown in Figure 3.7a were calculated by first finding the median CDNC for each day, and then calculating statistics for those median values. Listing the number of data points and number of days the data are from also gives an idea of how much the average data might be affected by cloud-to-cloud variability and day-to-day variability.
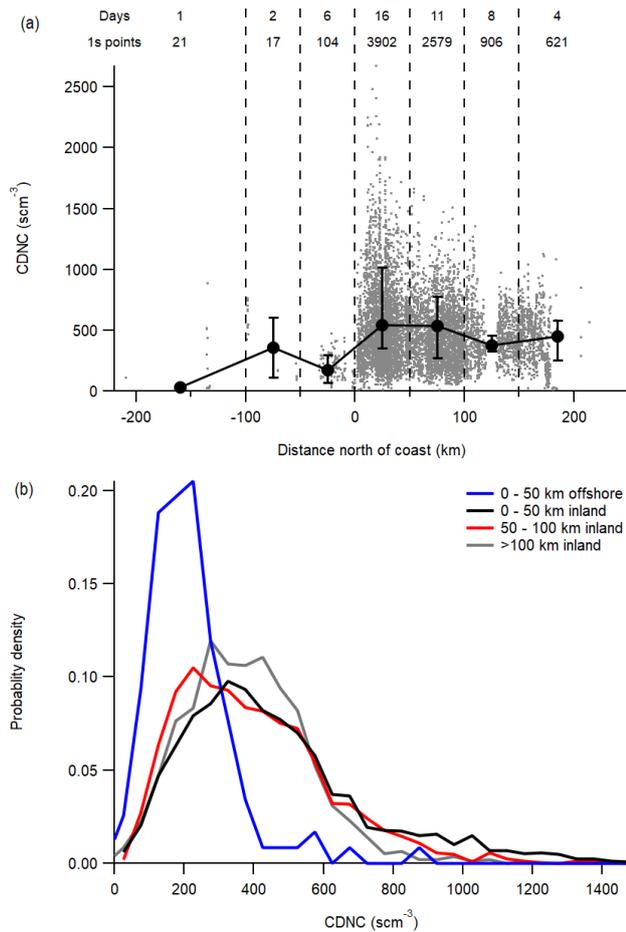
Figure 3.7 - Measured CDNC versus distance inland for all data below 1km. Panel (a) shows all data as a function of distance. Daily medians in each bin were calculated; the markers and error bars then show the median, minimum, and maximum of these daily medians. Panel (b) shows histograms at different distances.

Over 50 km offshore, there are few data points and from only a few individual days. These measurements are from specific case studies (e.g. Flamant et al., 2018) rather than more routine survey-type flights. Less than 50 km offshore, there was more frequent sampling of clouds from 7 individual days and almost 2 minutes of cloud data. The CDNC values here were more consistent, and most days had a median CDNC in the range 100 – 300 scm^{-3}, with a campaign average of 175 scm^{-3}. CDNC in the pristine south Atlantic is generally less than ~80 cm^{-3} (Bennartz, 2007). This suggests that the background CDNC of offshore clouds in the DACCIWA region is representative of moderately polluted clouds. Moving inland, several differences are apparent. The peak CDNC for 1s data points was significantly higher, with some values over 1500 scm^{-3}; these clouds are directly affected by the thickest urban plumes. However, such extreme values were not representative of clouds across the whole region.

Individual values of CDNC are often highly variable due to the different histories of individual air parcels. Between 0 and 100 km inland, the daily average values of CDNC inland were in the range 270 – 1020 scm^{-3}, with a campaign median of 540 scm^{-3}. Over 100 km inland, daily medians ranged from 250 – 580 scm^{-3}, with a campaign average of 410 scm^{-3}. The average CDNCs up to 100 km inland were a factor of 3 higher than the offshore values. It is tempting to conclude that this enhancement is due to local urban emissions from the coastal cities being entrained into the clouds. However, an enhancement factor of 2 persisted over 100 km inland, where the urban plumes would be largely diluted. Figure 3.7b shows that the entire CDNC distribution was shifted to higher values inland compared to offshore but inland was broadly similar regardless of distance

inland from the coast. There was also an extra tail in the distribution due to higher values of CDNC from city plumes, which diminished further from the coast, but this was only a small fraction of the whole distribution. City plumes were apparent in some cases, as they are in Figure 3.7, but large enhancements over the regional background were highly localised.

3.2.4   Linking spatial and diurnal variations of aerosols, clouds, and dynamics

We explored the variation in CDNC at different times of day; these are shown in Figure 3.8a. The spatial variation in CDNC showed some diurnal changes. Before 0900 CDNC did not change with respect to distance from the coast. In the late morning and early afternoon a pattern emerged showing lower CDNC offshore and enhancements up to a factor of 2 – 3 inland compared to just offshore. In the late morning this enhancement persisted up to 250km inland. By the early afternoon these enhancements in CDNC may have been more limited over 100 km inland, though data coverage here was only from one or two days. CDNC is determined by the supersaturation in an updraft, and the concentration of aerosols that activate at that supersaturation.

Figure 3.8b shows the spatio-temporal variations in CCN concentration. Here the meridional trends are more mixed. The CCN concentrations show a modest decrease with distance inland before 0900, becoming generally higher later in the day. Between 0900 – 1500 there was high variability, but there was little meridional variability, with the highest enhancements of only ~25%. Peak concentrations were highest just inland, on days where city plumes were intercepted at this altitude. After 1500 there was a clearer trend of enhancements, up to 80%, inland, but these data were only from 1 – 3 individual days (depending on location), so the significance of the result cannot be determined.

Figure 3.8c shows the average vertical velocities measured in the same clouds as Figure 3.8a. Up to 50 km offshore, the average vertical velocity was lower at all measured times of day, compared to inland values. This was particularly true in the early afternoon, where the average vertical velocity just offshore presented as downdrafts, meaning the clouds were dissipating. This pattern of lower vertical velocities offshore and higher inland is indicative of a sea breeze circulation. This is consistent with Figure 3.3, which showed sea breeze cloud cover peaking up to 50 km inland in the early afternoon. The highest average updrafts were 50 – 100 km inland in the afternoon. This also corresponds with the highest average CDNCs measured. In the morning, the average vertical velocities offshore were lower than those inland, but they were still positive. Additionally, the average updrafts inland in the morning were fairly modest at ~0.2 ms^{-1} and largely invariant with latitude, with a few exceptions. In the afternoon, the average inland updrafts were up to 1 ms^{-1}, indicative of the clouds becoming more convective as the surface temperatures peaked, and surface flux increased as the clouds started to break up.

To summarise, Figure 3.8 shows increases in CDNC of a factor of 2 – 3 inland compared to offshore. However, the corresponding increases in CCN concentrations were generally more modest; at some times of day they were up to 25% or up to 80% higher, but at others the CCN concentration decreased inland. The meridional trend in CDNC appears qualitatively to match better with the trend in average updraft velocity than to CCN concentrations. Taken together, this suggests a small enhancement in regional average CDNC due to local aerosol emissions, but the majority of the difference in CDNC was likely due to differences in dynamics.
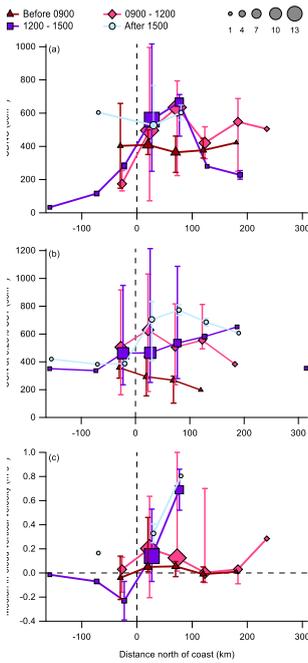
Figure 3.8 - Spatial variation in CDNC (a), CCNC (b), and in-cloud updraft velocity (c), relative to distance from the coast at different times of day. The data shown are from all data measured below 1km. The marker size denotes the number of different days the measurements are from. The markers and error bars use the same averaging scheme as in Figure 3.7. Data points without error bars show only data from one single day.

3.2.5   Parcel model simulations

In order to investigate the relative sensitivites of CDNC to aerosols and dynamics, we ran parcel model simulations using the Aerosol-Cloud and Precipitation Interactions Model (ACPIM, Connolly et al., 2009). ACPIM uses bin microphysics and aerosol thermodynamics to solve the drop growth equation numerically using Kohler theory, so does not rely on empirical parametrisations of cloud drop activation.

The model simluated an air parcel rising at a prescribed updraft velocity, starting at 95% humidity, 296 K, and 960 hPa, which are typical of conditions just below cloud base over Togo. As the parcel rose, the additional condensed water was distributed between the aerosol particles to form cloud drops. Aerosol size distributions from SMPS and AMS compositions were averaged over regions at various distances offshore or inland over SWA, and used to initialise the model for several runs with different updraft velocities. Inorganic aerosols were represented by ammonium sulphate, and organics by fulvic acid. By using fixed, representative thermodynamic starting conditions, varying the aerosol and updraft velocities allows us to determine the relative sensitivites of CDNC to both variables. This is not intended to be an exact simulation, but a sensitivity analysis using physically reasonable approximations.

Figure 3.8c showed statistics of daily average vertical velocity measured in clouds, these are not necessarily indicative of the updrafts at cloud base when particles activate, as the data will be biased low due to the inclusion of downdrafts. Figure 3.9 shows statistics of the daily 75th percentile of vertical velocity- this is likely to be more indicative of typical updrafts at cloud base when clouds form, and therefore more useful to consider in parcel model simulations.
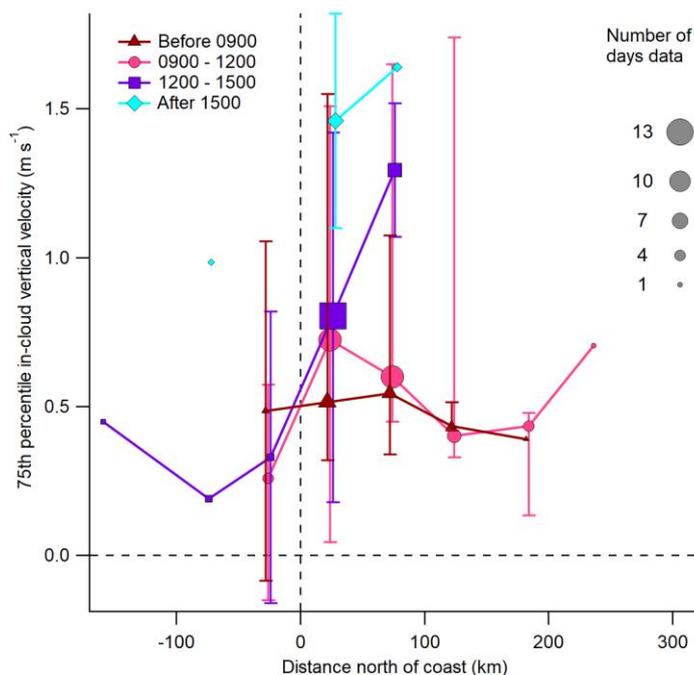

Figure 3.9 – As in Figure 3.8c, but showing statistics using the 75th percentile for each day, which are more likely to be indicative of updraft velocities at cloud base when particles activate

Aerosol size distributions and relative compositions from the respective regions were used in ACPIM at varying updraft velocities, spanning the range showed in Figure 3.9. The resultant simulated CDNCs are shown in Figure 3.10. For updrafts up to 0.4 ms^{-1} no difference was seen in the CDNC values, as the only particles that were activated were in the size range (larger than 200 nm) where the size distributions were the same. At higher updraft velocities, there was more difference between the different aerosol inputs, but this difference was much less than the difference in CDNC at different updraft velocities. For a typical inland updraft of 1.25ms^{-1}, the effect of using inland aerosol compared to offshore was to increase the simulated CDNC by around 15%. This enhancement is insignificant compared to the difference in CDNC using the inland versus offshore updraft velocities from Figure 3.9 (0.3 rather than 1.25 ms^{-1}), which caused a doubling of CDNC.
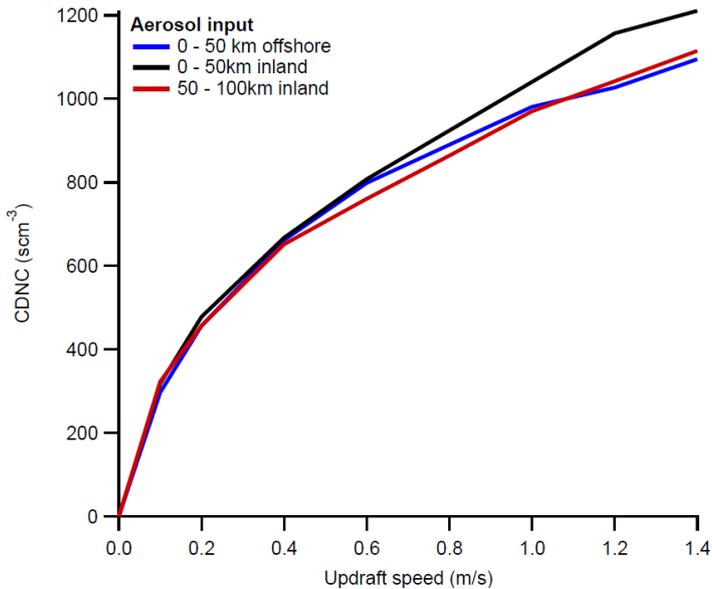
Figure 3.10 – Sensitivity of simulated cloud base CDNC to varying updraft velocity, derived using ACPIM simulations with average aerosol size distributions and composition from measurements

3.3 Summary and conclusions

These results have provided an overview of diurnal and spatial variation in low-level cloud cover in southern West Africa, and insight into factors affecting in situ cloud properties. Low-level cloud cover developed overnight but peaked around 1000 UTC, reaching over 90% on average in some regions. This average smooths out variations, and on many days and nights cloud cover reached 100%. Additional sea breeze clouds formed up to around 50km inland in the late morning, peaking around 1200 UTC. The low-level clouds broke up in the early afternoon and by 1600 the average coverage was below 20%, and cloud-free in many regions on many days. Orography was the main factor determining regional variation in low-level cloud cover, with peaks on the upwind side of slopes and troughs on the leeward sides.

CDNC showed both meridional and diurnal variations. Offshore CDNC were generally 100 – 300 cm^{-3}. Apart from in the early morning, CDNC increased inland compared to offshore. Peaks of over 1500 cm^{-3} were also seen associated with city plumes, but the increases inland were typically more like a factor of 2 – 3 inland compared to offshore. Our analysis showed that this enhancement in CDNC inland was likely due to differences in dynamics, with stronger updrafts inland compared to offshore. Additionally, a sea breeze circulation peaking in the early afternoon meant clouds measured offshore were dissipating, and this will likely have reduced the CDNCs.

What this means is local aerosol emissions may have a much more limited effect on CDNC in the region than previously expected, due to the high background aerosol concentrations. Consequently, the classical Twomey effect of these local emissions may not be as significant as first thought, compared to that for clean background clouds with CDNC <100 cm^{-3}. Regional and climate modelling studies should investigate the effects of dynamical processes on clouds over the region, as well as varying aerosol concentrations.

4   The role of Urban Plumes in Modification of Cloud Properties (DLR, UCA)

4.1   Comparison of cloud microphysical properties to aerosols in city plumes

The ATR42 (SAFIRE) flew 20 scientific flights accounting for nearly 70 h of observations over Ivory Coast, Ghana, Togo, Benin and Gulf of Guinea with altitudes ranging from 60m up to 7km (Figure 4.1). The region has been studied under generally enhanced polluted conditions, thereby observing increased CCN-prone (>0.1 µm) aerosol number concentrations, with a median and interquartile range of 780 and 540-1200 cm-3, respectively. The altitude profile of aerosols larger than 0.1 µm is depicted in Figure 4.2, showing generally a decrease in concentrations with altitude, although the trend is contrasted by eventual long-range transport (LRT) of biomass burning (advection from the south) or of desert dust (from the north). In terms of fine (< 1 µm) aerosol mass concentration (Figure 4.3) a comparable trend is observed, with free tropospheric background being occasionally strongly enhanced due to advection of LRT plumes. From analytical limitation in the estimate of PM1 here (which does not take in account desert dust), the free tropospheric enhancements observed in Figure 4.3 is attributed to biomass burning emissions transported from central Africa. The median and interquartile range of PM1 is 6.7 µg m^{-3} and 4.6-10.0 µg m^{-3}, respectively, being mostly composed of Organics (56%), followed by Sulfate (25%) and minor contribution of the other species.
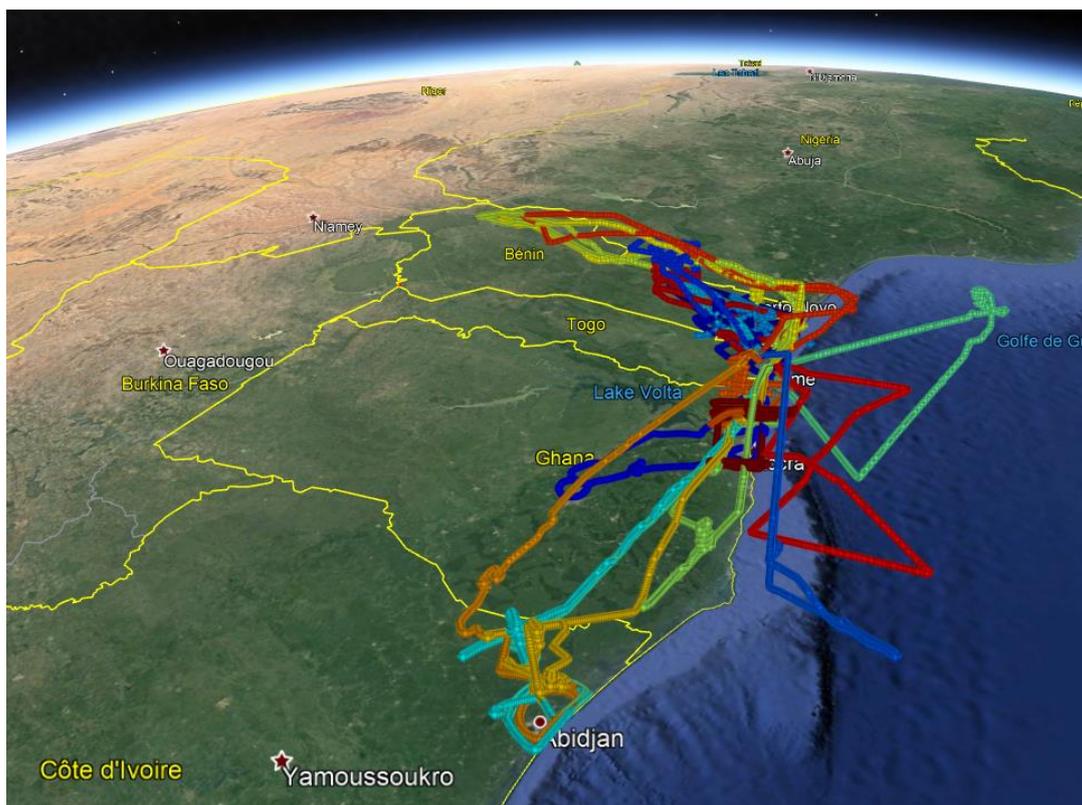

Figure 4.1 - ATR42 (SAFIRE) flight trajectories during DACCIWA color-coded according to flight number. This figure summarizes 20 scientific flights over Benin, Togo and Ghana accounting for almost 70 h of atmospheric observations on altitudes ranging from 60m up to 7km.
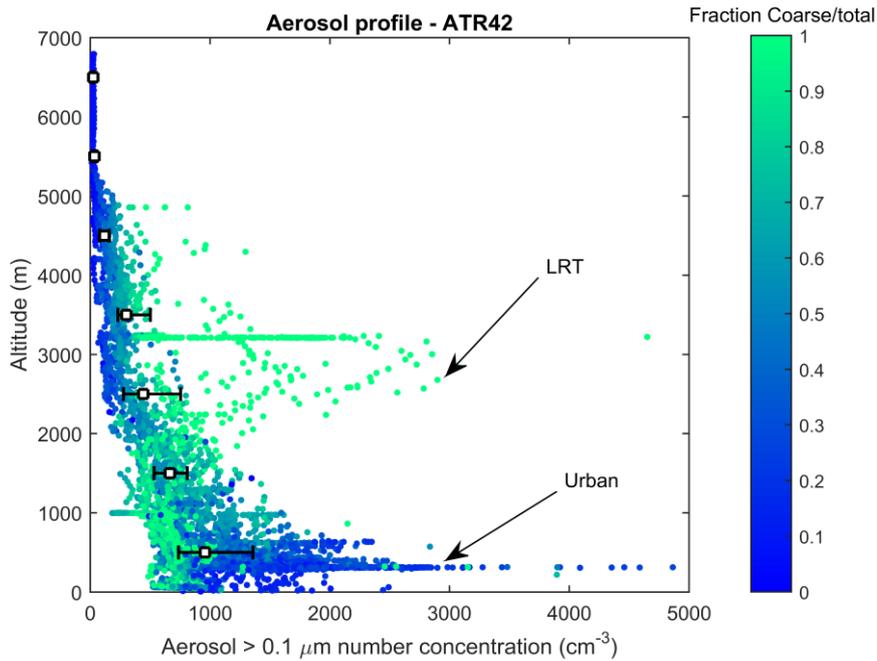
Figure 4.2 - Aerosol (>0.1 μm) number concentration profiles observed from ATR42 for the field campaign. The color shows the fraction of aerosol number larger than 0.1 μm relative to total, used to discriminate Long Range Transport (LRT, mostly in the coarse mode) from urban (mostly in the ultra-fine range) local pollution aerosol. The median values and interquartiles (25th and 75th percentiles) for 1km height bins are added (black boxes and lines with whiskers).
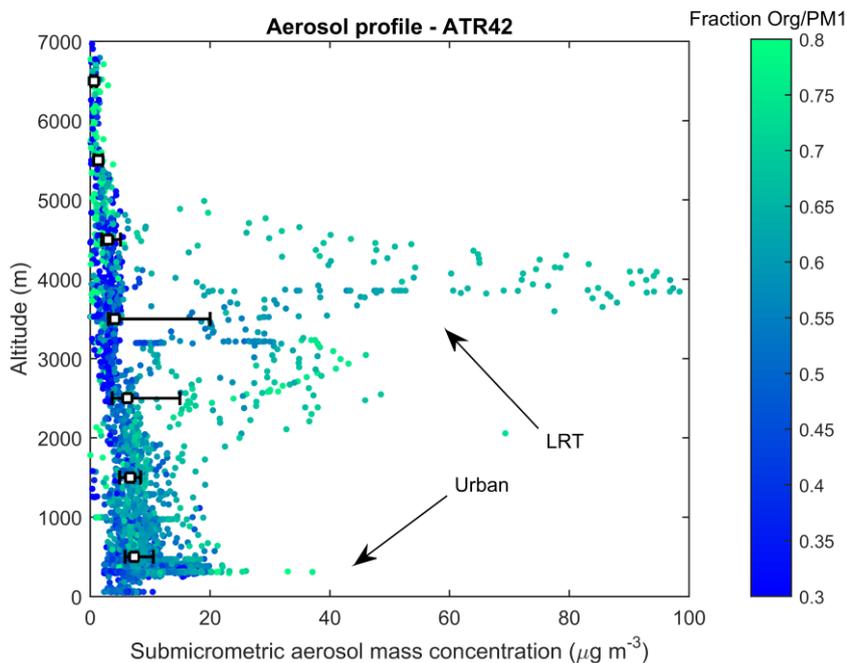
Figure 4.3 - Submicron aerosol mass concentration profiles observed from ATR42 for the field campaign. The color shows the fraction of Organics relative to the sum of Organics, SO4, NO3, NH4, Chl and BC. The arrows indicate enhancements associate to Long Range Transport (LRT) and urban plumes. Black boxes show median and range bars the interquartile range per 1km height bins.

Beyond the overall presence of typically high aerosol concentrations throughout the region, the number concentrations of aerosols larger than 0.1 μm were significantly enhanced in the outflow of

large urban centers, such as Abidjan, Accra, Lomé and Kumasi (Figure 4.4). By filtering between in-plume and continental background based on the methodology described in Brito et al (2018), the number concentration of accumulation mode aerosols were about twice as high within the urban plumes (~1400 cm^{-3}) as compared to continental background (700 cm^{-3}) (Figure 4.5). This high background is thought to be a mix of multiple regional sources, including smaller and very abundant local fires, pollution from smaller urban conglomerations, complex atmospheric circulation patterns (Flamant et al., submitted), and subsidence of LRT biomass burning plumes into the boundary layer largely taking place to the south of the DACCIWA region.
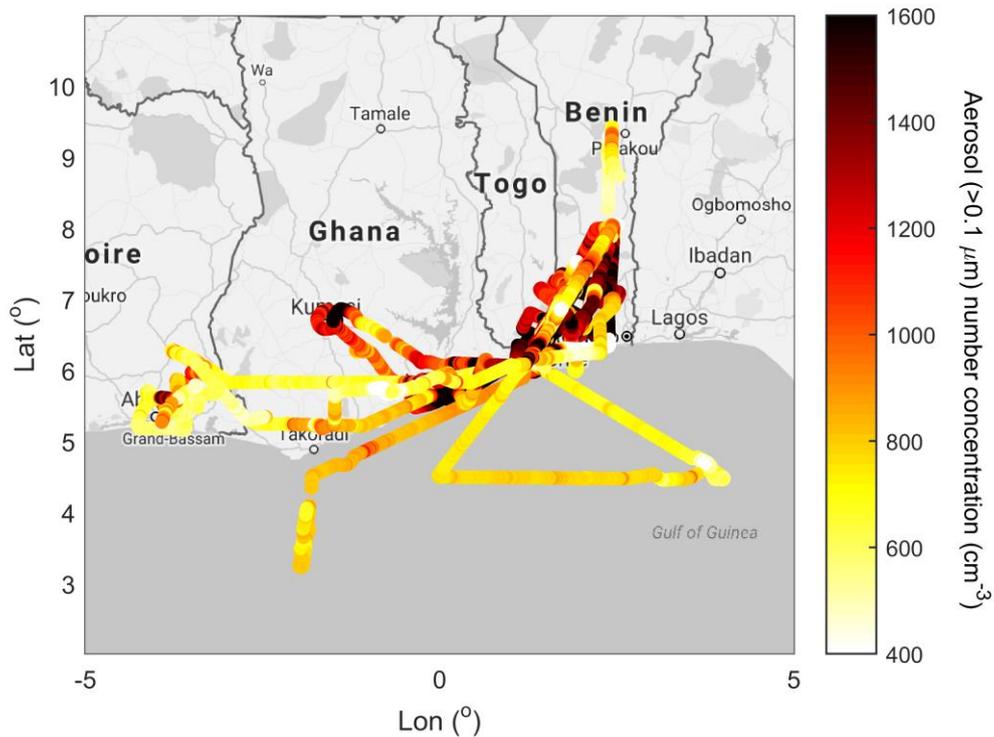
Figure 4.4 - Spatial distribution of aerosol (>0.1 µm) number concentration for flight trajectories below 2000 m.
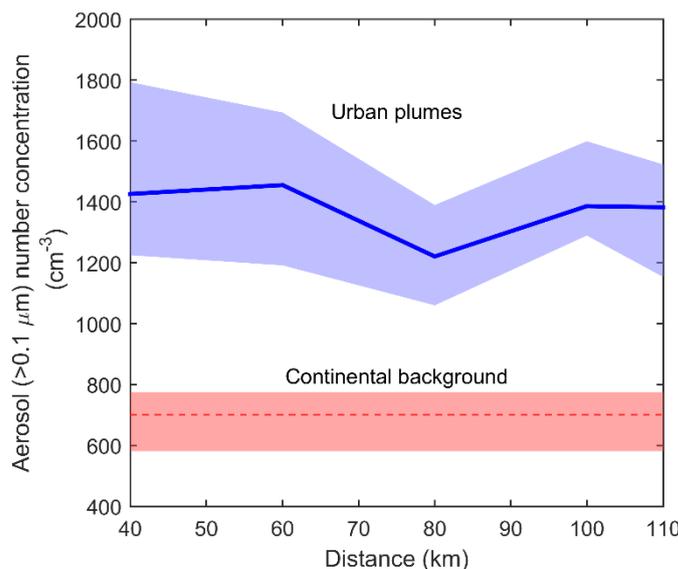
Figure 4.5 - Regional background (marked in red) and in-plume (blue) concentrations for aerosol (>0.1 µm) number concentration calculated according to the methodology described in Brito et al., 2018. The in-plume data has been segregated into 20km bins from the identified urban sources, namely Abidjan, Accra and Lomé. The lines (straight blue and dotted red) represent the median values and the shaded areas the interquartile ranges.

Figure 4.6 shows vertical profiles of in-situ measured cloud properties in the 2-50 µm size range as observed with the ATR42. These statistics are composed of about 10 000 data points, namely about 2.7h of combined cloud measurements. Most of the sampled clouds were low-levels clouds, with a median sampling altitude of 1100 m.
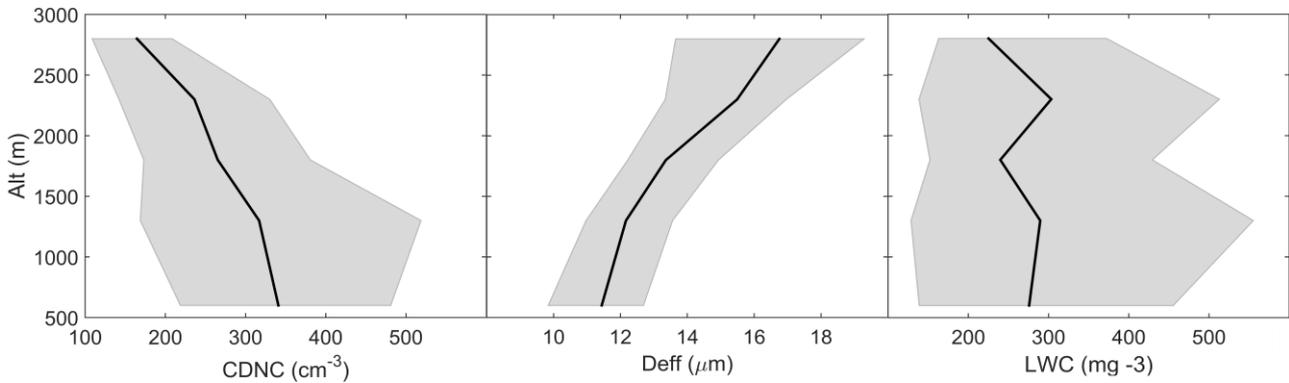

Figure 4.6: Cloud droplet number concentration (CDNC), effective diameter (Deff) and liquid water content (LWC) profiles in the 2-50 µm size range as observed by the ATR42 during DACCIWA. The lines represent the median values and the shaded area the interquartile ranges.
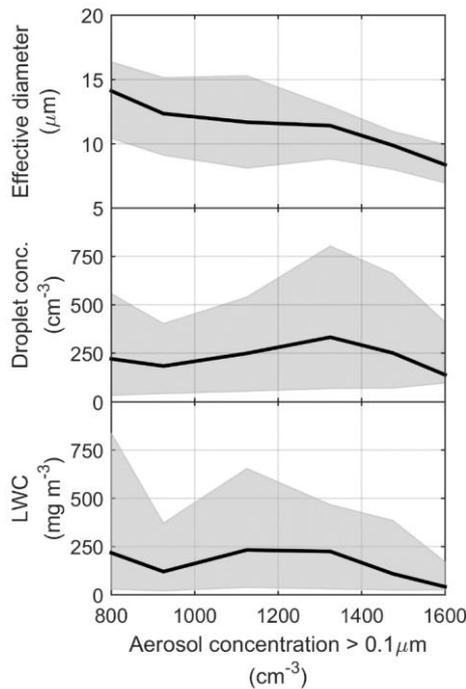

Figure 4.7: Cloud droplet number concentration (CDNC), effective diameter (Deff) and liquid water content (LWC) profiles in the 2-50 µm size range as observed by the ATR42 during DACCIWA binned according to the observed aerosol (> 0.1 µm) number concentration in the vicinity of the cloud. Data are limited to 1200 m altitude and were sampled above land. Median and interquartile range are shown as a line and shaded area respectively.

By combining the cloud properties shown in Figure 4.6 with aerosol (> 0.1 µm in size) number concentrations (see Figure 4.5) for altitudes below 1200 m we derive a simple analysis on the general sensitivity of cloud properties to aerosol numbers (Figure 4.7). Whereas cloud droplet number concentration and LWC do not reveal a clear trend as a function of aerosol number concentration (not within observed increased pollution levels and/or not due to limited data statistics), a clear decreasing trend of the effective droplet diameter with increasing aerosol concentrations is evidenced. On average, the effective droplet diameter is decreasing from 14.8 µm at 800 particles cm^{-3} to 8.0 µm at 1600 particles cm^{-3}.

4.2   Investigation of cloud microphysics in specific city plumes using gas-phase tracers

4.2.1   Introduction

Tropical West Africa (TWA) is a region with strong increases in anthropogenic emissions due to large growth rates in population density. At the same time this region is poorly covered by operational atmospheric monitoring. Therefore weather forecast and climate models are known to have strong deficits in TWA (IPCC2013). To explore this region, microphysical properties of shallow clouds in Tropical West Africa (TWA) were measured with the Cloud Aerosol Spectrometer CAS (Voigt et al., 2017) onboard the DLR Falcon with the goal to investigate effects of aerosol and pollution on clouds. The CAS was extensively calibrated and characterized in the laboratory and the size dependent sampling area of the instrumental optics was determined.

Figure 4.8 - Cloud measurements with the DLR Falcon during DACCIWA 2016 and emissions from domestic fires and road traffic in TWA (from Knippertz et al., 2015)

Both, CO and cloud condensation nuclei particle concentrations were used to investigate and distinguish pollution levels of air masses within the boundary layer. Figure 4.9 shows the concentration of aerosol >100 nm measured on the SAFIRE ATR at altitudes below 1300m along the flight tracks. Enhanced aerosol concentrations were detected over urban and densely populated rural areas. This goes in line with CO measurements on the DLR Falcon, with enhancements larger than 170 ppbv in densely populated areas in TWA.
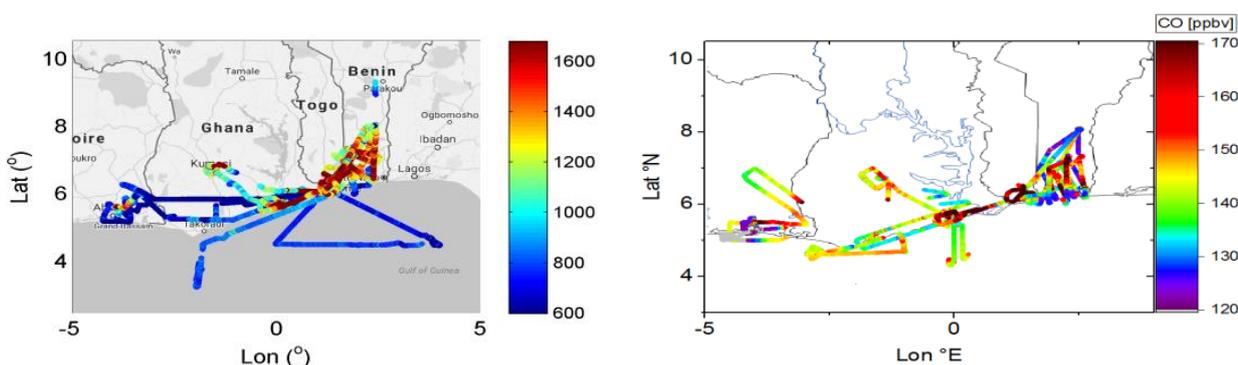
Figure 4.9 - (left) Aerosol concentration (n/cm^{-3}) > 100nm measured by the SAFIRE and (right) CO mixing ratio detected by the Falcon for all DACCIWA flights in June/July 2016.

CO was then used as tracer to characterize pollution levels of low level clouds and their microphysical properties. An average CO mixing ratio between 140 ppbv and 150 ppbv was measured throughout the campaign. For discrimination an upper threshold of 135 ppbv for the moderately polluted case and a lower threshold of 155 ppbv for the substantially polluted case was introduced.

4.2.2   Results – Shallow Clouds

 A novel dataset of in-situ cloud measurements were collected in TWA by three research aircraft. Microphysical properties of shallow clouds were determined. The effective droplet diameter of shallow clouds below 2 km altitude increases with altitude. As a result for the TWA region, polluted clouds contain higher droplet number concentration than less or moderately polluted clouds. Smaller droplet sizes were measured in polluted clouds, as the ambient water is distributed on more cloud particles. Fig. 4.10 shows the vertical statistics over individual 500 m altitude bins between 500 m and 2000 m for effective droplet diameter and number concentration for both, the moderately polluted and polluted case, as described above.
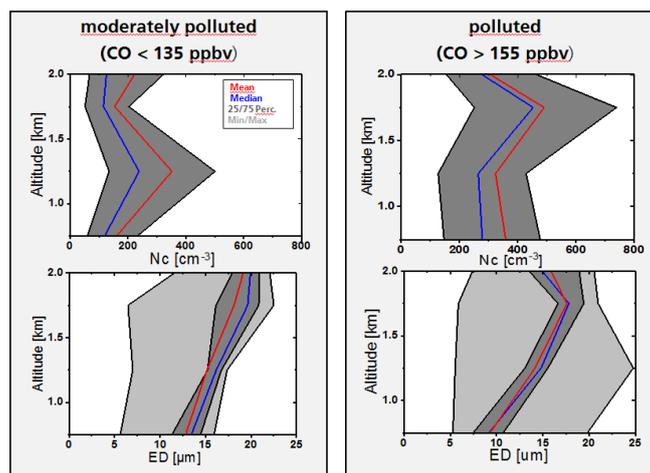

Figure 4.10 - Cloud droplet number concentration Nc in the size range of 0.6 to 50µm and effective diameter ED in moderately and heavily polluted clouds in TWA measured with the CAS onboard the Falcon in July 2016.

Further, the origin and the distribution of the pollution levels of CO in TWA were investigated in more detail. In particular, the question on the origin of the high pollution levels in the TWA hinterland outside of big cities was posed.

To address this question, CO measurements < 2 km altitude on the Falcon were averaged on horizontal 0.05°*0.05° grids and linearly interpolated and were compared to the latest high resolution CO data of the EDGAR emission inventory version 4.2 (2008).

4.2.3   Results – Anthropogenic emissions

Although comparing data from the EDGAR emission inventory version 4.2, which gives CO source strength, with in situ measurements, EDGAR strongly under-predicts anthropogenic CO emissions in TWA, in particular in rural areas. Data from the Luminocity3D project show a high population density in Togo in the rural areas outside of the large cities Lomé and Cotonou.

Luminocity3D uses the *Global-Human-Settlement-Layer*, provided by the EU, which uses a synopsis of census and satellite data to derive a population density. The high population density in *rural* areas may contribute to anthropogenic emissions in TWA. Cleaner conditions were found above the sea with CO concentrations upstream of the DACCIWA region between 130 and 150 ppb being observed (figure 4.11). These values are, however, considerably enhanced compared to typical clean tropical background values of around 80 ppb and the upstream accumulation mode number concentrations of 800 cm^{-3} are also more similar to moderately polluted conditions. This indicates that whilst there is likely to be a contribution to regional pollution arising from rural communities it is in addition to an appreciable contribution from central African burning.
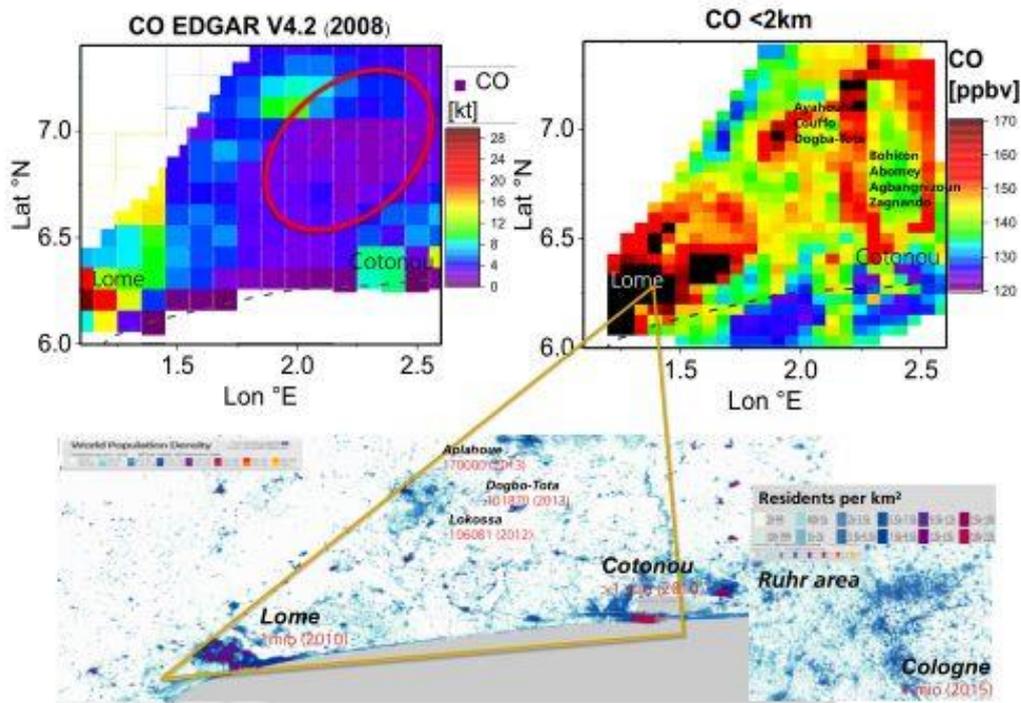
Figure 4.11 - (upper panel) CO emissions from EDGAR V4.2 inventory and CO measurements on the falcon interpolated to a vertical grid, (lower panel) Population density in Togo and the Ruhr area from the Luminocity3D project. A high population density exists outside of large cities in Togo.

4.2.4   Implications

Population growth in TWA has to be taken into account in emission inventories. Strong anthropogenic emissions modify shallow cloud properties in TWA. Cloud observations will be compared to weather prediction and climate models in TWA in order to assess and improve model results.

5 Microphysical processes limiting aerosol influences on cloud and precipitation (UNIVMAN)

This section refers to work using the MONC model described in Section 2.1.

5.1 How well are DACCIWA clouds simulated using MONC?

5.1.1 Development of clouds and boundary layer
The MONC simulations produce a cloud layer with an initial mean cloud base around 350 m and a cloud top of 600 m is shown in Figure 5.1 (CASIM_NO_PROC). After sunrise at 0537 UTC, surface fluxes increase sharply from around 0700 UTC, resulting in a deeper boundary layer (BL) and lifting of the cloud layer from around 0800 UTC.
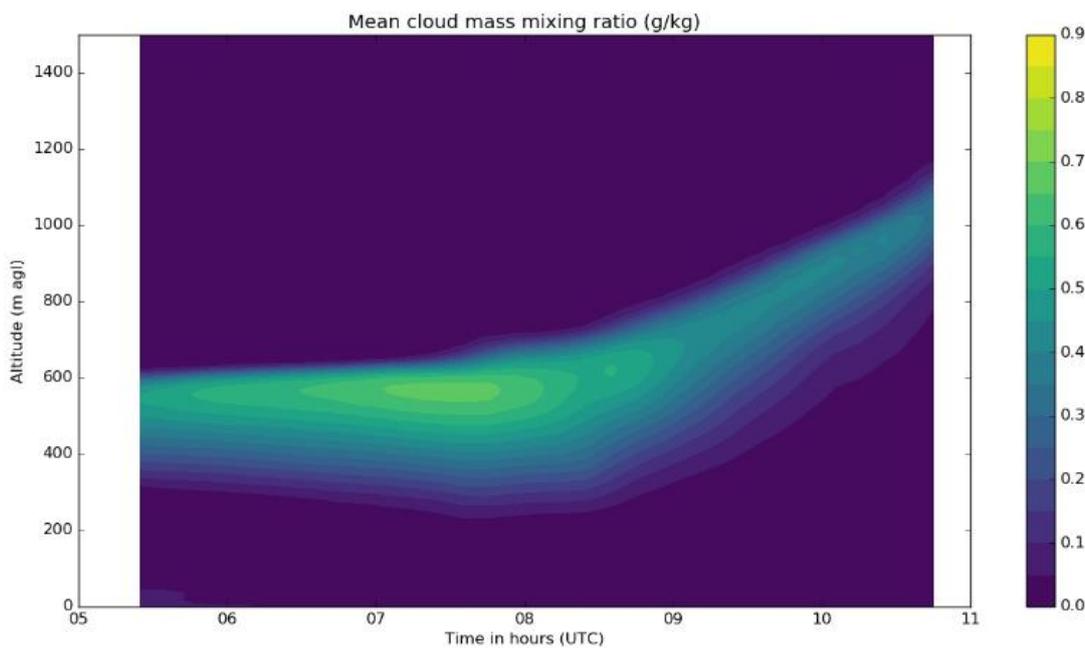
Figure 5.1 - Time-height plot of the mean cloud mass mixing ratio (g kg^{-1}) within the model domain. Values calculated as temporal means every 10 minutes.

Comparison of the cloud base height with ceilometer results from Savé (WP1) show that the general trend is well captured by the model. Cloud top long wave radiative cooling was found to be crucial for the development and maintenance of the cloud, through the generation of an overturning circulation within the cloud layer – without any long wave cooling, the model was unable to sustain the cloud layer, resulting in complete dissipation by the end of the spin-up period.
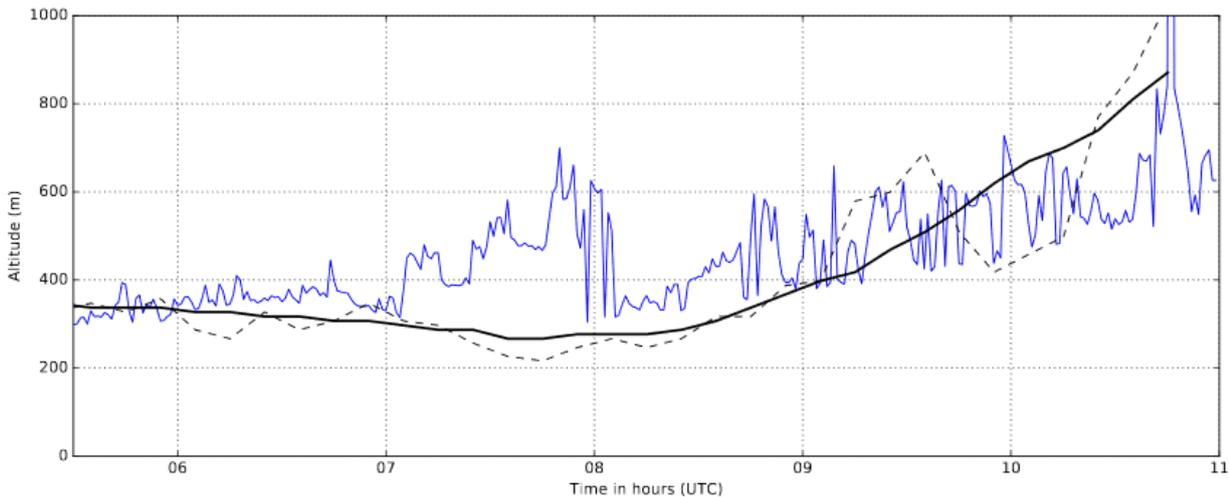
Figure 5.2 - Time series of cloud base height at Savé on 5 July 2016 (blue) derived from ceilometer measurements and 10 minute averages of cloud base height diagnosed from CASIM_NO_PROC using a threshold cloud liquid water mass mixing ratio of 0.1 g kg^{-1}. Solid black line – domain mean value; dashed black line – the value at the centre of the model domain.

Shortly after spin-up, the CASIM_NO_PROC experiment shows a well-mixed cloud-topped BL capped by a temperature inversion at 600m agl. A stable layer exists from the surface up to 150m agl (consistent with long wave cooling of the surface during the night), with a thin fog layer which dissipates by 0630 UTC. By 1100 UTC, the increased surface fluxes produce a deeper, convective BL, with an unstable layer at the surface. A well-mixed layer exists between 50 – 400m agl (sub-cloud region), with signs of a second shallower well-mixed layer directly below the top of the BL, where liquid water potential temperature gradually increases with height. The model captures the deepening of the BL as seen in the observations, with a simulated height of 1.1 km by 1100 UTC, compared with 1 km as detected by the radiosonde.

5.1.2   Comparison of LWP using two cloud schemes

Liquid Water Path (LWP) from the CASIM_NO_PROC simulation was compared with observations from the vertically pointing ground-based microwave radiometer at Savé. The model was found to simulate the evolution of LWP in a manner that is broadly consistent with the measurements, with observations for the most part lying within ±2 standard deviations of the simulated LWP values. Peak local values of LWP also occurred at approximately the correct time in the model as well (after 0800 UTC when surface fluxes increase). No precipitation was produced by the model, consistent with measurements at Savé.

To assess the impact of reducing the cloud scheme complexity, the results from the CASIM_NO_PROC experiment are compared to the SIMPLE_CLOUD experiment. Figure 5.3 shows the comparison of spatial distribution of LWP for each case as the simulations progress. This confirms that the cloud is more spatially homogeneous in the SIMPLE_CLOUD simulation, resembling largely featureless stratus in comparison to the stratocumulus seen in CASIM_NO_PROC.
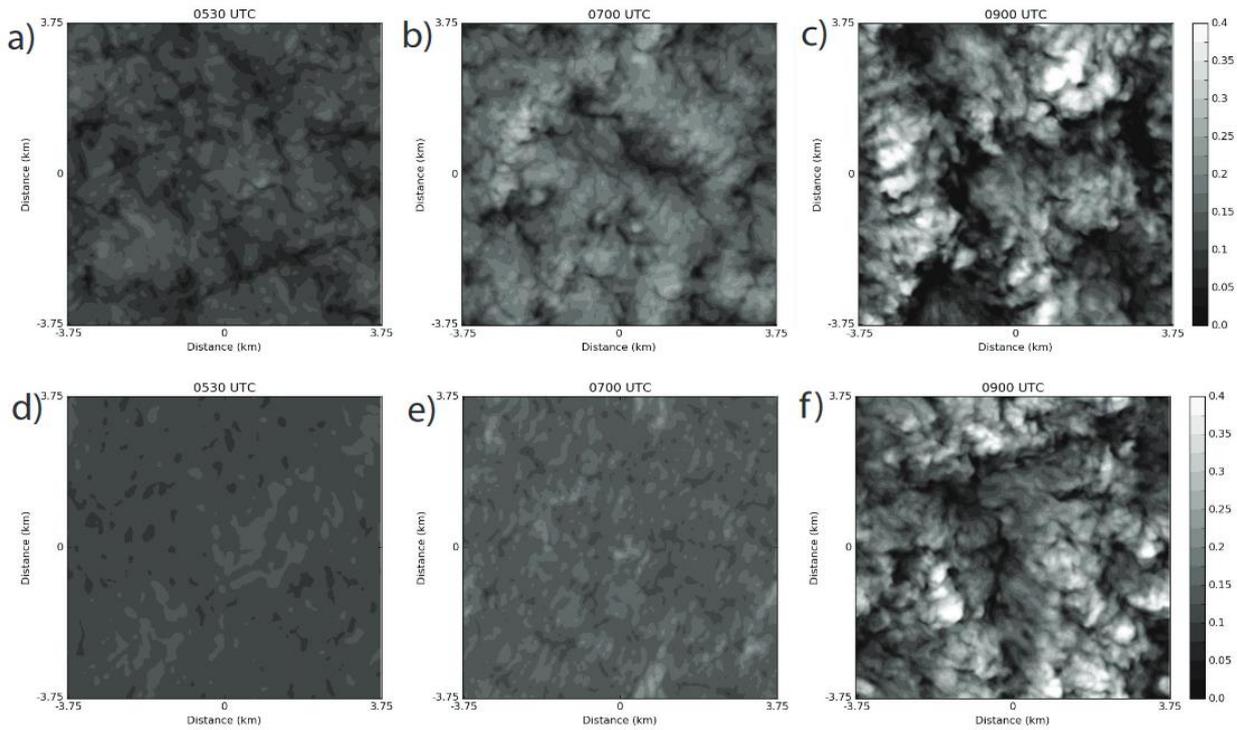
Figure 5.3 - Spatial distribution of LWP (kg m⁻²) within the model domain at 0530, 0700 and 0900 UTC for CASIM_NO_PROC (top row) and SIMPLE_CLOUD (bottom row)

A comparison of the time series of mean LWP in the domain, Figure 5.4, shows similar curve shape with a peak around mid-morning, but with notable difference, despite both cases not precipitating. By 0700 UTC, CASIM_NO_PROC has higher LWP, the peak LWP occurs in the same place, but persists for longer in the SIMPLE_CLOUD case. Cloud base is also higher for the SIMPLE_CLOUD case.
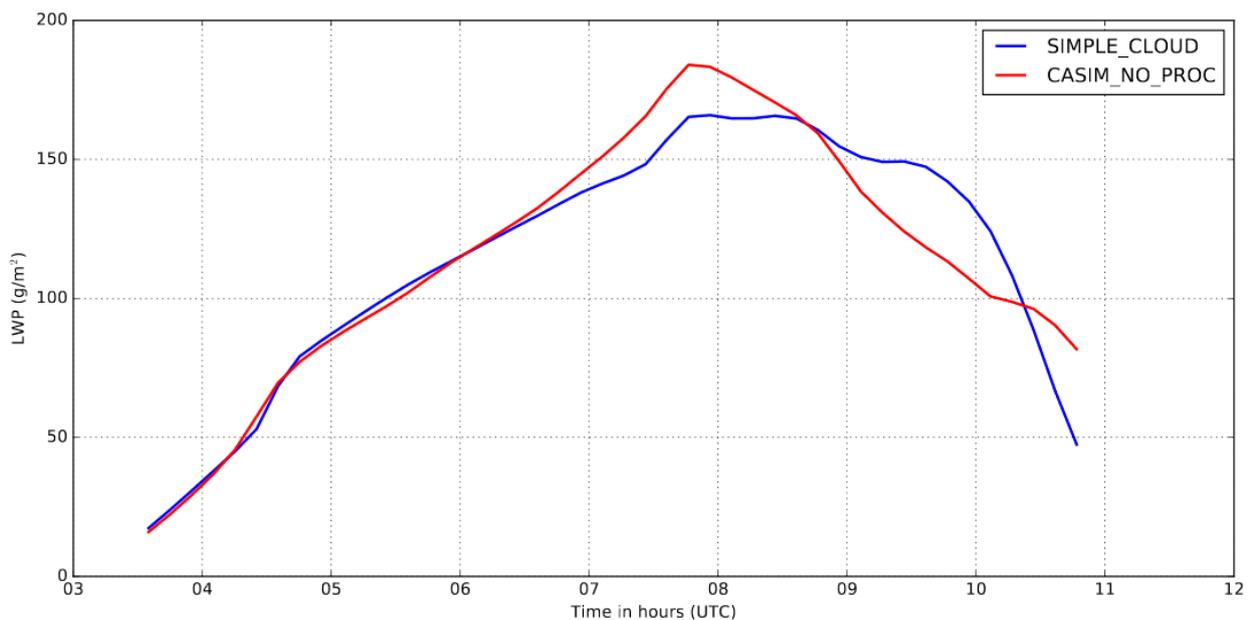
Figure 5.4 - Time series of LWP (g m⁻²) from CASIM_NO_PROC (red) and SIMPLE_CLOUD (blue). LWP is calculated from 200 m to top of the model domain.

Droplet sedimentation effects (as a result of gravitational settling) can explain the difference in LWP evolution; this is not represented in SIMPLE_CLOUD. This was confirmed by a test simulation of

CASIM_NO_PROC with droplet sedimentation switched off (auto conversion on) effectively yielding the same results as SIMPLE_CLOUD.

Sedimentation is found to ultimately increase LWP by the removal of liquid water from the entrainment zone near cloud top, which in turn reduces evaporative cooling and long wave radiative cooling: two processes that control the sinking of relatively dry air from the free troposphere into the cloud layer. The absence of droplet sedimentation in SIMPLE_CLOUD results in slightly higher LWC at cloud top during spin-up relative to CASIM_NO_PROC. In the 1.5 hrs after spin-up (0530 – 0700 UTC), the larger LWC within the entrainment zone of the SIMPLE_CLOUD case promotes stronger evaporative cooling relative the CASIM_NO_PROC, which increases the downward heat flux at cloud top, reduces moisture fluxes and reduces the circulation strength in the BL. This results in a slower rate of LWP growth with time relative to CASIM_NO_PROC as shown in Figure 5.4. The removal of liquid water mass from cloud top due to droplet sedimentation in CASIM_NO_PROC effectively acts to shield the cloud layer from the effects of entrainment, allowing the LWP to grow faster with time. This effect of sedimentation on LWP breaks down after 0800 UTC once heat fluxes dominate and the surface layer becomes unstable.

For this case study it was noted that at other ground sites the LLC onset times were much earlier (0000 UTC at Kumasi and 2100 UTC at Ife-Ife). An earlier LLC onset would allow more time for the sedimentation effects to impact LWP before sunrise (assuming sedimentation-entrainment feedback is valid). To investigate the absence of surface driven mixing, both experiments were re-run with surface fluxes set to zero, short wave radiation turned off and with the forcing of the low level jet (LLJ) still included. This showed clearly that when nocturnal conditions are maintained. CASIM_NO_PROC maintains a higher LWP by around 33% relative to SIMPLE_CLOUD by 1100 UTC.

5.1.3   Effect of Reduced CDNC on LWP
A further experiment with a prescribed initial cloud droplet number concentration of 250 cm^{-3} (compared to the CASIM_NO_PROC experiment where predicted number concentrations are 400-700 std cm^{-3}, agreeing with the median in-situ measurement of 500 std cm^{-3}), was performed to check the expected increase in the effects of sedimentation on LWP and cloud base height (as droplet sedimentation rates are inversely proportional to number concentration). This simulation produced excessive variability in the LWP field, and cloud bases too low when compared to in-situ measurements. The depth of the BL was also too shallow by the end of the simulation. Around 0830 UTC, cloud base touches the surface and liquid water is removed from the domain mainly by gravitational settling of cloud droplets; this results in a lower LWP compared to CASIM_NO_PROC.

5.1.4   Effect of increase vertical wind on cloud
Investigation of the aircraft in-situ cloud microphysics data (UNIMAN) (Section 3) suggests that the breakup of stratiform cloud in the SWA region may be related to changes in vertical wind observed during the day as the surface heats up. A further experiment was performed with doubled prescribed surface sensible heat flux values (CASIM_dblshf). This increases maximum vertical velocity values by up to 1.2 ms^{-1} after 0800 UTC for CASIM_dblshf compared to CASIM_NO_PROC and there is a broadening of the vertical velocity probability density function. By the end of the simulation, cloud top height is increased and the cloud is patchier for the CASIM_dblshf case, but higher peak LWP values were noted for the CASIM_NO_PROC simulation, as shown in Figure 5.5.
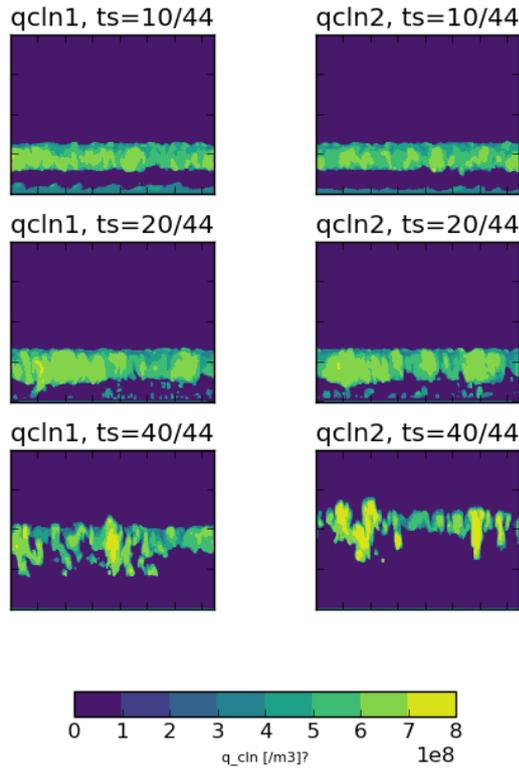
Figure 5.5 - Vertical cross-section of cloud liquid number for CASIM_NO_PROC (left column) and CASIM_dblshf (right column) at timesteps (ts) indicated.

5.1.5   Effect of aerosol on radiation

The CASIM_NO_PROC simulation was re-run to include radiation diagnostics, along with a simulation using half the aerosol number and mass (CASIM_halfaer) to investigate the effect of aerosol on the top of atmosphere long and shortwave upwelling radiation.
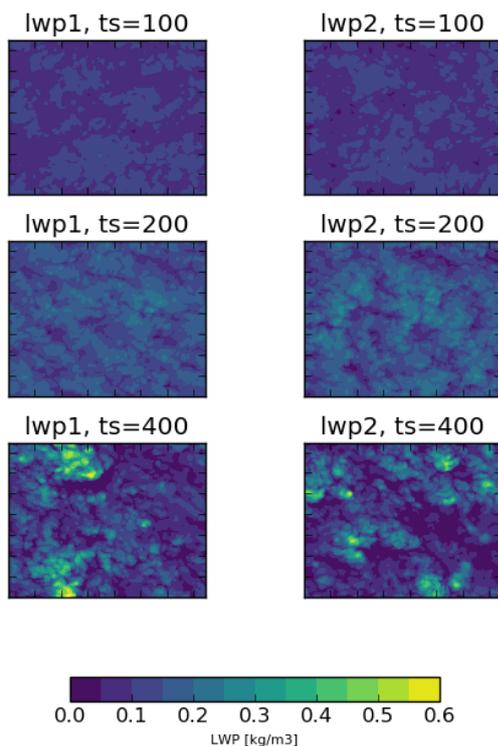
Figure 5.6 - Maps of LWP at indicated timesteps (ts, #/440) for CASIM_NO_PROC (left column) and CASIM_halfaer (right column).

Figure 5.6 reveals that there are definite changes noted in the spatial variation in LWP in the domain. Cloud top and cloud base are similar for the two cases, with lower more homogenous cloud liquid number values throughout the cloud deck in CASIM_halfaer compared to CASIM_NO_PROC. The impact this has on the radiation at the top of atmosphere towards the end of the simulations can be seen in Figure 5.7, where although there are changes in the spatial distribution of the peaks in both short and long wave outgoing radiation, the range of values across the domain are similar. This suggests that changes in aerosol do not have an overall large impact on the cloud radiative properties in this region, though it must be remembered that the aerosol fields are passive in this experiment.
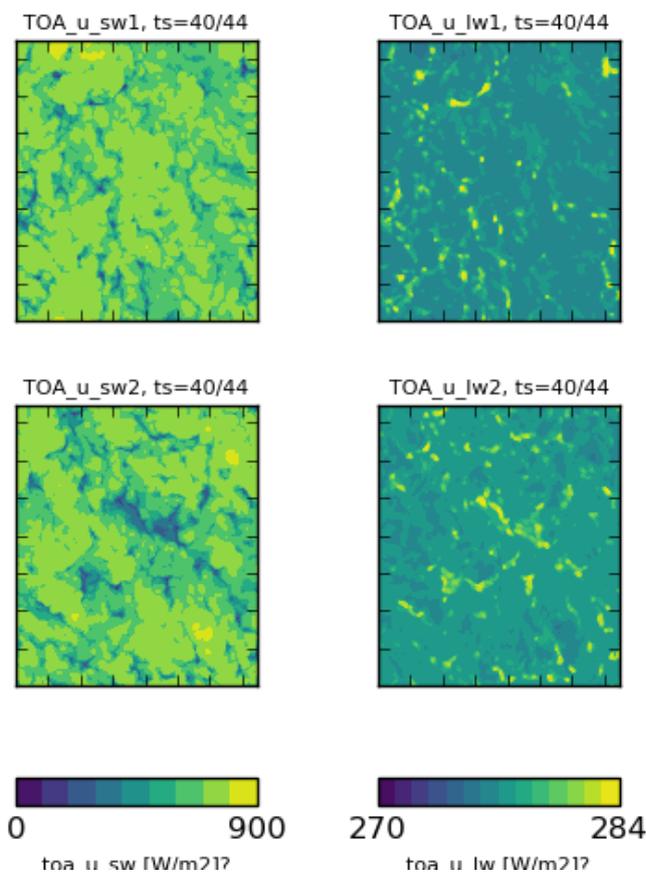
Figure 5.7 - Top of atmosphere upwelling short (left) and long (right) wave radiation [W/m^{-2}] for CASIM_NO_PROC (top) and CASIM_halfaer (bottom)

5.2 Summary and Conclusions:

Large eddy simulations of LLCs over SWA have been performed using MONC constrained and validated using in-situ measurements collected during DACCIWA. Cloud top long wave radiative cooling during the night was required for the formation and maintenance of the clouds.

The evolution of LLCs over SWA is found to be sensitive to the effects of droplet sedimentation; liquid water is removed from the entrainment zone near cloud top and reduces the magnitude of evaporative cooling during entrainment mixing. This could potentially play an important role in regulating the surface radiation budget for the region. Coupling of MONC to an interactive land-

surface scheme is needed to be able to fully assess the impacts of droplet sedimentation on the diurnal cycle of LLCs in this region.

The simulation closest to the observations was the one that had the closest match to the observed droplet number concentrations (for prescribed subsidence and surface fluxes). There are relatively high background pollution levels in SWA that are dominated by the long-range transport of biomass burning aerosols from central Africa. This is likely to limit the susceptibility of the LLCs to perturbations from local pollution sources, however, the effects of droplet size on cloud top entrainment rates should not be ignored when considering the diurnal cycle of clouds in the region.

Results suggest possibility of complex feedback chain involving aerosols, sedimentation, entrainment, liquid water path and surface energy fluxes. Work is still ongoing to investigate the effects of varying dynamics on the simulations.

6   Quantifying Cloud Aerosol Interactions in Southern West Africa (UNIVLEEDS)

This section refers to work using the UM model described in Section 2.2.

6.1   Aims

This work aims to determine the sensitivity of the key meteorological and climatological parameters upon aerosol concentration within the DACCIWA region. The lifetime aerosol effect predicts that as aerosol concentration, and hence cloud condensation nuclei concentration, increases, then if the amount of available liquid water remains the same the liquid droplets in clouds will be more numerous and smaller. Smaller droplets are less able to aggregate via the autoconversion process to form drizzle sized or larger droplets, hence precipitation is suppressed. The suppressed precipitation causes a reduction in the rate of removal of water from the cloud and hence the cloud lifetime is increased. The increase in cloud lifetime has implications for radiative transfer through the atmosphere and hence provides a climatological radiative forcing.

Of course the radiative and precipitation impacts predicted by the lifetime effect may have impacts upon the dynamics and thermodynamics of the atmosphere, which may feed back onto the cloud properties.

6.2   Results

Here we present the impact of aerosol concentrations upon precipitation and outgoing radiation from our model with those predicted by the lifetime effect. Figure 6.1 shows the droplet concentration, the amount of rain near the surface, the low cloud coverage, and the top of atmosphere outgoing longwave and shortwave radiative fluxes as a function of time during the simulations. The measurements are averaged over the entire domain.

We see that as predicted by the lifetime effect, cloud droplet number concentration is increased by the increase in aerosol number concentration because there are more aerosol particles to act as CCN. Also as predicted by the lifetime effect the rain amount is decreased by an increase in aerosol number concentration. This is due to the reduction in autoconversion of cloud droplets to drizzle size droplets due to the reduction in droplet size. Representing this change can only be performed by a 2-moment cloud microphysics model such as CASIM.

However, contrary to the predictions, the reduction of rain does not cause an increase in cloud coverage. In fact, the low cloud fraction is decreased in the model with higher aerosol number concentration. This decrease in cloud fraction results in a lower albedo, and hence less outgoing top of atmosphere shortwave radiation during the day and also into a generally lower top of atmosphere longwave radiative flux (although the longwave flux is not a monotonic relationship to aerosol at all times of day).

Figure 6.2 shows maps of precipitation and low cloud cover for the first two days of the simulations. We see that the simulations show the same broad scale special patterns in these fields but with differences in coverage. Initially the whole domain is covered with light precipitation. This is due to the initial conditions inherited from the global simulations which include a convective parameterisation. Such parameterisations are known to often incorrectly produce extensive regions of drizzle and not enough heavy rain. As the simulations spin up they rapidly diverge. At 0300 on the first day of simulation the lowest aerosol concentration simulation contains much more widespread drizzle than the highest aerosol concentration simulation. This situation persists to a greater or lesser extent throughout the simulations and an obvious diurnal cycle can be seen with

drizzle becoming more widespread from the evening through to sunrise before reducing again. There is a clear negative correlation between the aerosol concentration and the areal coverage of drizzle overnight.
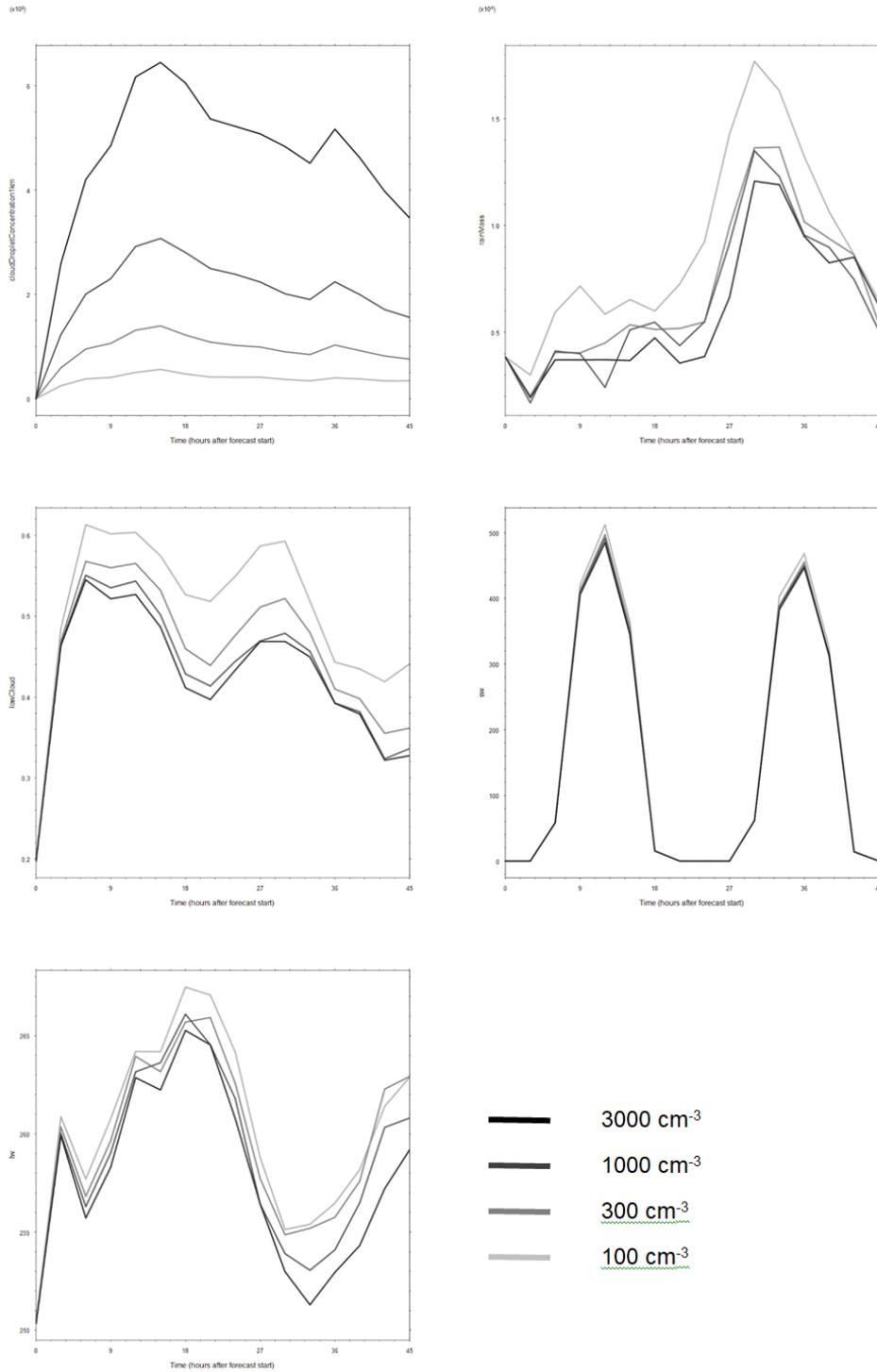
Figure 6.1 - Time series showing cloud droplet concentration at 1 km altitude, rain mass in the lowest atmosphere level, low cloud amount, top of atmosphere outgoing short wave radiative flux and top of atmosphere outgoing longwave radiative flux for two days of simulation. The simulation began at midnight on 4th June 2016.
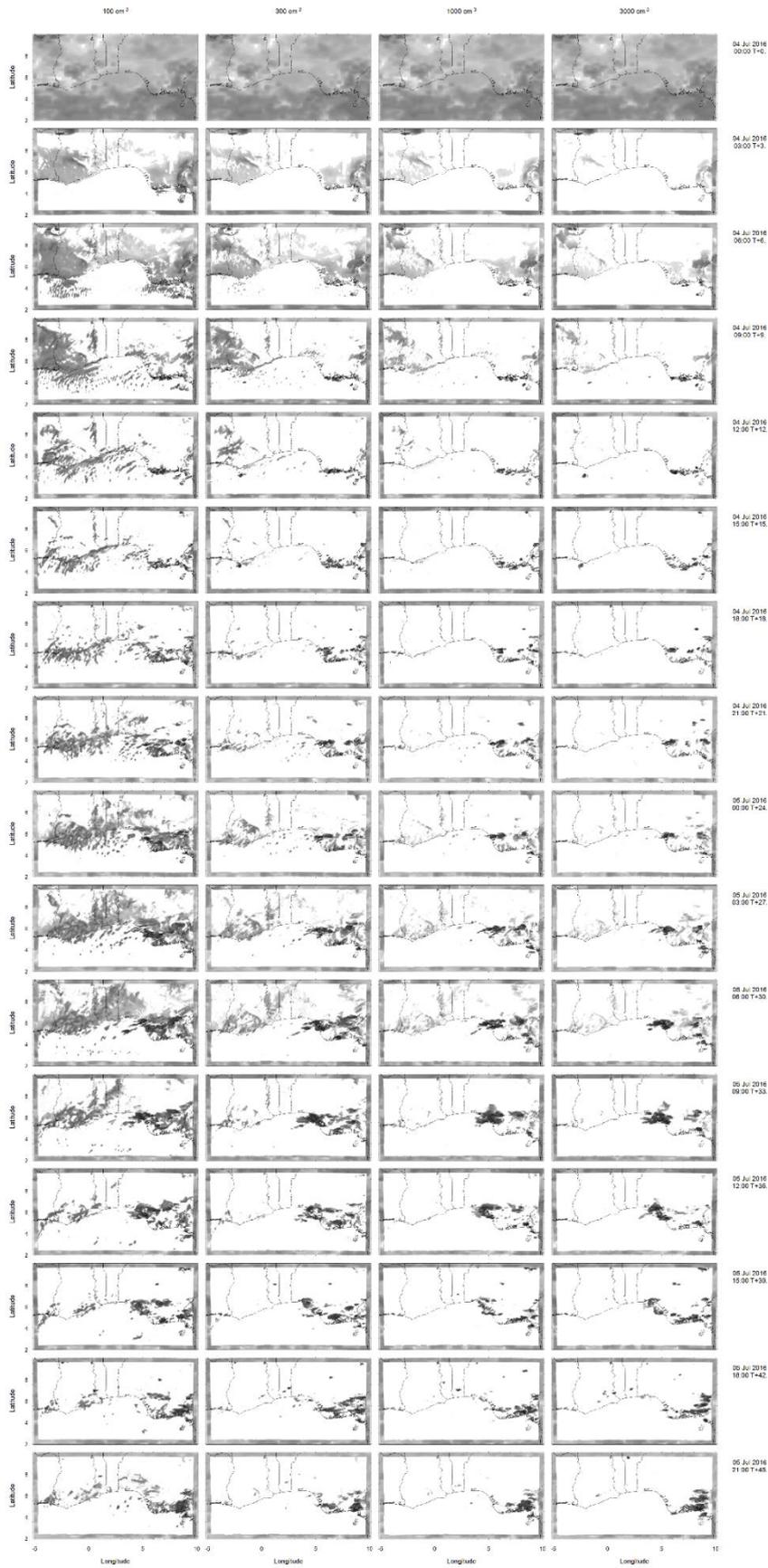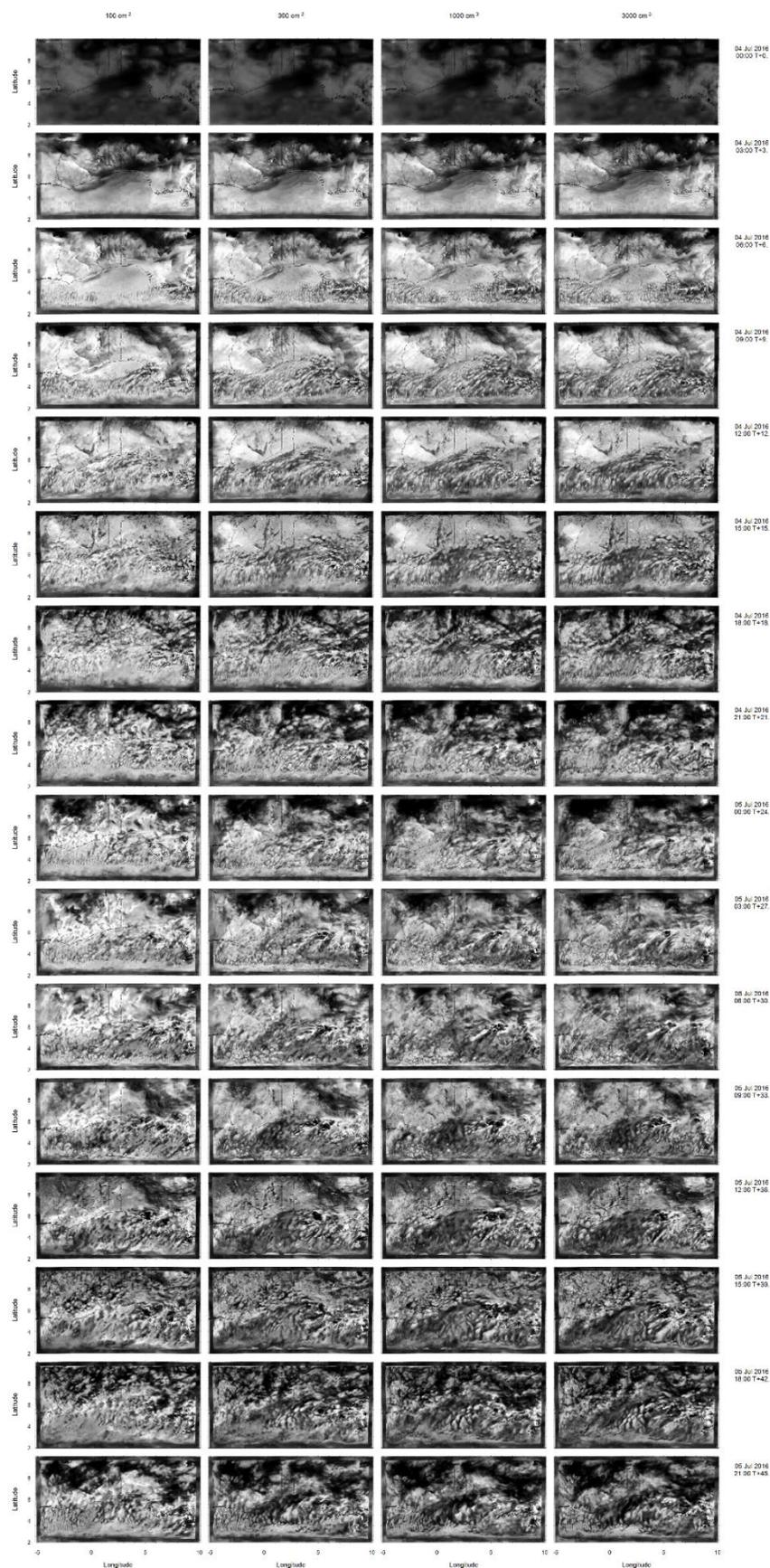
Figure 6.2 - Maps showing the mass of rain in the lowest model level (as a proxy for rain rate) and the low level cloud cover from the four simulations (one simulation per column) as a function of time (three hourly intervals between rows).

The low cloud coverage takes slightly longer to diverge than the precipitation and the differences aren't obvious until 0600 on the 1st day of the simulation. At this time the differences are subtle over land but obvious over the ocean where the cloud is much more broken in the higher aerosol concentration simulations. The differences become more obvious over land as the simulations progress. By 1800 on day 1 of the simulation the change in cloud cover is widespread over the entire domain and the difference is particularly pronounced around the Ghana, Togo, Benin and Nigeria Coastline. In general, the higher aerosol concentrations results in more broken cloud, both on resolved scales (seen as more pixel-to-pixel variation in Figure 6.2) and on unresolved scales (seen by fewer bright white 100% covered pixels in Figure 6.2). The amplitude of the diurnal cycle in low cloud amount is similar in all simulations. But the mean cloud amount is reduced when aerosol concentration is increased.

6.3 Discussion

The finding that cloud amount decreases with increasing aerosol number concentration is counter to the prediction made by the lifetime effect. However, the predictions of the lifetime effect are based on a number of key assumptions listed here

1) Increasing aerosol concentration increases available CCN and increases droplet number concentrations in cloud.
2) The available liquid water is the same and hence the cloud droplet diameter decreases for larger aerosol number concentrations.
3) Smaller droplets cause a reduction in precipitation for higher aerosol number concentrations.
4) The drizzle depletes cloud water, meaning that higher aerosol concentrations with less drizzle maintain cloud for longer.

Assumption 1 has been validated in our simulation, as can be seen in Figure 6.1, with cloud droplet number concentration at 1 km altitude increasing by approximately a factor of 3 between each simulation corresponding to the approximately factor of 3 increase in aerosol concentration.

All simulations have identical initial conditions, so have the same initial available liquid water. This can be seen in Figure 6.3. The processing rates for conversion of cloud droplet water content into precipitation water content were not available as output from the simulations. However, the expected change in precipitation is clearly observed as seen in Figures 6.1 and 6.2.
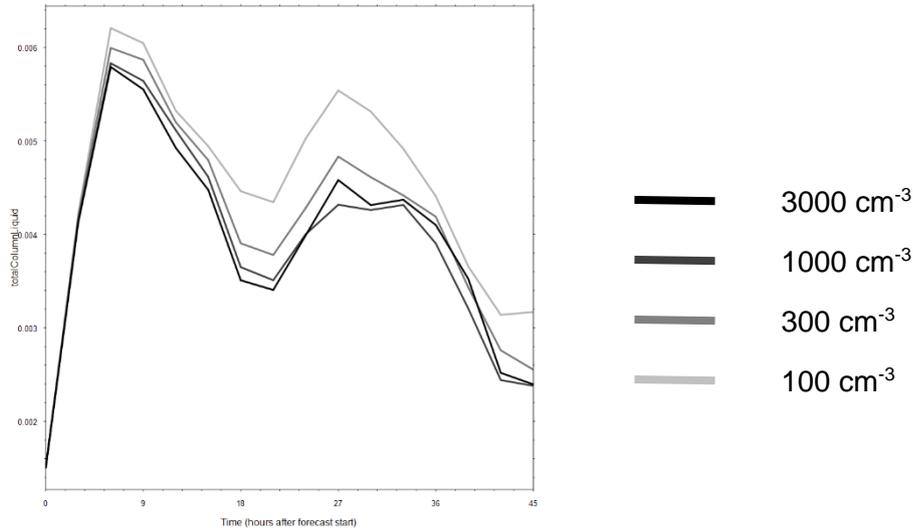
Fig 6.3 - Total column liquid water content as a function of time for the four simulations averaged over the whole domain. The simulation began at midnight on 4th June 2016.

However, if we examine the total column liquid water as seen in the time series in Figure 6.3, we see that the total column liquid increases during initial spin up of resolved scale convection until 0600. The increase is greatest in the lower aerosol, higher drizzle cases and the lowest aerosol concentration case maintains the greatest liquid water content for the duration of the simulated period.

In addition, Figure 6.4 shows a series of model vertical profiles of liquid water content over a 2° square region at the coast of Ghana (we average over a small region to avoid problems with averaging profiles over widely varying topography). These show that in the higher aerosol simulation cloud base is higher in altitude and cloud penetrated higher into the free troposphere (reference the BL heights in Figure 6.2). This is particularly the case around 1800. Note that this analysis has not attempted to determine if the reduction in peak liquid water content in high aerosol runs in Figure 6.4 is due to reduced in-cloud liquid water or reduced number of cloudy grid cells.
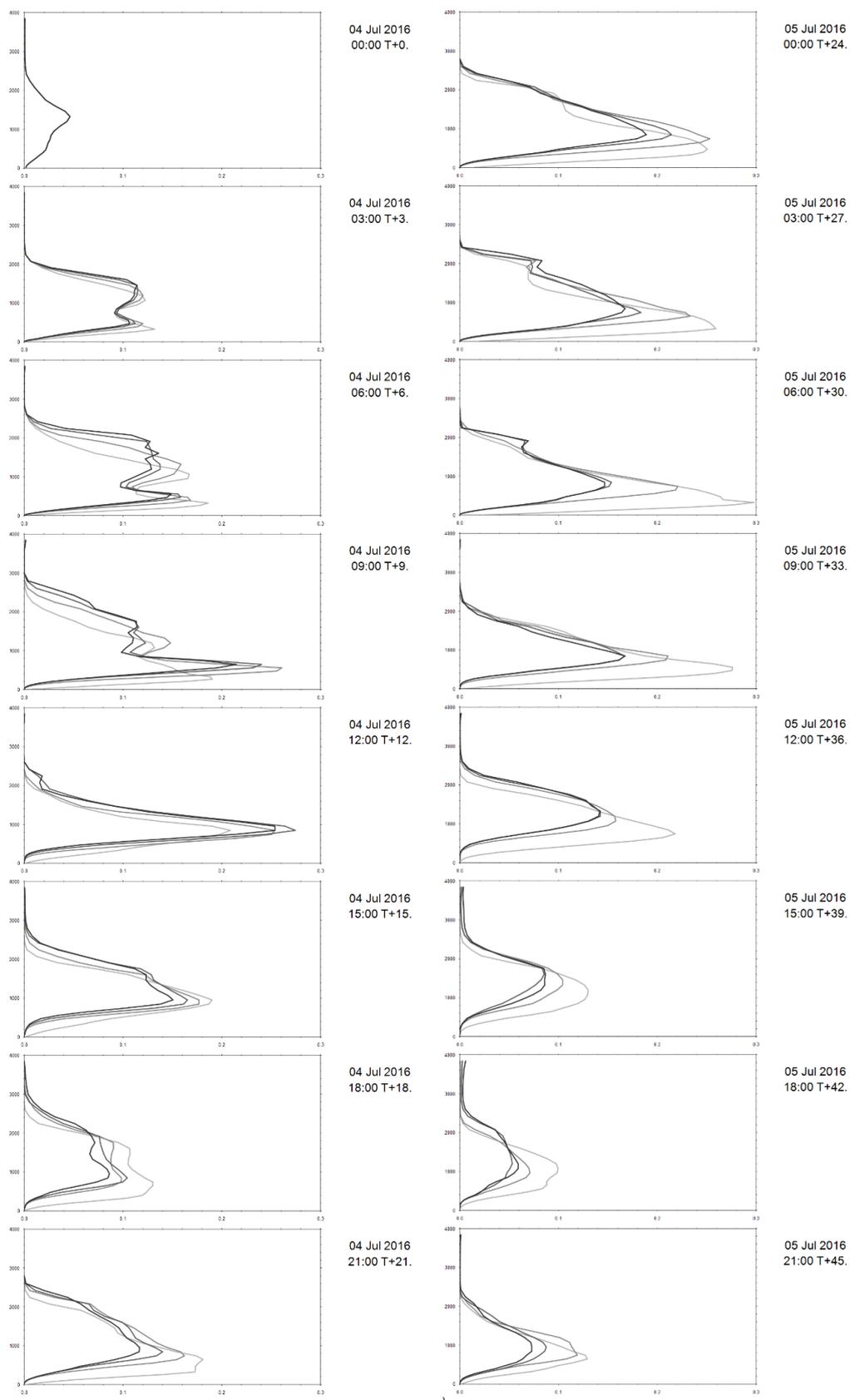
Figure 6.4 - Profiles of liquid water content for the four simulations. The profiles were averaged over a 2° square centred on lon 1°, lat 6° near the Ghana coast.

It should be noted that the Smith scheme used here defines the amount of liquid water simply as a function of relative humidity, with liquid water able to exist for relative humidity of 85% and above.

The differences in total column liquid water must therefore be due to increases in the relative humidity of grid cells. Relative humidity is clearly a function of specific humidity and temperature. We find that in the lowest aerosol case the specific humidity close to the surface is significantly greater than the other cases from 0600 on day 1 of the simulations onwards. The remaining simulations are rather similar. There is a general trend for the simulation with lower aerosol to have lower temperature near the surface. It is tempting to attribute these differences to evaporation of drizzle near the surface generating moist cold pools. However, it should be noted that drizzle is a net sink of liquid water from the atmosphere meaning that over the whole domain it should reduce specific humidity and increase potential temperature (due to latent heat release). These changes in near surface potential temperature and specific humidity must therefore be driven by differences in either surface fluxes or redistribution of heat and moisture.
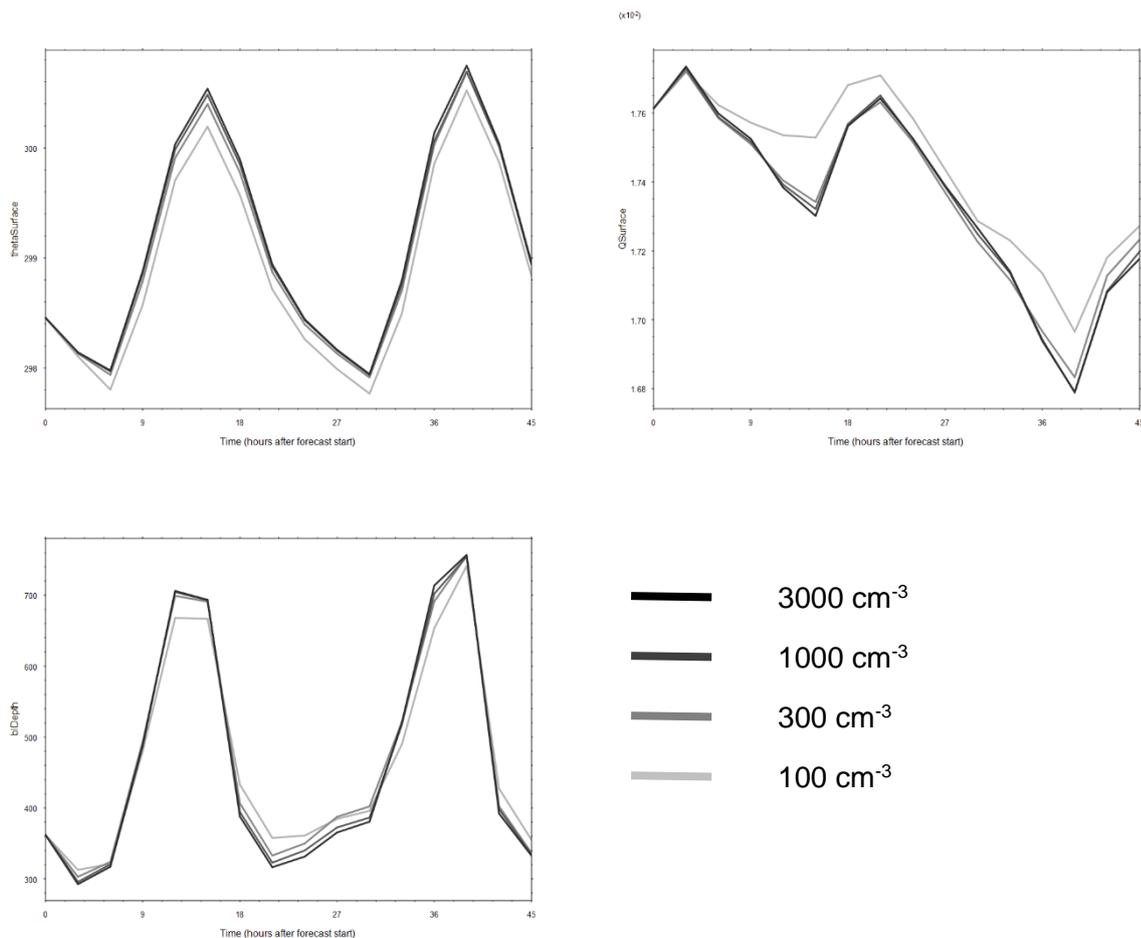
Figure 6.5 - Time series of potential temperature in the lowest model level, specific humidity in the lowest model level and boundary layer depth.

We do not find a trend in surface fluxes which can explain the trend in specific humidity or potential temperature. However, we do find that the lowest aerosol case has a boundary layer depth that is lower during the day and deeper during the night. This implies that as the boundary layer grows during the day, less warm dry free tropospheric air is mixed into the boundary layer. This could explain why the near surface is cooler and moister and why there is more cloud.

The cause of the changes in boundary layer depth have not been fully explored. Some possible explanations are

1) At night higher drizzle concentrations in the lower aerosol cases generate cold pools which could increase turbulent mixing in an otherwise stable environment and cause a deeper boundary layer in the lower aerosol simulations.

2) During the day, in the high aerosol simulations where little drizzle is formed, much of the latent heat released in cloud, can be reabsorbed at similar altitudes by evaporation of rain caused by daytime heating of the boundary layer or entrainment of warm dry free tropospheric air. In the lower aerosol simulations with more drizzle, liquid water is transported downward before evaporation. This causes a warming aloft and a cooling below. This could stabilize the boundary layer and suppress boundary layer growth.

3) Through mass conservation, convection which penetrates the boundary layer top must reduce the boundary layer growth rate. The higher aerosol cases which have cloud penetrating to higher altitudes may have boundary layer growth suppressed in this manner especially during the diurnal cycle's convection maxima, expected in the evening. This may contribute to the reduction of boundary layer depths at this time.

6.4 Conclusions

This work has explored the predicted cloud lifetime effect which links aerosol concentration and cloud cover. The prediction is that increases in aerosol result in increased cloud droplet number, reduced drizzle formation, suppression of precipitation, reduction of depletion of cloud liquid water and enhance cloud lifetime and cloud coverage. We are able to investigate these processes in the DACCIWA region using the Unified Model due to the introduction of a new microphysical parameterisation known as CASIM which includes multi-moment representation of cloud and precipitation droplets and permits idealised setup in which sensitivity studies can be performed.

We found that increasing aerosol concentration from 100 cm^{-3} to 300 cm^{-3}, 1000 cm^{-3} and 3000 cm^{-3} resulted in increased droplet concentration and supressed precipitation as expected. However, we found the opposite to the expected impact upon cloud cover, i.e. increasing aerosol concentration caused a reduction in cloud cover.

The changes in cloud cover were correlated with changes in relative humidity (as expected from the cloud scheme used in the Unified Model) and the changes in relative humidity were linked to expected changes in temperature and specific humidity, i.e. simulations with more cloud cover had higher relative humidity, higher specific humidity and lower temperature near the surface. Surface fluxes could not explain these changes. The differences may be explained by changes in boundary layer depth, with higher aerosol concentration simulations having shallower boundary layers during the night and deeper boundary layers during the day. This implies more entrainment of warm dry free tropospheric air during daytime boundary layer growth which reduces relative humidity and cloud cover.

The reasons for the boundary layer depth changes have not yet been fully explored. But some causes could be precipitation generated cold pools, vertical redistribution of latent heat by drizzle and suppression of boundary layer growth by convection overshooting the boundary layer top.

7   Numerical simulation of the aerosol-cloud radiation feedback during DACCIWA with COSMO-ART (KIT)

This section refers to work using the COSMO-ART model described in Section 2.3.

7.1   Introduction

This study focuses on the assessment of the aerosol impact on clouds and the atmospheric dynamics over SWA using a two-day process study. The following research is based on two particular themes. Firstly, the investigation of aerosol impacts on meteorological characteristics over SWA and the spatial and temporal scales they exhibit. We investigate changes in radiation and precipitation in response to changing aerosol. The other theme is focused on the impact of clouds and humidity on aerosols. Humidified aerosol layers may have a large radiative forcing, which in turn could affect dynamics, transport and clouds across the region.

7.2   Results

As indicated in previous studies, a coastal front is observed that develops during daytime and propagates inland in the evening (Atlantic Inflow). Increasing the aerosol amount in COSMO-ART leads to reduced propagation velocities with frontal displacements of 10-30 km to the south and a weakening of the nocturnal low-level jet (Figure 7.1).
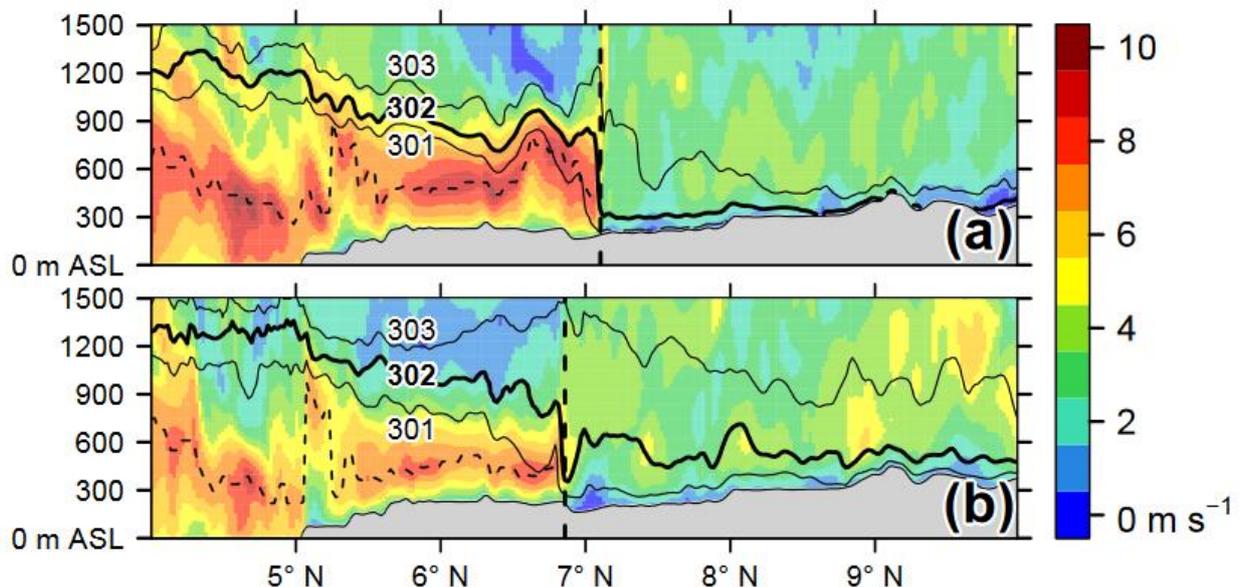
Figure 7.1 - Meridional vertical transects (m ASL) of wind speed (shading, m s⁻¹) along 5.75 °W (central Ivory Coast) for 2 July 21 UTC for the clean (a) and the polluted case (b). The solid black contours show the potential temperature for 301, 302 and 303 K while the bold isentrope (302 K) is used for the identification of the AI front (vertical dashed line). The horizontal dashed line shows the NLLJ wind speed maximum (jet axis) in the AI post-frontal area. The gray shading indicates the topography.

This is related to a subtle balance of processes related to the decrease in near-surface heating: (1) flow deceleration due to reduced land-sea temperature contrast and thus local pressure gradient, (2) reduced turbulence favouring frontal advance inland and (3) delayed stratus-to-cumulus transition of 1-2 h via a later onset of the convective boundary layer. The spatial shift of the Atlantic Inflow and the temporal shift of the stratus-to-cumulus transition are synergized in a new conceptual

model (Figure 7.2). We hypothesize a negative feedback of the stratus-to-cumulus transition on the Atlantic Inflow with increased aerosol.

To assess whether the reduction of incoming shortwave radiation due to clouds is related to a change in the cloud water content and therefore the optical thickness of the clouds or due to the Twomey effect with a change in cloud droplet number concentration (CDNC) and effective radius, Figure 7.3 exhibit the Empirical Cumulative Distribution Function (ECDF) with respect to the COSMO-ART realizations of the CDNC (Fig. 7.3a), cloud droplet effective radius (Fig. 7.3b), cloud water (Fig. 7.3c) and precipitation (Fig. 7.3d). This figure corresponds to the cloud and precipitation patterns presented in Figure 7.4 for 2 July, 15 UTC. A strong susceptibility of the CDNC and effective radii towards a change in the aerosol amount can be observed (Fig. 7.3). The factor variation from 0.1 to 4.0 leads to an increase in the median CDNC by one order of magnitude from 100 to 1000 cm^{-3} (Fig. 7.3a) and a reduction in the median effective radius from 9 to about 3.5 µm. When considering the green and red curves in Figure 7.3, which are related to an aerosol change symmetrically around the reference case (black), the effect on the CDNC and effective radius is nonlinear. An aerosol increase (solid green and red lines) has significantly stronger impacts than the aerosol decrease (dashed green and red lines).

In contrast to these remarkable changes, the effect on cloud water and precipitation (Fig. 7.3c,d, respectively) is insignificant. Except in the polluted case (solid red lines) all realizations show similar ECDFs, indicating that the aerosol increase neither leads to a cloud water increase due to precipitation suppression or due to enhanced water vapor condensation on the aerosol particles nor a cloud water decrease via enhanced evaporation. The polluted case shows a tendency of precipitation decrease (increase) for the weak (strong) precipitating areas, related to an increase (a decrease) in cloud water. This effect of greater local rainfall amounts is in agreement with the findings of Saleeby et al. (2014) likely via the convective-cloud invigoration mechanism. However, the deviations from the other realizations are small. Figure 7.3 reveals that the aerosol impact on radiation via the Twomey effect is very likely dominating the cloud-radiation interaction, whereas the cloud optical thickness impact (via a change in the amount of cloud water) is of minor importance. The weak precipitation response to the changing aerosol amount underlines the finding that the radiation and its variation is the key player in the observed changes over SWA due to the ADE in and outside of clouds and the Twomey effect.

The results exhibit radiation as the key player governing the aerosol effects on SWA atmospheric dynamics via the aerosol direct effect and the Twomey effect, whereas impacts on precipitation are

small (Fig. 7.3).
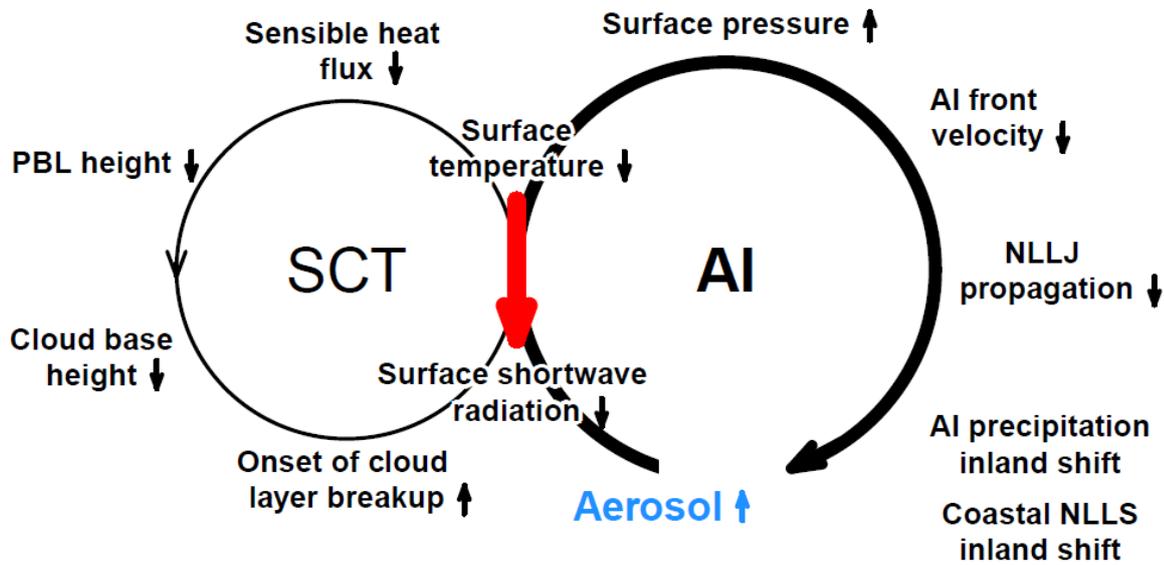
Figure 7.2 – Scheme of the aerosol-related atmospheric feedbacks summarizing the findings of the process study simulations on 2–3 July 2016. The main loop is labelled AI (Atlantic Inflow) and the additional loop SCT (Stratus-to-Cumulus Transition). The small arrows in upward and downward direction denote whether a quantity reacts with a decrease (downward) or increase (upward) to the increase of aerosol mass and number (blue) as the initial perturbation. The red arrow shows the linkage between AI and SCT via the decrease in shortwave radiation and surface temperature and a potential pathway for a negative feedback of SCT on AI.
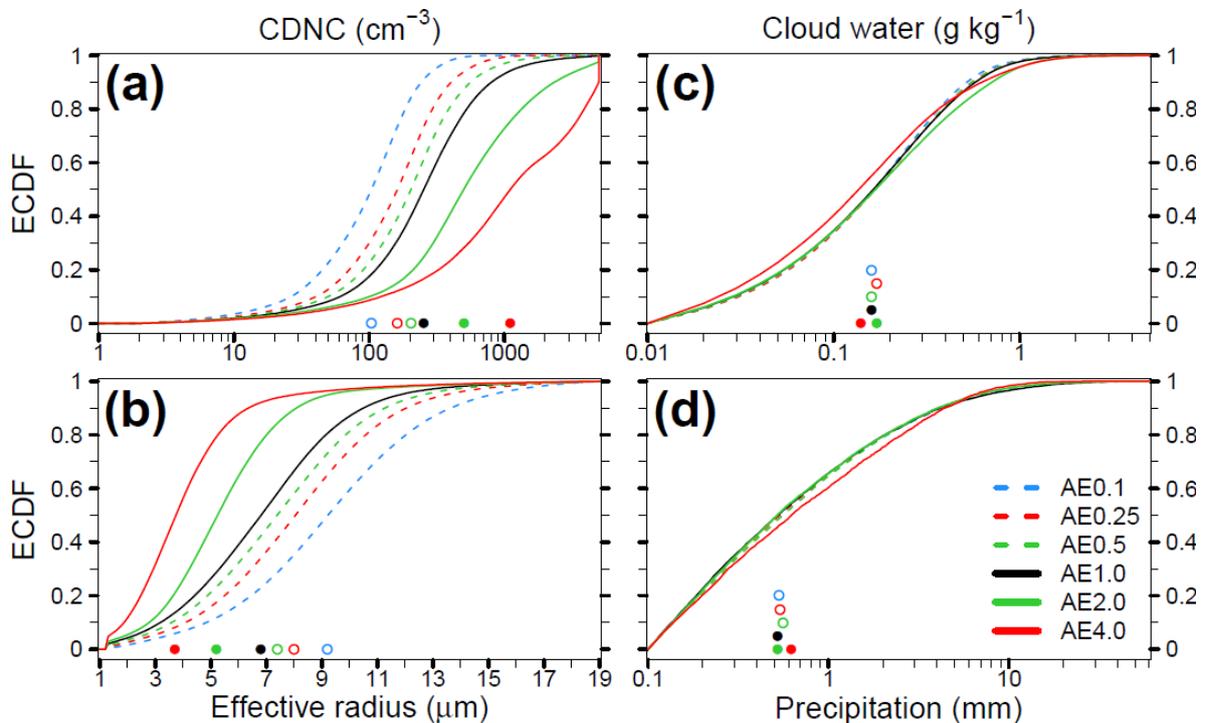
Figure 7.3 – Empirical Cumulative Distribution Function (ECDF) of (a) CDNC (cm^{-3}), (b) cloud droplet effective radius (m), (c) cloud water (g kg^{-1}) and (d) precipitation (mm) for the six experiments of Table 2.1 considering the full vertical column over the inland area of SWA on 2 July, 15 UTC. The circles and dots highlight the median values. Dashed lines and circles relate to realizations with fewer aerosols than the reference case and solid lines and dots refer to simulations with aerosol amounts greater/equal the reference case.

Given the marked diurnal cycle in SWA due to AI the further analysis is separated into three characteristic phases: (a) Atlantic Inflow progression phase (15 - 02 UTC), when winds from the Gulf of Guinea accelerate in the less turbulent evening and night-time boundary layer, (b) Moist morning phase (03 - 08 UTC), when the passage of the Atlantic Inflow front leads to overall cool and moist conditions over land and (c) Daytime drying phase (09 - 15 UTC) (Fig. 7.4), in which the Atlantic Inflow front re-establishes with the inland heating initiated after sunrise. This diurnal cycle imprints, via the relative humidity, also the Aerosol Liquid Water Content (ALWC). We analysed the impact of relative humidity and clouds on the aerosol liquid water content. As shown by other studies, the accumulation mode particles are the dominant contributor of aerosol liquid water. We find aerosol growth factors of 2 (4) for submicron (coarse) mode particles, leading to a substantial increase of mean aerosol optical depth from 0.2 to 0.7. A further model realization is realized, which neglects the ALWC in the radiative transfer calculations (No-ALWC).
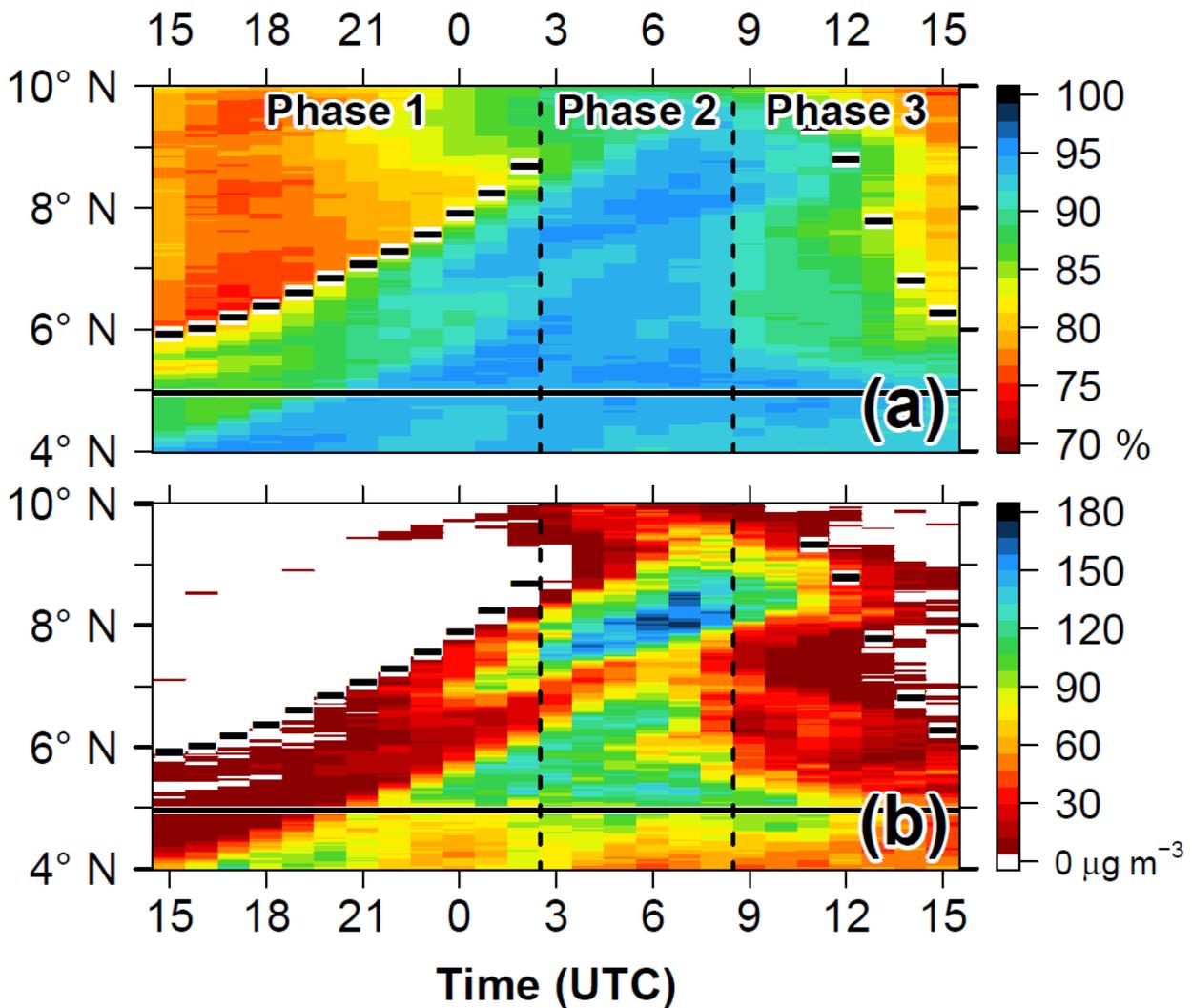
Figure 7.4 - Hovmöller diagram of the median (a) RH (%) and (b) total ALWC (g m-3) in the lowest 1500 m AGL as zonal mean over Ivory Coast (7.5 °W–3° W, 4–10° N) between 2 July 15 UTC and 3 July 15 UTC. The horizontal bars denote the zonal mean location of the 302 K isentrope at 250 m AGL, the horizontal solid line the zonal mean coast line and the vertical dashed lines separate the three phases: AI progression phase (Phase 1), Moist morning phase (Phase 2) and Daytime drying phase (Phase 3).
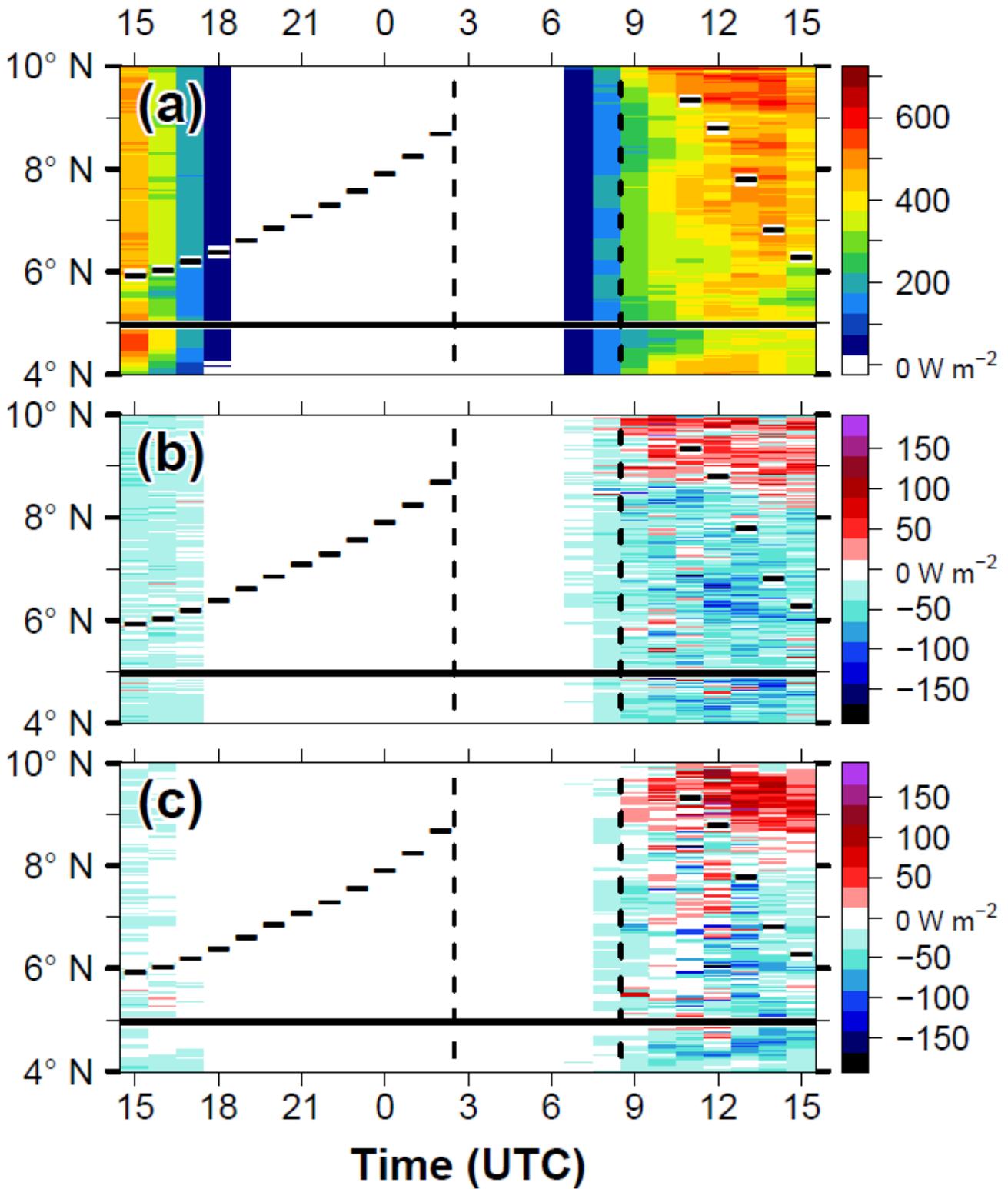
Figure 7.5 Hovmöller diagram of SSR (W m⁻²) for (a) Reference, (b) Reference minus No-ALWC for ICA and (c) Reference minus No-ALWC for OCA as zonal mean over Ivory Coast (7.5 W–3 W, 4–10 N) between 2 July 15 UTC and 3 July 15 UTC. The horizontal bars denote the zonal mean location of the 302 K isentrope at 250 m AGL of Reference, the horizontal solid line the zonal mean coast line and the vertical dashed lines the three phases introduced in Figure 7.4.

Considering the aerosol liquid water content leads to a decrease in shortwave radiation (SSR) of about 20 W m⁻² (Fig. 7.6), while longwave effects (SLR) appear to be insignificant, especially during night-time. The estimated relationships between total column aerosol liquid water and radiation are -305 39 W g⁻¹ (shortwave in-cloud), -114 +- 42 W g⁻¹ (shortwave off-cloud) and about -10 W g⁻¹

(longwave). The results highlight the need to consider the relative humidity dependency of aerosol optical depth in atmospheric models, particularly in moist tropical environments, where their effect on radiation can be very large

7.3 Summary

Changing the aerosol number and mass in COSMO-ART, the aerosol direct effect (ADE) and indirect effect (AIE) was quantified, indicating a considerable sensitivity of the AI frontal location towards changes in the aerosol amount. With increasing aerosol the AI front shows reduced propagation velocities over Ivory Coast leading to frontal displacements of 10-30 km. Longwave cooling influences the AI pre-frontal area but even after sunset the positive temperature anomaly from daytime solar heating persists and dominates. In addition to the effect on AI, the decrease in near-surface heating leads to a delayed Stratus-to-Cumulus Transition (SCT) via a later onset of the convective boundary layer. We synergized this subtle aerosol-atmosphere feedback in a new conceptual model combining the AI and SCT loops. Furthermore, we hypothesize that the additional radiation deficit due to the later SCT leads to a further weakening of AI. The results exhibit the radiation as the key player governing the aerosol effects on SWA atmospheric dynamics during boreal summer, via ADE and the Twomey effect. In contrast, effects on precipitation are small.

8 Investigation into the role of coastal anthropogenic sources on cloud formation (UPMC)

This section refers to work using the WRF-CHIMERE model described in Section 2.4.

8.1 Objectives

The objective of this study is to quantify the impact of the coastal anthropogenic sources on the cloud formation. Aerosol-cloud interaction is largely controlled by the amount of aerosols and then anthropogenic emissions over important population centres such as the Southern West Africa (SWA). These interactions are both on direct and indirect effects. In this study, we focus on the indirect effect only to quantify the impact on the cloud life-cycle.

DACCIWA experimental studies have shown that low clouds are persistent during the morning in this SWA region. During the afternoon, these low clouds are broken and magnitude and speed of this process remains poorly understood. In this study, we focus on one specific day, corresponding to IOP measurements including aircraft measurements: the 5 July 2016, when a degree of high cloudiness was observed.

In order to evaluate the effect of aerosols on the daytime evolution of low cloud, we propose to compare three numerical simulations:

(i) no AEx10: with no aerosol effects included in the model. It means that the WRF-CHIMERE modelling system is used off-line. The meteorology is calculated without knowledge of the aerosol variability and is used a climatology for aerosol. The meteorological fields are used by CHIMERE to calculate the aerosol emissions, transport, chemistry and deposition. The anthropogenic emissions are multiplied by ten for all emitted species. Even if this increase seems to be unrealistic, this corresponds to a scenario of 'huge' emissions just to quantify a possible maximum of emissions.

(ii) AE–HTAP: The "online" mode of the WRF-CHIMERE system is on. Several times per hour, WRF sends meteorological fields to CHIMERE and CHIMERE sends aerosol information to WRF. This first configuration uses the HTAP anthropogenic emissions as it.

(iii) AE–HTAPx10: This configuration is the same configuration as AE-HTAP, except that the anthropogenic emissions are also multiplied by ten for all emitted species.

One has to note that the 'regular' HTAP emissions correspond to the year 2010 and the DACCIWA studied case to the year 2016. Between the two, real anthropogenic emissions increased a lot. A realistic representation of anthropogenic emissions is thus probably between the two configurations AE-HTAP and AE-HTAPx10.

For all other possible sources, mineral dust, biogenic, biomass burning and sea salt, the emissions fluxes are the same in the three configurations.

8.2 Observational dataset

The three simulations are compared to all the available observations. These include routines satellite products and the DACCIWA IOP measurements provided from both aircraft flights and in-situ surface measurements. The comparison of the three simulations to the data was used to determine if: (i) the model is close to the observations or not, (ii) if aerosol-dynamical coupling significantly changes the predicted results, and (iii) if the addition of this coupling improves the simulation or not.

The following observations are used for the comparisons:

- The radiosonde in Savé was used to compare the vertical structure of the boundary layer and the lower troposphere where surface measurements are performed.

- The ceilometer in Savé provided more details on the vertical structure of the boundary layer, with precise information on the altitude of the cloud base and on aerosols layers.

- Aircraft measurements: The model results are compared to the ATR and Falcon aircrafts data (Twin Otter measurements are not presented but may be included in the final analysis). This included temperature, relative humidity, liquid water mixing ratio, wind speed and direction, gases (NO2) and aerosol (from AMS and OPC)

- MeteoSat (MSG) visible satellite images are used to examine the spatial variability of the clouds.

8.3   Comparison of model results to observations

8.3.1   Cross section of LWC
The measured and modelled cloud liquid water mixing ratio was analysed using vertical cross-sections along the flight trajectory. Results are presented in Figure 8.1 and show the modelled cloud structure in terms of the altitude of its base and depth.

a) ATR - no AE

b) Falcon - no AE

c) ATR - AE - HTAP

d) Falcon - AE - HTAP

e) ATR - AE - HTAP x10

f) Falcon - AE - HTAP x10
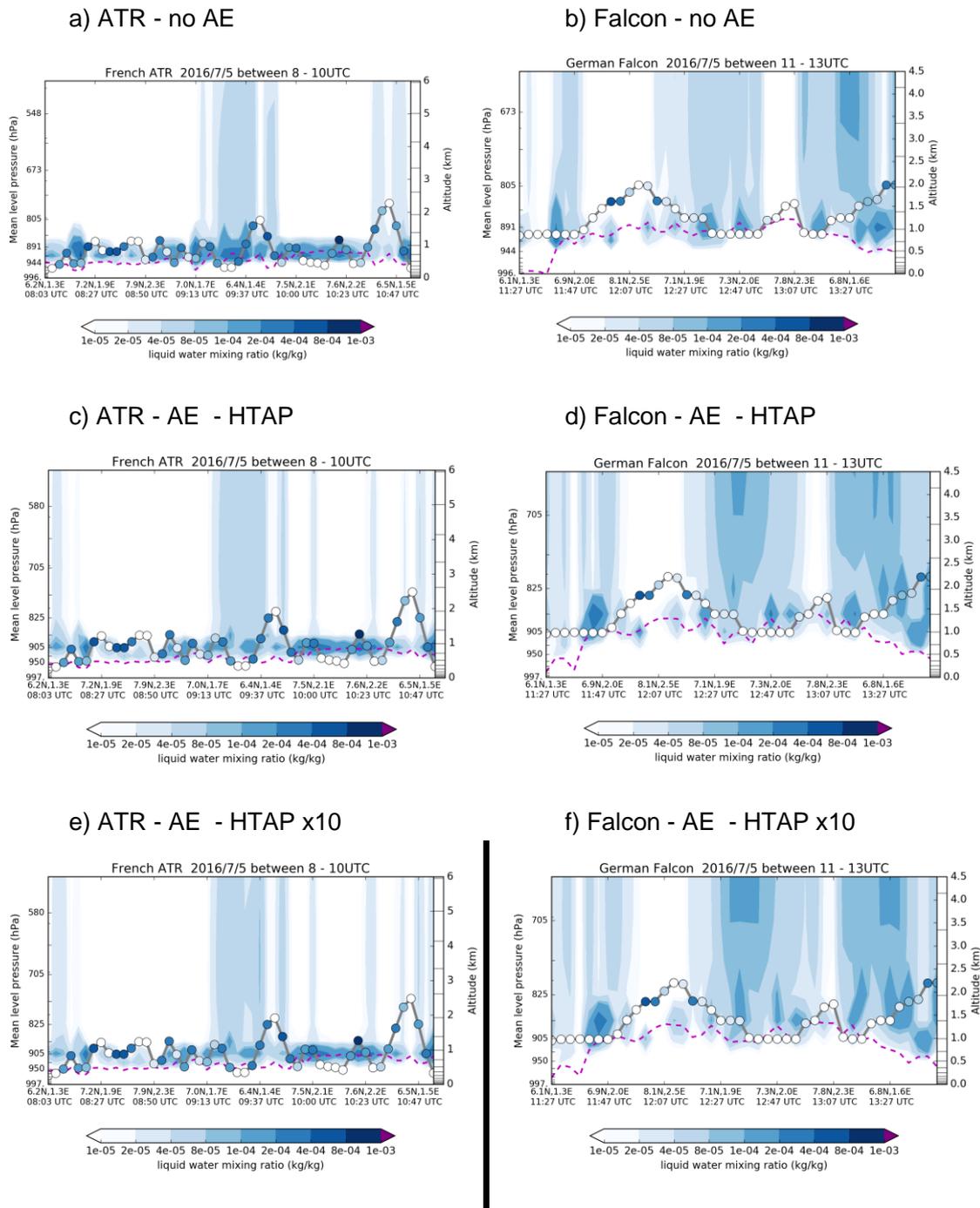
Figure 8.1 - Vertical cross section (altitude – time/position) along the ATR (left) and Falcon (right) flight trajectories on 5 July 2016 for the liquid water mixing ratio. Observations are presented with the coloured dots at the altitude of the aircraft (grey line). The WRF-CHIMERE modelled fields corresponds to the colour shadings with the same colour map that for the observations for three simulations: (i) without Aerosol Effect and HTAP anthropogenic emission multiplied by 10 (no AE – HTAP x10), (ii) with AE and HTAP standard (AE – HTAP), (iii) with AE and HTAP anthropogenic emission multiplied by 10 (AE – HTAP x10). Modelled PBL height is the violet dashed line.

During the ATR flight between 0800 and 1100 UTC, the clouds are located at about 500 m above the surface. The clouds are present during the entire flight seen by the measurements as well as by the model. The altitude and depth of the clouds is similar for the three simulations. There are no clear improvements with the AE.

During the Falcon flight between 1100 and 1400 UTC, the clouds are sparse spatially and located at about 1000 m above the surface. The cloud frequency is well reproduced by the model. The altitude and depth of the clouds is similar for the three simulations. There is no clear improvements with the indirect aerosol effect. This may be due to the short time of the simulation.

Figure 8.2 - Photography from the Falcon cockpit showing high cloudiness on 5 July 2016 flight at 1230 UTC

Figure 8.2 shows a complex vertical structure with cloudy layer below and above the aircraft. The horizontal resolution of the model is too coarse to reproduce these fine scale structures.

8.3.2   Break up time and vertical wind structure

Figure 8.3 presents soundings at Savé for the mean wind speed and from the surface to 5000m AGL. For the two soundings, regardless of whether Aerosol Effects are switched on or not, the meteorological model is able to retrieve the main characteristics of the vertical structure. A low level jet at 11:00UTC and at 1000m AGL is resolved as is a minimum of wind speed at 2000 AGL and a reinforcement of the wind speed above 3000m AGL. At the end of the afternoon, at 17:00UTC, the low level jet disappears but the vertical structure remains the same above 3000m AGL.
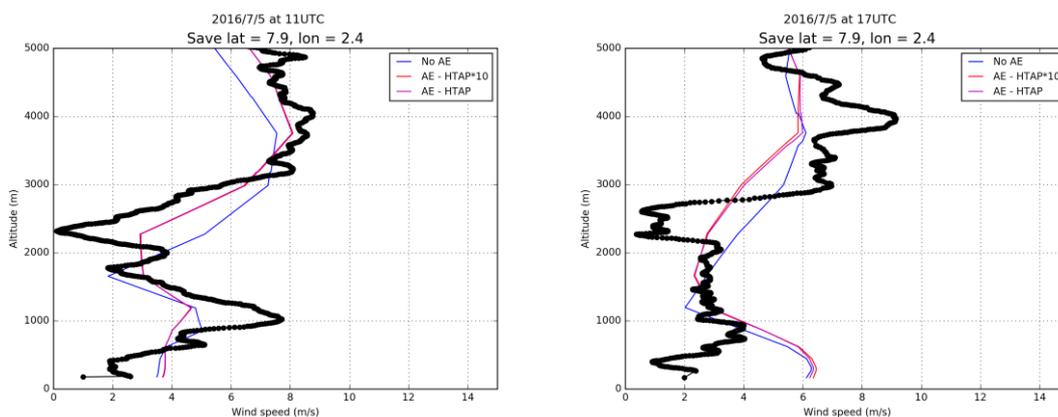
Figure 8.3: Vertical profiles along the radiosonde trajectories of the wind speed on 5 July 2016 launch at 1100 UTC for the liquid water mixing ratio. Raw observations at 1 Hz are averaged every 3 minutes (black dots) and the 4D modelled fields are interpolated along the balloon trajectory every 3 minutes for three simulations: (i) without Aerosol Effect and HTAP anthropogenic emission multiplied by 10 (no AE – HTAP x10), (ii) with AE and HTAP standard (AE – HTAP), (iii) with AE and HTAP anthropogenic emission multiplied by 10 (AE – HTAP x10).

The results show that there is some improvement in the model reproduction of the observed vertical structure of wind speed with the Aerosol Effect included. Though these changes are small these differences between the two simulations are important with changes of the wind speed of ~ 1-2 m/s.

8.3.3   Ceilometer Cloud base

Finally, we compare the model results to the ceilometer data recorded at Savé and in Figure 8.4. The Ceilometer is able to record the vertical structure of the lower troposphere and to provide information of the aerosol layers and cloud altitude and base. The first (coloured) figure shows the direct output of the instrument available on the database. It shows a thin cloud layer at ~500m AGL during the morning, increasing in altitude up to 1000m AGL. From these data, the cloud base is extracted and superimposed onto the model output. The model results are presented as vertical cross-section of liquid water mixing ratio.

For the three model configurations, the cloud base is well modelled during the first half of the day. During the afternoon, the comparison is more difficult since the ceilometer recorded various altitudes, ranging from 1500m to 5000m. The comparison between the models shows that the coupling between aerosol and clouds changes the vertical structure of the modelled clouds as well as the intensity of the amount of the liquid water. It is difficult to quantify whether the aerosol effect provides a better simulation or not in the regard using only the ceilometer data for comparison.
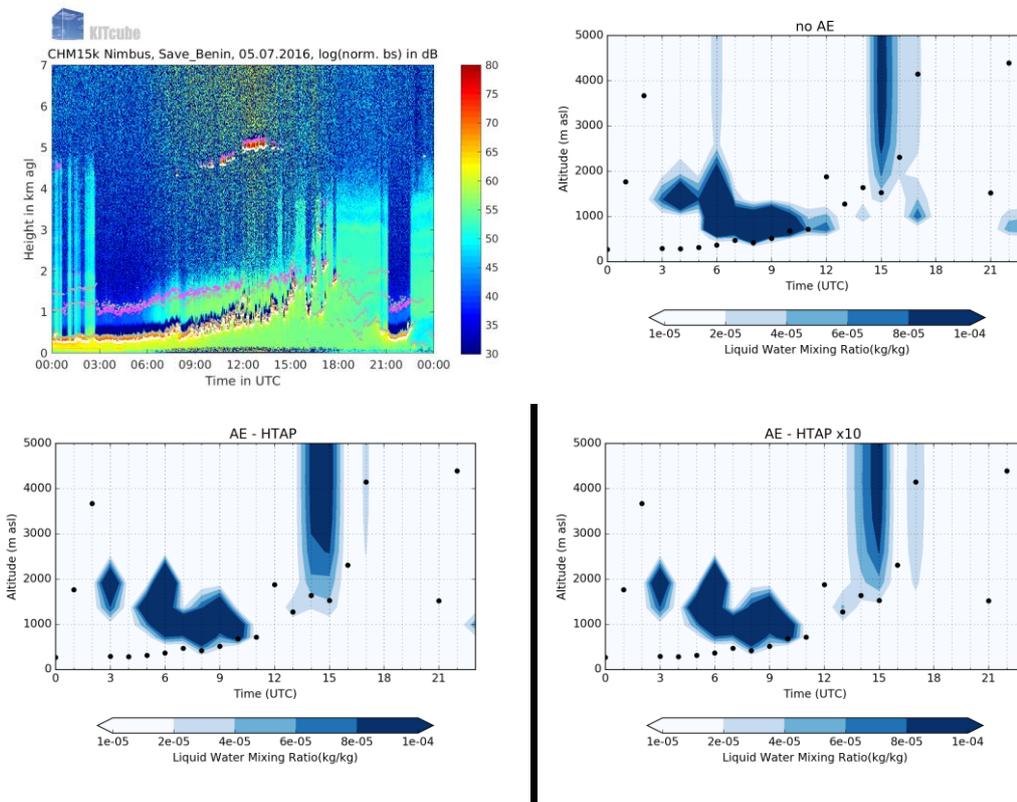
Figure 8.4 - Diurnal cycle of cloud vertical distribution on 5 July 2016 at Savé (Benin). (Top left) Ceilometer data providing cloud base height and depth (in m). (Other panels) Observed cloud base height (in m) and modelled liquid water mixing ratio retrieved along the radiosonde trajectories launched at 1100 UTC. Raw observations at 1 Hz are averaged every 3 minutes (black dots) and the 4D modelled fields are interpolated along the balloon trajectory every 3 minutes for three simulations: (i) without Aerosol Effect and HTAP anthropogenic emission multiplied by 10 (no AE – HTAP x10), (ii) with AE and HTAP standard (AE – HTAP), (iii) with AE and HTAP anthropogenic emission multiplied by 10 (AE – HTAP x10).

8.4   Investigation of the effect of aerosols on the cloud field

Here, we investigate the diurnal cycle of cloud cover during the break up of low clouds. We also analyse the impact on precipitation patterns and on the vertical wind structure.

8.4.1   Cloud break up time

In this section, we analyse the brake up time of clouds between 1200 UTC and 1500 UTC. We present visible images obtain by MSG, then we compare to the modelled Cloud Optical Depth (COD) to investigate the evolution of the spatial pattern of clouds.

1200 UTC   **1300 UTC**

1400 UTC   **1500 UTC**
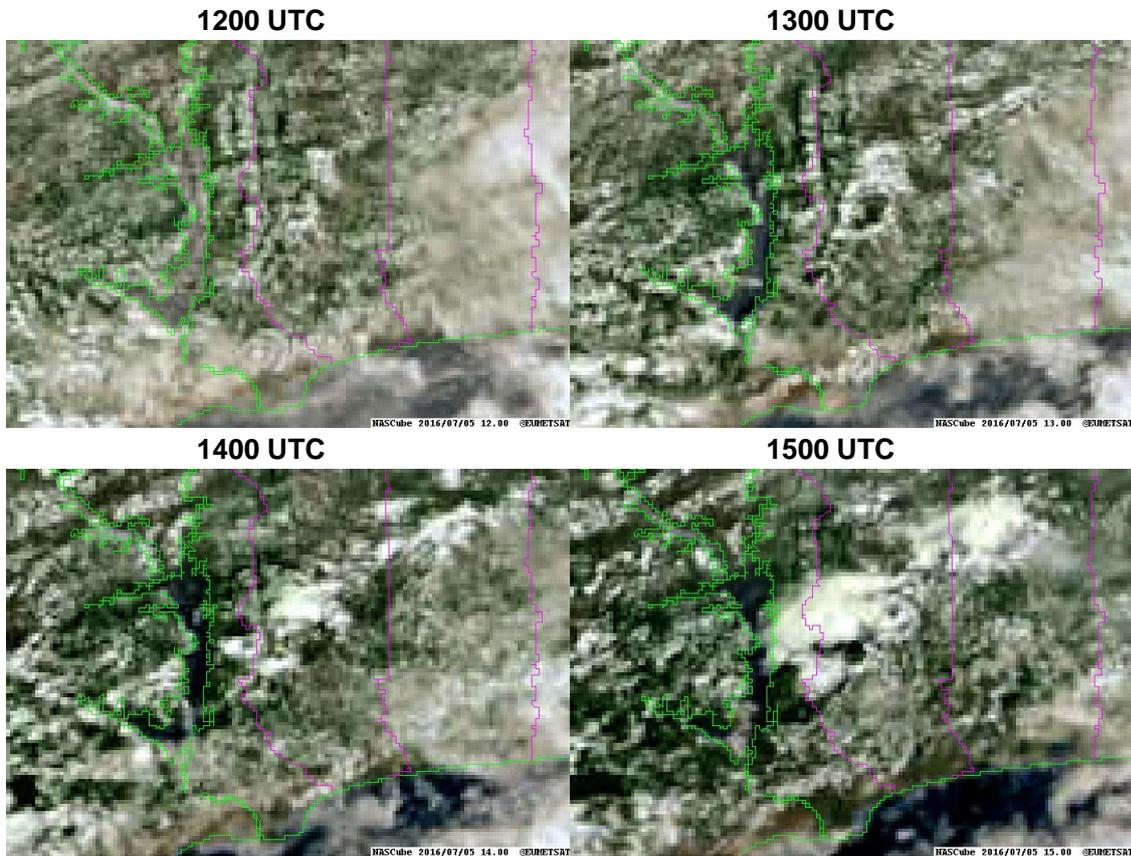

Figure 8.5 - EUMETSAT visible images on 5 July 2016 between 1200 and 1500 UTC over the evaluation domain (5.5°N-8.6°N; 1.1°W-3.2°E). Downloaded from the NASCube website (Lille University).

MSG images show that the cloud cover is very broad and continuous at 1200 UTC. From 1200 to 1500 UTC, the cloud cover becomes patchier with some large clouds, which suggest organized convection at 1500 UTC. It is worth notifying that the cloudiness stay important close the coast.

The modelled cloud cover is in good agreement with the MSG images. The simulation without AE is less in agreement, although the simulations with AE predict more clouds, especially in the coastal area between Lomé (Togo) and Cotonou (Benin). With AE, the model reproduces the clouds over the ocean (at 1200 and 1300 UTC) that are seen with satellite images. There are only tiny differences for the two simulations with the AE using HTAP standard and HTAP by 10.
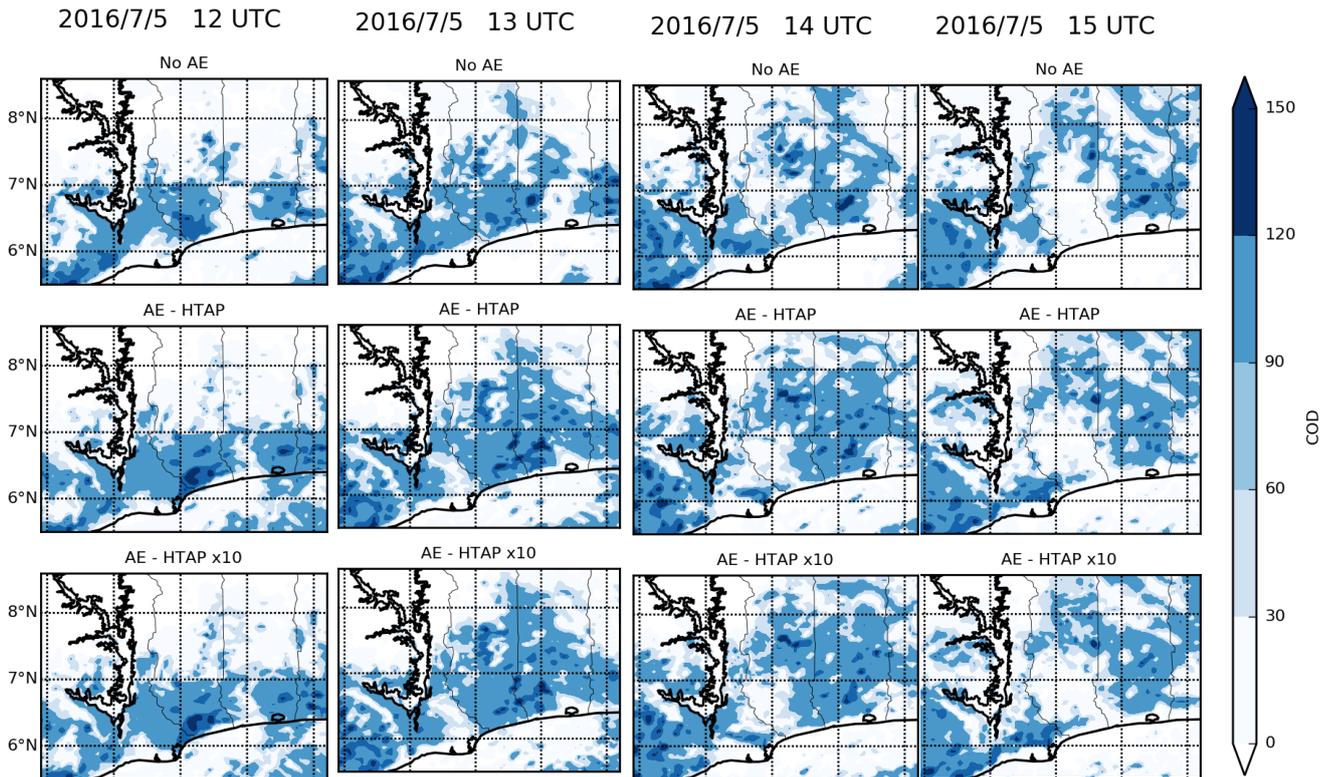
Figure 8.6: Map of WRF-CHIMERE hourly modelled Cloud Optical Depth (COD) on 5 July 2016 between 1200 and 1500 UTC over the evaluation domain (5.5°N-8.6°N; 1.1°W-3.2°E) for three simulations: (i) without Aerosol Effect and HTAP anthropogenic emission multiplied by 10 (no AE – HTAP x10), (ii) with AE and HTAP standard (AE – HTAP), (iii) with AE and HTAP anthropogenic emission multiplied by 10 (AE – HTAP x10).

8.4.2   Impact on precipitation and vertical wind structure

In this section, the effect of AE on local meteorology was investigated. The AE changes the radiation reaching the surface, which in turn changes the thermal convection, the PBL height, the precipitation and the wind structure in the lowermost troposphere.

The daily cumulative precipitation on 5 July and the vertical profile of the wind speed at Cotonou (Benin) were analysed for all three simulations.

The three simulations depict an area of low precipitation rate (from 7°N to 8°N) and of moderate precipitation (from the ocean to 7°N). Without AE, the model does not predict cumulative precipitation greater than 1 mm/day close to the coast, over the ocean and over the continent. There is little difference between this pattern and those of the two simulations with AE, showing that the precipitation (and cloud cover) are not very sensitive to the anthropogenic aerosol level.

We have seen that the model with AE improves the accuracy of the model for the clouds. This result should be linked with a modification of the vertical structure of the atmosphere when the AE are turned on.
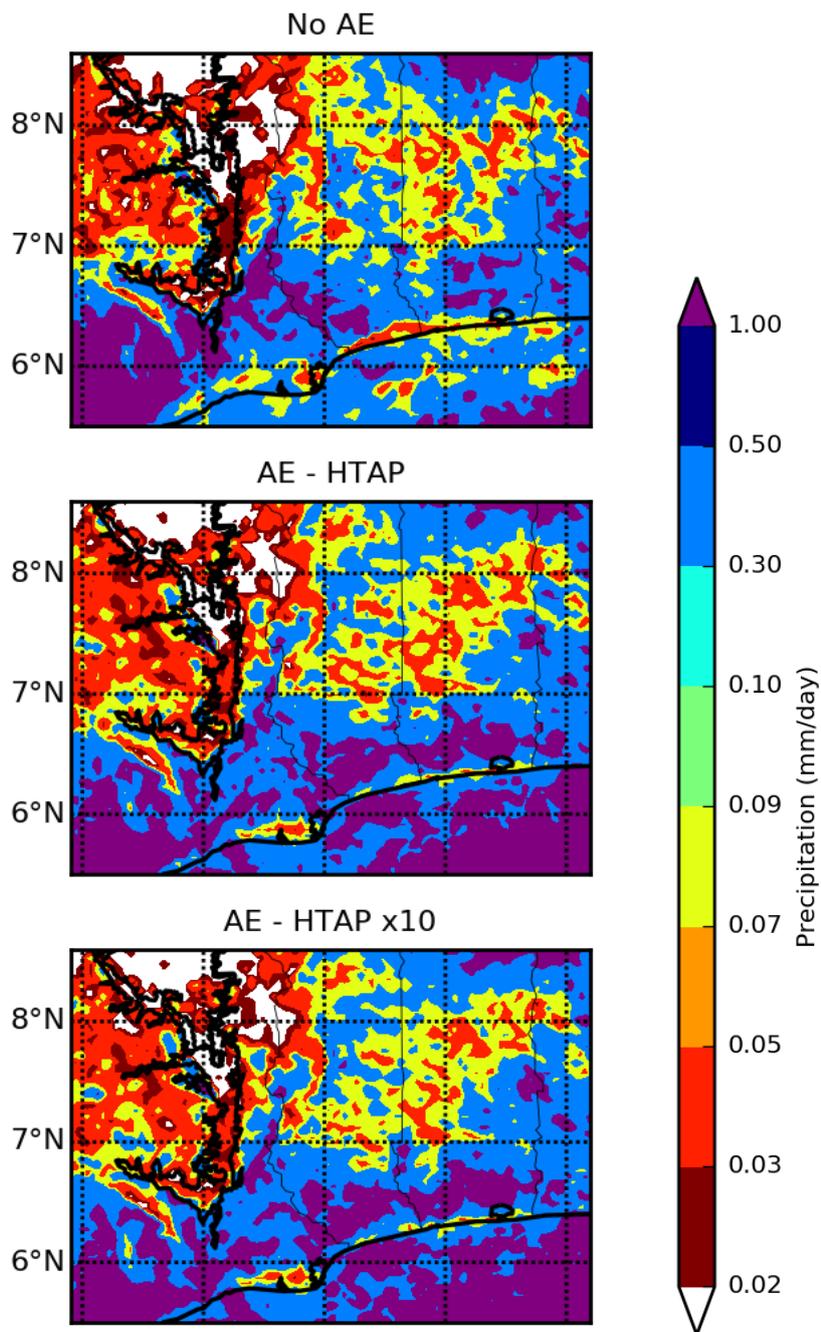
**Figure 8.7: Map of WRF-CHIMERE daily modelled precipitation rate (mm/day) on 5 July 2016 between 1200 and 1500 UTC over the evaluation domain (5.5°N-8.6°N;1.1°W-3.2°E) for three simulations: (i) without Aerosol Effect and HTAP anthropogenic emission multiplied by 10 (no AE – HTAP x10), (ii) with AE and HTAP standard (AE – HTAP), (iii) with AE and HTAP anthropogenic emission multiplied by 10 (AE – HTAP x10).**
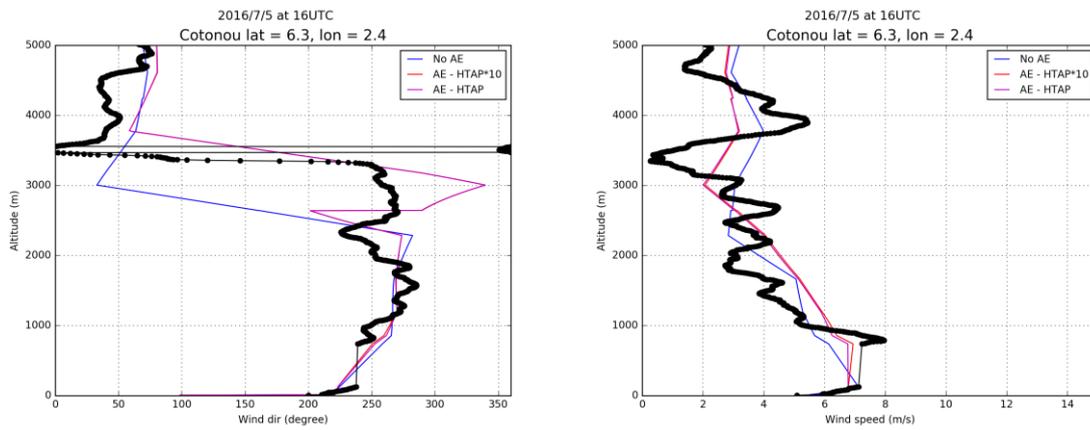
Figure 8.8: Vertical profiles along the radiosonde trajectories of the wind direction and speed on 5 July 2016 launch at Cotonou (Benin) at 1600 UTC. Raw observations at 1 Hz are averaged every 3 minutes (black dots) and the 4D modelled fields are interpolated along the balloon trajectory every 3 minutes for three simulations: (i) without the Aerosol Effect and with HTAP anthropogenic emission multiplied by 10 (no AE – HTAP x10), (ii) with AE and HTAP standard (AE – HTAP), (iii) with AE and HTAP anthropogenic emission multiplied by 10 (AE – HTAP x10).

The radiosonde launched at Cotonou at 1600 UTC was in a period when the cloud cover was patchy. Observations of wind direction show that the altitude of the wind shear is located at 3500 m asl, which corresponds to the wind speed minimum. In the PBL (below 1 km), there is a maximum of wind speed at about 800 m ASL.

The model reproduces the wind direction change more accurately with the AE. There is an important difference of about 1 km for the wind shear altitude. Moreover, the modelled wind speed is also in better agreement with observations throughout the PBL when AE is included. The differences of the two simulations with AE are negligible, which indicates little dependence on the difference in emissions between 2010 and present day.

9   Summary of major findings

DACCIWA has identified several important contributors to the regional aerosol budget across the southern West African region. The large urban centers of Abidjan, Accra, Lomé, and Cotonou are important sources of particulates, though at present these cities are smaller and less well developed than Lagos and so the plumes are quite distinct. There is also a large population of people, close to 4 million, which is dispersed across the rural region between these cities and inland, and observations show that these regions may well be a significant source of pollution based on CO measurements from aircraft. Whilst these sources have clearly been identified and do have an influence on the aerosol load across the region, they are superimposed on an elevated regional background of aerosol from biomass burning sources in central Africa across the DR Congo, Angola, Botswana and Namibia. These aerosols are entrained into easterlies in the lower free troposphere and are advected over the tropical eastern Atlantic Ocean. Whilst observations of elevated biomass burning from this region have previously been observed aloft over West Africa during the monsoon season in AMMA, the presence of such aerosol in the boundary layer over the West African continent is a new and important finding. DACCIWA has shown that this aerosol, once entrained into the oceanic boundary layer and advected into West Africa, elevates background pollution levels (discussed in D3.4) by up to 10 μgm^{-3} and provides a high concentration of particulate across the region that needs to be considered when assessing aerosol-cloud interactions across the region.

In polluted plumes, analysis of aircraft data shows cloud droplet number concentrations of around 200-700 cm^{-3} are elevated compared to the wider region which has a mean of around 150-500 cm^{-3}. The equivalent cloud droplet effective diameters (5-20 µm and 7-23 µm respectively) show a reduction of droplet size in the plume as to be expected. Even offshore, upwind of the region, cloud droplet concentrations were around 100-300 cm^{-3}, which compared to clean marine stratocumulus clouds that have cloud droplet number concentrations of less than 100 cm^{-3} indicates significant perturbation of the cloud system over the ocean to the south of the region. The lower cloud droplet number concentration over the ocean compared to the DACCIWA region is partly a result of changes in updrafts resulting from land-ocean surface heating.

Analysis of satellite data shows the strong diurnal cycle of cloudiness across the region with significant overnight development reaching peak average cloud cover of over 90% in some regions by 1000 UTC. By early afternoon this cloud had largely dissipated on most days. There was clear evidence of sea breeze influence generating more convective clouds around midday up to 50km inland. Orography was the main influence on the spatial variability of cloud cover with higher cloud incidence upstream of elevated terrain and greater clearance to the lee.

The relationships between the evolution of low level clouds and their microphysics has been investigated using large eddy modelling simulations that are constrained and validated by observational data. These have shown that sedimentation is important in the low level clouds across the DACCIWA region. This process removes liquid water from cloud top and in doing so reduces evaporative cooling at cloud top during entrainment. This is important since a greater proportion of water is retained in the cloud layer and cloud cover is maintained for longer into the day, impacting upon the surface radiation budget as a result. The effect appears to be important to correctly predict the cloud diurnal cycle in the DACCIWA region. This effect also reduces the sensitivity of low level cloud to the more widely recognised effect of reduced aerosol number leading to increased precipitation through increase in collision-coalescence since fewer, smaller cloud droplets lead to enhanced sedimentation of liquid water away from cloud top. The simulations are consistent with the observations in that the aerosol number concentrations closest

to those observed provide simulated clouds that behave most closely to those observed. These used a high background of aerosol consistent with the input of long range transported pollution which reduces the susceptibility of cloud radiation effects to changes in aerosol.

The Met Office Unified Model run in Numerical Weather Prediction mode was used to carry out a series of limited area runs over the DACCIWA domain to examine whether cloud-aerosol microphysical interactions affected cloud lifetime. This is hypothesized to occur as a result of reduced precipitation, caused by inhibition of the autoconversion rate of cloud droplets to drizzle since smaller and more numerous cloud droplets are present in polluted clouds. The simulations showed that, contrary to this cloud lifetime effect, the cloud amount decreased with increasing aerosol number concentration. The reasons for this have been examined in detail. The simulations show that as aerosol concentrations increase cloud droplet numbers also increase in a manner consistent with the observations. The simulated clouds showed suppression of precipitation with increased aerosol in the way that is to be expected from the cloud lifetime effect. The reductions in cloud cover were correlated with changes in relative humidity resulting from higher levels of specific humidity and lower temperatures. The simulations suggest that this is driven by shallower night-time boundary layers and deeper boundary layers during the day in model runs with higher aerosol loading. Deeper boundary layers drive stronger entrainment of warm, dry air. The reasons have not been fully elucidated to date but investigation is focusing on the vertical redistribution of moisture by drizzle, the generation of cold pools resulting from precipitation or overshooting of convection.

Increased numbers of aerosol were shown to have a significant impact on the dynamics of the nocturnal low level jet. This was diagnosed using a set of COSMO-ART simulations with variable aerosol number and mass to quantify both the aerosol direct effect and aerosol indirect effect. The simulations show that as aerosol concentrations increase the propagation speed of the nocturnal surface layer front reduces over Ivory Coast, leading to frontal displacements of 10-30 km to the south during the course of the night. Longwave cooling influences the pre-frontal area but even after sunset the positive temperature anomaly from daytime solar heating persists and dominates. In addition, the decrease in near-surface heating caused by additional aerosol leads to a delayed Stratus-to-Cumulus Transition (SCT) via a later onset of the convective boundary layer. This subtle aerosol-atmosphere feedback was incorporated into a new conceptual model combining the interactions governing the inflow of Atlantic air and the processes governing the SCT. This has led to the hypothesis that the additional radiation deficit due to the later SCT leads to a further weakening of the Atlantic Inflow. The results exhibit radiation as the key player governing the aerosol effects on the Southern West African atmospheric dynamics during boreal summer. In contrast, effects on precipitation are small.

WRF-CHIMERE simulations of a case study period that took place during the intensive measurement campaign were used to assess the extent to which two way aerosol coupling between the chemistry and dynamics schemes are important in capturing the main features of west African monsoonal flow And cloud structure. The results show that the model captures the broad cloud structures reasonably well regardless of whether two-way aerosol coupling with clouds and dynamics is incorporated into the model. The model representation of the vertical wind structure was also broadly similar though the inclusion of aerosol coupling improved comparison with observational data of 1 - 2 ms^{-1}. The effect of aerosol coupling on the development of cloud during the course of the day was also examined. The two-way coupling of aerosol did not affect the affect the development of the cloud structure during the morning hours and the model representations did a good job of reproducing measurements. However two-way aerosol coupling had a larger role to

play in the afternoon, changing both the vertical structure and also the amount of liquid water. It was harder to compare directly with ceilometer measurements during this period.

Break-up of the low level cloud during the afternoon is represented better in WRF-CHIMERE if two-way aerosol coupling is included compared to MSG satellite imagery, though there is little difference between simulations with 2010 emissions and a simulation with a factor of 10 increase in aerosols. The model shows moderate precipitation over land close to the coast (south of 7N) and little precipitation north of this region. There is little influence of two way aerosol coupling on the precipitation over land but higher drizzle rates are observed over the ocean when this coupling is included. A comparison with radiosonde launches in Benin shows that two way aerosol coupling in WRF-CHIMERE represents wind shear at the wind speed maximum in the vertical profile (~3.5 km) is better represented when aerosol coupling is included. There are clearly some dynamical processes that are better represented using two-way aerosol coupling between CHIMERE and WRF but some, including precipitation, show very little sensitivity. The simulations with greatly increased aerosol do not behave significantly differently from the 2010 HTAP emissions runs supporting the result that regional aerosol pollution is already sufficiently widespread as a result of long range transported biomass burning in addition to regional sources that the regional climate is likely to be relatively insensitive to further changes in pollution.

10 References

Athanasopoulou, E., Vogel, H., Vogel, B., Tsimpidi, A. P., Pandis, S. N., Knote, C. and Fountoukis, C., 2013: Modeling the meteorological and chemical effects of secondary organic aerosols during an EUCAARI campaign. Atmospheric Chemistry and Physics, 13, 625-645.

Baldauf, M., A. Seifert, J. Foerstner, D. Majewski, M. Raschendorfer and T. Reinhardt, 2011: Operational convective-scale numerical weather prediction with the COSMO model: description and sensitivities. Mon.Weather Rev., 139 (12), 38873905, doi: 10.1175/MWRD- 10-05013.1.

Bennartz, R.: Global assessment of marine boundary layer cloud droplet number concentration from satellite, J. Geophys. Res., 112(D2), D02201, doi:10.1029/2006JD007547, 2007.

Briant, R., Tuccella, P., Deroubaix, A., Khvorostyanov, D., Menut, L., Mailler, S. and Turquety, S.: Aerosol–radiation interaction modelling using online coupling between the WRF 3.7.1 meteorological model and the CHIMERE 2016 chemistry-transport model, through the OASIS3-MCT coupler, Geosci. Model Dev., 10(2), 927–944, doi:10.5194/gmd-10-927-2017, 2017.

Brito, J., Freney, E., Dominutti, P., Borbon, A., Haslett, S. L., Batenburg, A. M., Colomb, A., Dupuy, R., Denjean, C., Burnet, F., Bourriane, T., Deroubaix, A., Sellegri, K., Borrmann, S., Coe, H., Flamant, C., Knippertz, P., and Schwarzenboeck, A.: Assessing the role of anthropogenic and biogenic sources on PM1 over southern West Africa using aircraft measurements, Atmos. Chem. Phys., 18, 757-772, https://doi.org/10.5194/acp-18-757-2018, 2018.

Connolly, P. J., Möhler, O., Field, P. R., Saathoff, H., Burgess, R., Choularton, T. and Gallagher, M.: Studies of heterogeneous freezing by three different desert dust samples, Atmos. Chem. Phys., 9(8), 2805–2824, doi:10.5194/acp-9-2805-2009, 2009.

Deetz, K. and Vogel, B., 2017: Development of a new gas-flaring emission dataset for southern West Africa, Geosci. Model Dev., 10, 1607-1620.

Deetz, K., Vogel, H., Knippertz, P., Adler, B., Taylor, J., Coe, H., Bower, K., Haslett, S., Flynn, M., Dorsey, J., Crawford, I., Kottmeier, C. and Vogel, B., 2018: Cloud and aerosol radiative effects as key players for anthropogenic changes in atmospheric dynamics over southernWest Africa. Atmospheric Chemistry and Physics Discussions, doi:10.5194/acp- 2018-186.

Flamant et al.: The Dynamics–Aerosol–Chemistry–Cloud Interactions in West Africa Field Campaign, *Bull. Amer. Meteor. Soc.,* doi:10.1175/BAMS-D-16-0256.1, 2018.

Flamant, C., Deroubaix, A., Chazette, P., Brito, J., Gaetani, M., Knippertz, P., Fink, A. H., de Coetlogon, G., Menut, L., Colomb, A., Denjean, C., Meynadier, R., Rosenberg, P., Dupuy, R., Schwarzenboeck, A., and Totems, J.: Aerosol distribution in the northern Gulf of Guinea: local anthropogenic sources, long-range transport and the role of coastal shallow circulations, Atmos. Chem. Phys. Discuss., https://doi.org/10.5194/acp-2018-346, in review, 2018.

Ghan, S. J., Leung, L. R., Easter, R. C. and Abdul-Razzak, H.: Prediction of cloud droplet number in a general circulation model, J. Geophys. Res. Atmos., 102(D18), 21777–21794, doi:10.1029/97JD01810, 1997.

Grosvenor, D. P., Field, P. R., Hill, A. A. and Shipway, B. J.: The relative importance of macrophysical and cloud albedo changes for aerosol-induced radiative effects in closed-cell stratocumulus: insight from the modelling of a case study, Atmos. Chem. Phys., 17(8), 5155–5183, doi:10.5194/acp-17-5155-2017, 2017.

Hill, A. A., Shipway, B. J. and Boutle, I. A.: How sensitive are aerosol-precipitation interactions to the warm rain representation?, J. Adv. Model. Earth Syst., 7(3), 987–1004, doi:10.1002/2014MS000422, 2015.

Iacono, M. J., Mlawer, E. J., Clough, S. A. and Morcrette, J.-J.: Impact of an improved longwave radiation model, RRTM, on the energy budget and thermodynamic properties of the NCAR community climate model, CCM3, J. Geophys. Res. Atmos., 105(D11), 14873–14890, doi:10.1029/2000JD900091, 2000.

Knippertz, P., Coe, H., Chiu, J. C., Evans, M. J., Fink, A. H., Kalthoff, N., Liousse, C., Mari, C., Allan, R. P., Brooks, B., Danour, S., Flamant, C., Jegede, O. O., Fabienne, L., Marsham, J. H., 2015b: The DACCIWA Project, BAMS, 1451-1460.

Knippertz, P., Evans, M. J., Field, P. R., Fink, A. H., Liousse, C., Marsham, J. H., 2015a: The possible role of l ocal air pollution in climate change in West Africa, Nature Climate

Liousse, C., Assamoi, E., Criqui, P., Granier, C., Rosset, R., 2014: Explosive growth in African combustion emissions from 2005 to 2030, 9, 1-10.

Lock, A. & Edwards, J., The parameterization of boundary layer processes. UM Documentation Paper 24, 2011.

Lock, A. P., Brown, A. R., Bush, M. R., Martin, G. M., Smith, R. N. B., Lock, A. P., Brown, A. R., Bush, M. R., Martin, G. M. and Smith, R. N. B.: A New Boundary Layer Mixing Scheme. Part I: Scheme Description and Single-Column Model Tests, Mon. Weather Rev., 128(9), 3187–3199, doi:10.1175/1520-0493(2000)128<3187:ANBLMS>2.0.CO;2, 2000.

Mailler, S., Menut, L., Khvorostyanov, D., Valari, M., Couvidat, F., Siour, G., Turquety, S., Briant, R., Tuccella, P., Bessagnet, B., Colette, A., Létinois, L., Markakis, K. and Meleux, F.: CHIMERE-2017: from urban to hemispheric chemistry-transport modeling, Geosci. Model Dev., 10(6), 2397–2423, doi:10.5194/gmd-10-2397-2017, 2017.

Miltenberger, A. K., Field, P. R., Hill, A. A., Rosenberg, P., Shipway, B. J., Wilkinson, J. M., Scovell, R. and Blyth, A. M.: Aerosol–cloud interactions in mixed-phase convective clouds – Part 1: Aerosol perturbations, Atmos. Chem. Phys., 18(5), 3119–3145, doi:10.5194/acp-18-3119-2018, 2018.

Smith, R. N. B.: A scheme for predicting layer clouds and their water content in a general circulation model, Q. J. R. Meteorol. Soc., 116(492), 435–460, doi:10.1002/qj.49711649210, 1990.

Shipway, B. J.: Revisiting Twomey's approximation for peak supersaturation, Atmos. Chem. Phys., 15(7), 3803–3814, doi:10.5194/acp-15-3803-2015, 2015.

Shipway, B. J. and Hill, A. A.: Diagnosis of systematic differences between multiple parametrizations of warm rain microphysics using a kinematic framework, Q. J. R. Meteorol. Soc., 138(669), 2196–2211, doi:10.1002/qj.1913, 2012.

Thompson, G., Eidhammer, T., Thompson, G. and Eidhammer, T.: A Study of Aerosol Impacts on Clouds and Precipitation Development in a Large Winter Cyclone, J. Atmos. Sci., 71(10), 3636–3658, doi:10.1175/JAS-D-13-0305.1, 2014.

UNO, 2015a: World Population Prospects 2015 Data Booklet (ST/ESA/SER.A/377), United Nations, Department of Economic and Social Affairs.

UNO, 2015b: World Urbanization Prospects: The 2014 Revision, (ST/ESA/SER.A/366), United Nations, Department of Economic and Social Affairs, Population Division.

Valcke, S.: OASIS3-MCT User Guide OASIS3-MCT 3.0. [online] Available from: http://oasis.enes.org (Accessed 15 May 2018), 2015.

van der Linden, R., Fink, A. H. and Redl, R.: Satellite-based climatology of low-level continental clouds in southern West Africa during the summer monsoon season, J. Geophys. Res., 120(3), 1186–1201, doi:10.1002/2014JD022614, 2015.

Vogel, B., H. Vogel, D. Bumer, M. Bangert, K. Lundgren, R. Rinke, and T. Stanelle, 2009: The comprehensive model system COSMO-ART Radiative impact of aerosol on the state of the atmosphere on the regional scale. Atmos. Chem. Phys., 9 (22), 86618680, doi:10.5194/acp-9-8661-2009.

Voigt et al.: ML-CIRRUS - The airborne experiment on natural cirrus and contrail cirrus, *Bull. Amer. Meteorol. Soc.*, doi: 10.1175/BAMS-D-15-00213.1, 2017.

Watts, P. D., Bennartz, R. and Fell, F.: Retrieval of two-layer cloud properties from multispectral observations using optimal estimation, J. Geophys. Res. Atmos., 116(16), D16203, doi:10.1029/2011JD015883, 2011.

Wendisch et al.: The ACRIDICON-CHUVA campaign: Studying tropical deep convective clouds and precipitation over Amazonia using the new German research aircraft HALO, *Bull. Am. Met. Soc.*, doi: 10.1175/BAMS-D-14-00255.1., 2016.

Wood, N., Staniforth, A., White, A., Allen, T., Diamantakis, M., Gross, M., Melvin, T., Smith, C., Vosper, S., Zerroukat, M. and Thuburn, J.: An inherently mass-conserving semi-implicit semi-Lagrangian discretization of the deep-atmosphere global non-hydrostatic equations, Q. J. R. Meteorol. Soc., 140(682), 1505–1520, doi:10.1002/qj.2235, 2014.Lock, A. P. and Lock, A. P.: The Numerical Representation of Entrainment in Parameterizations of Boundary Layer Turbulent Mixing, Mon. Weather Rev., 129(5), 1148–1163, doi:10.1175/1520-0493(2001)129<1148:TNROEI>2.0.CO;2, 2001.